

**UNIVERSITA' VITA-SALUTE SAN RAFFAELE**

**CORSO DI DOTTORATO DI RICERCA  
INTERNAZIONALE IN MEDICINA MOLECOLARE**

**Curriculum in Experimental and Clinical Medicine**

**DEVELOPMENT OF A NOVEL  
SIGNATURE INTEGRATING CLINICAL,  
IMAGING AND EPIGENETIC  
INFORMATION TO TAILOR PELVIC  
NODAL TREATMENT IN PROSTATE  
CANCER**

DoS: Prof. Alberto Briganti



Second Supervisor: Prof. Christopher P. Evans

Tesi di DOTTORATO di RICERCA di Marco Bandini

Matricola. 015666

Ciclo di dottorato XXXV

SSD MED/24

Anno Accademico 2021/2022

## CONSULTAZIONE TESI DI DOTTORATO DI RICERCA

Il sottoscritto/I Marco Bandini  
Matricola/*registration number* 015666  
Nato a/*born at* Forlì  
Il/on 17 Settembre 1989

Autore della tesi di Dottorato di ricerca dal titolo / *author of the PhD Thesis titled*  
**Development of a novel signature integrating clinical, imaging and epigenetic  
information to tailor pelvic nodal treatment in prostate cancer**

X AUTORIZZA la Consultazione della tesi / *AUTHORIZES the public release of the thesis*

NON AUTORIZZA la Consultazione della tesi per ..... mesi /*DOES NOT AUTHORIZE the public release of the thesis for ..... months*


a partire dalla data di conseguimento del titolo e precisamente / *from the PhD thesis date, specifically*

Dal / *from* ...../...../..... Al / *to* ...../...../..... Poiché /*because*:

- l'intera ricerca o parti di essa sono potenzialmente soggette a brevettabilità/ *The whole project or part of it might be subject to patentability;*
- ci sono parti di tesi che sono già state sottoposte a un editore o sono in attesa di pubblicazione/ *Parts of the thesis have been or are being submitted to a publisher or are in press;*
- la tesi è finanziata da enti esterni che vantano dei diritti su di esse e sulla loro pubblicazione/ *the thesis project is financed by external bodies that have rights over it and on its publication.*

E' fatto divieto di riprodurre, in tutto o in parte, quanto in essa contenuto / *Copyright the contents of the thesis in whole or in part is forbidden*

Data /Date 10/11/2022

Firma /Signature ..... 

## DECLARATION

This thesis has been:

- composed by myself and has not been used in any previous application for a degree.

Throughout the text I use both 'I' and 'We' interchangeably.

- written according to the editing guidelines approved by the University.

Permission to use images and other material covered by copyright has been sought and obtained.

All the results presented here were obtained by myself, except for:

1. Pathological tumor assessment – done in collaboration with Dr. Roberta Luciano' and the Pathology Department, IRCCS Ospedale San Raffaele (methods sections 7.7, and data presented in Figure 49)
2. Sequencing of tumor DNA – done in collaboration with Dr. Francesca Giannese, Dr. Caterina Oneto, Dr. Dejan Lazarevic and the Center for Omics Sciences, IRCCS Ospedale San Raffaele (methods sections 7.8.1)
3. Bioinformatic analysis – done in collaboration with Dr. Giulia Maria Scotti and the and the Center for Omics Sciences, IRCCS Ospedale San Raffaele (methods sections 7.8.2 and result section 6.2)

All sources of information are acknowledged by means of reference.

## **ABSTRACT**

Radical prostatectomy (RP) is a treatment option for men with localized prostate cancer. Extended pelvic lymph node dissection (ePLND) at the time of RP is recommended only in patients at risk of lymph node invasion (LNI), where a more accurate disease staging can tailor further adjuvant treatments. The risk of LNI is assessed through preoperative models, such as the Briganti nomograms, which are based on clinical features. They allow for sparing ePLND in a significant proportion of patients, but their accuracy is still suboptimal. Unfortunately, ePLND is associated with significant risks of complications. Therefore, improving our ability to detect LNI in prostate cancer would be key to avoid ePLND-related morbidity. Multiparametric MRI (mp-MRI) proved to be the most accurate imaging technique for local staging prior to RP, improving also the ability to predict LNI. For this reason, mp-MRI tumor features have been included in the latest version of the Briganti nomogram. Beside this, epigenetic expression of prostate cancer cells showed to be highly informative of the biological behavior of prostate cancer, even in terms of lymph node dissemination. Thus, exploring epigenetic patterns within biopsy tumor samples may further improve the prediction of LNI.

Based on these premises, we aimed at developing a novel predicting model that included clinical, radiological, and epigenomic data. To accomplish this aim, we recruited 172 patients with localized prostate cancer diagnosed via combined target and systematic prostate biopsy and undergoing radical prostatectomy and ePLND. Epigenetic profiles of tumor DNA from target and systematic cores were sequenced via reduce representation bisulfite conversion. Gene pathways involved in gene transcription and regulation were significantly associated with LNI. Similarly, gene pathways involved in the transcription of potassium channels were associated with LNI, but only when target samples were considered. We identified 508 and 511 highly differentially methylated CpGs sites within target and systematic samples respectively, that were associated with LNI. The resulting epigenetic signatures were then integrated with conventional risk-factors, such as PSA at biopsy, T-stage at mp-MRI, and ISUP Gleason grade group at target biopsy, to develop two LNI predicting models. After train-test validations, we achieved an AUC of 86.0% for the target model and 82.7% for the systematic model. Both models outperformed Briganti nomograms for LNI prediction at internal validation.

This thesis work reported unprecedented epigenetic profiling of biopsy tumor samples from patients with localized prostate cancer. Novel epigenomic pathways were found to be associated with LNI. Additionally, we successfully developed two novel models for LNI prediction that integrated clinical, mp-MRI and epigenetic features and that outperformed previous tools, pending further validations.

# 1. Table of Contents

<b>1. TABLE OF CONTENTS .....</b>	<b>1</b>
<b>2. ACRONYMS AND ABBREVIATIONS.....</b>	<b>4</b>
<b>3. LIST OF FIGURES AND TABLES .....</b>	<b>6</b>
<b>4. INTRODUCTION.....</b>	<b>9</b>
<b>4.1 – EPIDEMIOLOGY .....</b>	<b>9</b>
<b>4.2 – BIOLOGICAL ORIGIN OF PROSTATE CANCER.....</b>	<b>11</b>
<b>4.3 – HISTOLOGICAL CHARACTERISTICS OF PROSTATE CANCER.....</b>	<b>11</b>
<b>4.4 – SCREENING OF PROSTATE CANCER.....</b>	<b>13</b>
4.4.1 – The PSA .....	13
4.4.2 – Recommendation for PSA screening.....	13
<b>4.5 – RISK FACTORS OF PROSTATE CANCER.....</b>	<b>18</b>
<b>4.6 – CLASSIFICATION OF THE DISEASE .....</b>	<b>19</b>
4.6.1 – the TNM classification system.....	19
4.6.2 – Classification according to clinical significance .....	19
4.6.3 – The D’Amico risk groups.....	21
4.6.4 – The novel EAU classification .....	22
<b>4.7– DIAGNOSIS.....</b>	<b>24</b>
4.7.1 – Predictors of the disease .....	24
4.7.2 – Prostate Cancer biopsy: from systematic biopsy to MRI-target approaches.....	24
4.7.3 – mp-MRI: methodological considerations .....	24
4.7.4 – The PI-RADS score .....	26
4.7.5 – Evidences supporting mp-MRI target biopsy .....	26
4.7.6 – Biomarkers for initial diagnosis.....	29
<b>4.8 – CONSERVATIVE TREATMENTS.....</b>	<b>29</b>
4.8.1 – Expected survival in prostate cancer patients .....	29
4.8.2 - Watchful waiting .....	29
4.8.3 – Active surveillance.....	30
4.8.4 – The Protec-T trial.....	31
<b>4.9 – ACTIVE TREATMENTS .....</b>	<b>32</b>
4.9.1 – The EAU risk stratification for active treatment .....	32
4.9.3 – Treatment for Intermediate-risk tumors.....	35
4.9.4 – Treatment for High-risk tumors .....	36
<b>4.10 – RADICAL PROSTATECTOMY.....</b>	<b>37</b>
4.10.1 – From open to robot-assisted radical prostatectomy .....	37
4.10.2 – Surgical techniques for robot-assisted radical prostatectomy .....	38
<b>4.11 – PELVIC LYMPH NODE DISSECTION (PLND).....</b>	<b>39</b>
<b>4.12 – HOW TO SELECT CANDIDATES FOR PLND .....</b>	<b>42</b>
4.12.1 – Prevalence of LNI according with the D’Amico risk group classification .....	42
4.12.2 – Predicting ability of different imaging tools .....	42
4.12.3 – LNI predicting models.....	43
4.12.4 – DNA methylation and LNI prediction .....	48
<b>5. AIMS OF THE RESEARCH PROJECT .....</b>	<b>54</b>
<b>6. RESULTS .....</b>	<b>56</b>
<b>6.1 – CHARACTERISTICS OF THE STUDY POPULATION.....</b>	<b>56</b>
6.1.1 – Clinical characteristics .....	56
6.1.2 – mpMRI features .....	56
6.1.3 – Biopsy sampling data .....	57
6.1.4 – Risk classification grouping.....	59

6.1.5 – Pathological features from radical prostatectomy specimens .....	59
6.1.6 – Follow-up and oncological outcomes.....	60
<b>6.2 – EPIGENETIC ANALYSIS.....</b>	<b>60</b>
6.2.1 – Cohort definition.....	60
6.2.2 – Validation of the Munbjerg signature.....	61
6.2.3 – Differential Methylation analysis.....	64
6.2.3.1 – Differential Methylation analysis for the combined (target and systematic cores) sample cohort.....	66
6.2.3.2 – Differential methylation analysis of the target core samples .....	75
6.2.3.3 – Differential Methylation analysis of the systematic core samples.....	81
6.2.3.4 – Overlap among differential methylation analyses of target, systematic, and combined samples using different cut-offs.....	87
6.2.4 – Developing models integrating epigenetic, clinical and mp-MRI features.....	94
6.2.4.1 – Identification of highly differentially methylated CpGs sites .....	94
6.2.4.2 – Developing epigenetic signatures with hypermethylated CpGs.....	97
6.2.4.3 – Integrating epigenetic, clinical, and mp-MRI features .....	97
6.2.4.4 – Comparison between developed models and existing clinical models .....	99
<b>7. MATERIALS AND METHODS.....</b>	<b>102</b>
<b>7.1 – COHORT DEFINITION.....</b>	<b>102</b>
7.1.1 – Patient selection and ethical approval .....	102
7.1.2 – Patient sample.....	102
<b>7.2 – MULTIPARAMETRIC MRI.....</b>	<b>103</b>
7.2.1 – mpMRI acquisition and cohort characteristics.....	103
<b>7.3 – TRANS-PERINEAL PROSTATE BIOPSY.....</b>	<b>104</b>
7.3.1 – Prostate biopsy indications and technique .....	104
<b>7.4 – BIOPSY CORE SELECTION.....</b>	<b>105</b>
7.4.1 Selection process of biopsy cores .....	105
<b>7.5 – EXTENDED PELVIC LYMPH NODE DISSECTION .....</b>	<b>106</b>
7.5.1 – Surgical technique for extended PLNDs .....	106
<b>7.6 – DEFINITION OF THE CLINICAL VARIABLES OF INTEREST .....</b>	<b>106</b>
7.6.1 – Clinical variables of the included population.....	106
<b>7.7 – PREPARATION OF THE CORE AND LYMPH NODE SPECIMENS .....</b>	<b>107</b>
7.7.1 – Specimen preparation.....	107
<b>7.8 – EPIGENETIC PROFILING FROM FFPE SPECIMENS OF PATIENTS WITH LOCALIZED (CTANYN0M0) PROSTATE CANCER.....</b>	<b>109</b>
7.8.1 – DNA methylation analyses.....	109
7.8.2 – Bio-Informatic analyses.....	110
7.8.2.1 – Validation of the Munbjerg signature .....	112
7.8.2.2 – Differential Methylation analysis .....	113
only for the 10% cut-off, since the application of the 25% cut-off did not lead to any significant results.....	116
7.8.2.3 – Identification of the highly differentially methylated CpG.....	116
7.8.2.4 – Development of epigenetic signatures .....	116
7.8.2.5 – Development of a model integrating clinical, mp-MRI and epigenetic features .....	117
<b>8. DISCUSSION .....</b>	<b>119</b>
<b>8.1 – THE RELEVANCE OF A NEW PROTOCOL FOR FFPE SAMPLE EXTRACTION AND EPIGENETIC ANALYSIS.....</b>	<b>120</b>
<b>8.2 – CHROMOSOMIC POSITIONS OF DIFFERENTIALLY METHYLATED CpG.....</b>	<b>122</b>
<b>8.3 – VALIDATION OF THE MUNDBJERG SIGNATURE.....</b>	<b>123</b>
<b>8.4 – ANALYSIS OF DIFFERENTIALLY METHYLATED CpG SITES AMONG SAMPLES FROM TARGET AND SYSTEMATIC BIOPSY CORE.....</b>	<b>125</b>
<b>8.5 – HIGHLY DIFFERENTIALLY METHYLATED CpGs SITES AND THEIR CORRELATION WITH GENE PATHWAYS.....</b>	<b>127</b>
<b>8.6 – DEVELOPING AN INTEGRATED MODEL FOR LNI PREDICTION .....</b>	<b>128</b>
<b>8.7 – STUDY LIMITATIONS.....</b>	<b>129</b>
<b>8.8 – CONCLUSIONS.....</b>	<b>130</b>

**9. REFERENCES.....132**



## **2. Acronyms and abbreviations**

Assessment of Prostate MRI Before Prostate Biopsies (MRI-FIRST)

American Urological Association (AUA)

American Joint Committee on Cancer (AJCC)

Androgen deprivation therapy (ADT)

Area under the curve (AUC)

Computer tomography (CT)

Deoxyribonucleic acid (DNA)

Diffusion weighted (DWI)

Dynamic contrast enhanced (DCEI)

European Association of Urology (EAU)

European trials, and especially with the European Randomized Study of Screening for

Extended pelvic lymph node dissection (ePLND)

External beam radiotherapy (EBRT)

Food and Drug Administration (FDA)

Image-guided RT (IGRT)

Intensity-modulated RT (IMRT)

International Agency for Research on Cancer (IARC)

Lymph node invasion (LNI)

Magnetic resonance imaging (MRI)

Magnetic resonance spectroscopy images (MRSI)

Met Prostaat MRI Meer Mans (4M)

Multiparametric MRI (mp-MRI)

National Comprehensive Cancer Network (NCCN)

Positron emission tomography (PET)

Prostate Cancer (ERSPC)

Prostate Evaluation for Clinically Important Disease: Sampling Using Image-guidance  
Or Not? (PRECISION)

Prostate Imaging Reporting and Data System (PI-RADS)

Prostate, Lung, Colorectal and Ovarian (PLCO)

Prostate-specific antigen (PSA)

Prostate-specific membrane antigen (PSMA)

United States (US)

United States Preventive Services Task Force (USPSTF)

Single nucleotide polymorphisms (SNP)

T2-weighted (T2WI)

Three-dimensional (3D)

Tumor, Node, Metastasis (TNM)

Volumetric arc radiation therapy (VMAT)

### 3. List of Figures and Tables

#### List of Figures

Figure 1.....	Page 10
Figure 2.....	Page 12
Figure 3.....	Page 14
Figure 4.....	Page 16
Figure 5.....	Page 17
Figure 6.....	Page 20
Figure 7.....	Page 23
Figure 8.....	Page 25
Figure 9.....	Page 27
Figure 10.....	Page 33
Figure 11.....	Page 45
Figure 12.....	Page 46
Figure 13.....	Page 47
Figure 14.....	Page 49
Figure 15.....	Page 51
Figure 16.....	Page 62
Figure 17.....	Page 63
Figure 18.....	Page 65
Figure 19.....	Page 67
Figure 20.....	Page 69
Figure 21.....	Page 69
Figure 22.....	Page 70
Figure 23.....	Page 72
Figure 24.....	Page 73
Figure 25.....	Page 74
Figure 26.....	Page 76
Figure 27.....	Page 76
Figure 28.....	Page 77
Figure 29.....	Page 77

Figure 30.....	Page 79
Figure 31.....	Page 80
Figure 32.....	Page 82
Figure 33.....	Page 84
Figure 34.....	Page 83
Figure 35.....	Page 84
Figure 36.....	Page 84
Figure 37.....	Page 86
Figure 38.....	Page 88
Figure 39.....	Page 89
Figure 40.....	Page 90
Figure 41.....	Page 90
Figure 42.....	Page 91
Figure 43.....	Page 92
Figure 44.....	Page 93
Figure 45.....	Page 95
Figure 46.....	Page 96
Figure 47.....	Page 101
Figure 48.....	Page 101
Figure 49.....	Page 108
Figure 50.....	Page 111
Figure 51.....	Page 115

**List of Tables**

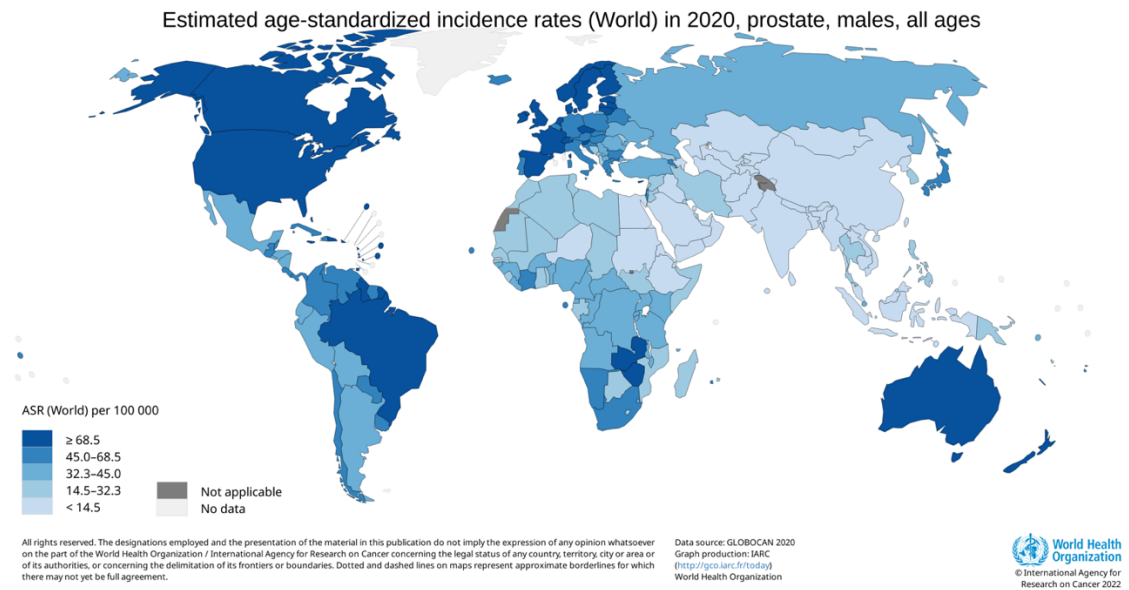
Table 1.....	Page 56
Table 2.....	Page 57
Table 3.....	Page 57
Table 4.....	Page 58
Table 5.....	Page 59
Table 6.....	Page 59
Table 7.....	Page 60
Table 8.....	Page 61

Table 9.....	Page 98
Table 10.....	Page 98
Table 11.....	Page 99
Table 12.....	Page 100
Table 13.....	Page 100

## 4. Introduction

### *4.1 – Epidemiology*

Epidemiological data from the International Agency for Research on Cancer (IARC) ranked prostate cancer as the second most commonly diagnosed cancer in men worldwide, with 1, 414 259 new cases in 2020(1). The estimated all-age incidence of prostate cancer in 2020 was 31 per 100 000 males, and the lifetime cumulative risk was 3.9%. Every year, prostate cancer claimed 375, 304 lives (data from 2020), making it the fourth most-common killer of men worldwide among all cancer types(2). Unfortunately, these numbers are expected to grow by 2040, with +71.6% and +91.1% for incidence and mortality, simply due to the growth and aging of the population(2). The burden of this disease presents intrinsic geographical heterogeneities. Indeed, there are significant variations in terms of incidence and mortality among countries(3). Australia, New Zealand, Northern America, and North-Western Europe present the highest incidence of the disease, while Eastern and South-Central Asia have the lowest, but rising (**Figure 1**). These geographical variations are promoted by several factors. Firstly, prostate cancer presents varying degrees of genetic susceptibility among different ethnicities(4). African descendants living in developed countries present the highest risk of developing and dying from prostate cancer, while Asians have the lowest(5). Secondly, inequalities in access to medical care engrave cancer incidence and mortality. Indeed, the use of prostate-specific antigen (PSA)-based screening and surgery for benign prostatic hyperplasia have shown to increase the diagnosis of latent forms of the disease, wherever they are routinely recommended(6). Additionally, variability of life expectancy among geographical areas also affects the prevalence of this tumor, which is usually diagnosed in men with advanced age. Indeed, men living in developing countries, where the life expectancy is short due to other competing causes, are less likely to die from prostate cancer than patients living in developed countries, where life expectancy is longer(7). In summary, prostate cancer incidence is widely heterogeneous among different geographical regions. Longer life expectancy, higher diagnostic rates of latent forms of prostate cancer and genetic predispositions have risen the incidence of the disease in developed countries in recent years.



**Figure 1** – Estimated age-standardized incidence rates (World) in 2020 for prostate cancer. Reprinted from GLOBOCAN 2020 Graph production: IARC (<http://gco.iarc.fr/today>) World Health Organization. ©2020, with permission from IARC/WHO.

#### ***4.2 – Biological origin of prostate cancer***

Behind the oncogenesis of prostate cancer, there is a complex interplay of multiple interactions among microenvironmental and macroenvironmental factors, inherent germline susceptibility, and acquired somatic genomic alterations(8). Prostate cancer arises from the prostate gland, which is located in the pelvis, around the more proximal tract of the male urethra(9). The prostate gland contains three main areas, namely the central, transition, and peripheral zones(10). Prostate cancer more frequently arises from the peripheral zone(11). Here, among the two types of prostatic epithelial cells, both luminal and basal can initiate the carcinogenic process (**Figure 2**). Prostate cancer has some unique biological characteristics that make it different from other types of cancer. First, it is hormone dependent. Indeed, both normal and cancerous epithelial cells express a high level of androgen receptors, and this explains why the growth of prostate cancer is driven by androgens, at least at the beginning of carcinogenesis(12). Another relevant characteristic of prostate cancer is that it often consists of a multifocal disease. Multiple foci of cancer may exhibit different genetic alterations with different attitudes to metastatic spreading and resistance to medical treatments. Thus, the clinical identification of prostate cancer through random prostatic sampling may not always comprehensively depict the features of a heterogeneous multifocal disease, where more aggressive tumor foci may remain undiscovered, then leading to unexpected progression(13). The main triggers of prostate carcinogenesis are chronic inflammation and infection from urine microbes. These agents may facilitate DNA alteration and selection of mutating clones through the activation of oxidative stress and generation of reactive oxygen species(14). Within an inflammatory environment, luminal proliferative epithelial cells may generate intermediate phenotypes that can be prone to accumulate genomic and epigenetic alterations, leading to prostatic intraepithelial neoplasia and malignant transformation. However, the mentioned biological mechanisms do not comprehensively explain the origin of prostate cancer and its natural course. Many more factors seem to play a role in the oncogenesis(15), and many others are still to be explored.

#### ***4.3 – Histological characteristics of prostate cancer***

The histological aspect of prostate cancer ranges from low-grade lesions, with similar



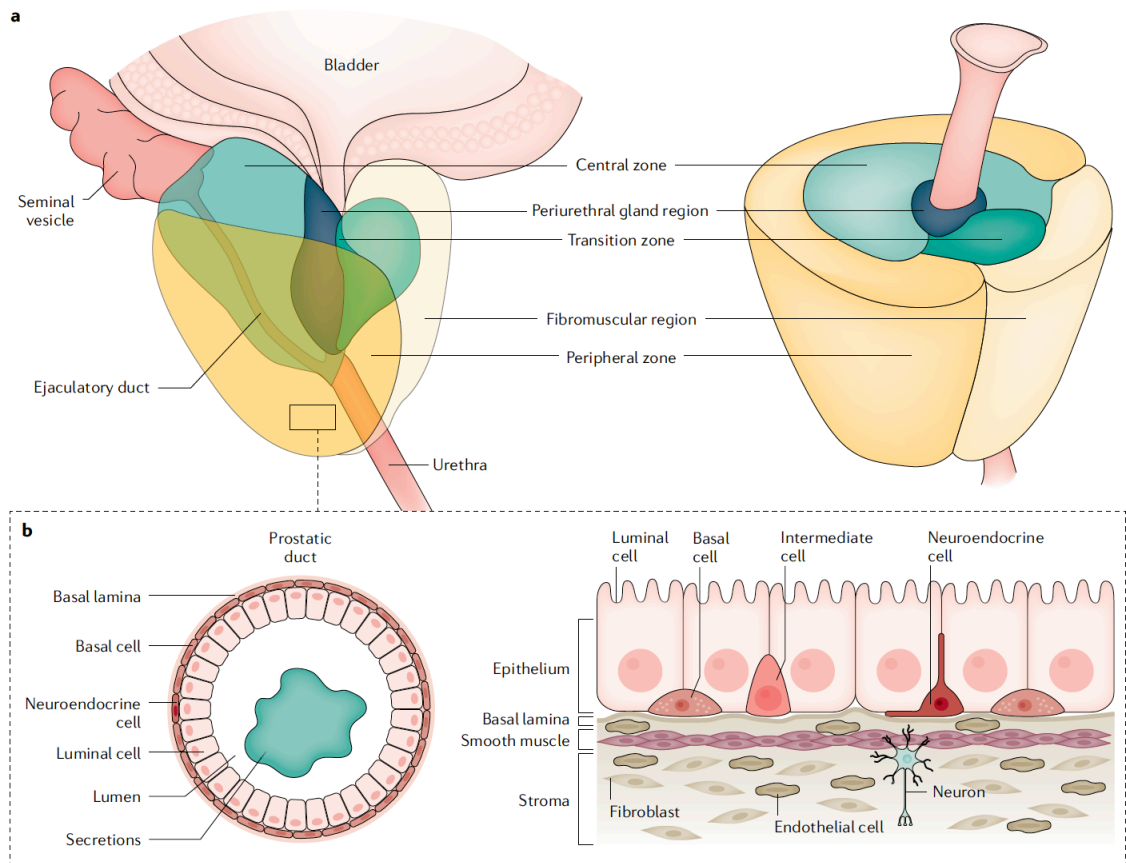


**Figure 2** – a) The adult prostate is composed of three main areas: the central, transition, and peripheral zones; prostate cancer more frequently arises from the peripheral zone. b) Each region comprises ducts and acini embedded in the stroma, which also contains other cell types: smooth muscle cells, fibroblasts, endothelial cells, and neurons. The ducts and acini comprise a single layer of columnar epithelium, surrounded by a layer of basal epithelial cells. Neuroendocrine cells are also present within the duct. Reprinted by permission from Springer Nature ("Springer Nature"), Nature Reviews Disease Primers, "Prostate cancer", Richard J. Rebello et al., ©2018

architecture of benign glands, to high-grade neoplastic glandular lesions, which instead present small, round acini lacking basal epithelium and interspersed between benign glands(16). The Gleason score is a grading system ranging from 6 to 10 and it is used to classify the aggressiveness of prostate cancer at the time of histological diagnosis. The Gleason patterns are assigned by the pathologist based on the microscopic appearance of prostate cancer in a way that an increasing number corresponds to increasing aggressiveness(17) (**Figure 3**). The Gleason score is calculated as the numeric sum of the two most prominent Gleason patterns. The Gleason score is nowadays converted to the International Society of Urological Pathology (ISUP) grade grouping which can range from 1 to 5, where group 1 accounts for Gleason score 3+3, group 2 for 3+4, group 3 for 4+3, group 4 for 4+4, 3+5, and 5+3, group 5 for 4+5, 5+4 and 5+5. The adoption of the ISUP grade grouping was introduced to better account for the prognosis of prostate cancer, which was not comprehensively estimated with the use of the Gleason score(18).

#### ***4.4 – Screening of prostate cancer***

##### ***4.4.1 – The PSA***

Prostate-specific antigen, or simply PSA, is a human glycoprotein produced by normal, as well as malignant cells of the prostate gland. PSA levels can be measured with a simple blood sample. Its value can be expressed as nanograms of PSA per milliliter (ng/mL)(19). The blood level of PSA can be elevated in patients with prostatic hyperplasia, as well as with prostate cancer(20). The PSA test was approved by the Food and Drug Administration (FDA) in 1986(21). Originally, PSA was only recommended for monitoring the progression of prostate cancer in men who had already been diagnosed with the disease. However, in 1994 following the results of a large cohort study(22), the FDA approved the PSA blood test in combination with digital rectal examination to facilitate the detection of prostate cancer in men 50 years and older(23).

##### ***4.4.2 – Recommendation for PSA screening***

The use of PSA-screening has been a controversial topic since its introduction in clinical practice. The PSA-screening was advocated as a possible way to reduce prostate cancer mortality by reducing the incidence of newly-diagnosed metastatic disease, as the test can

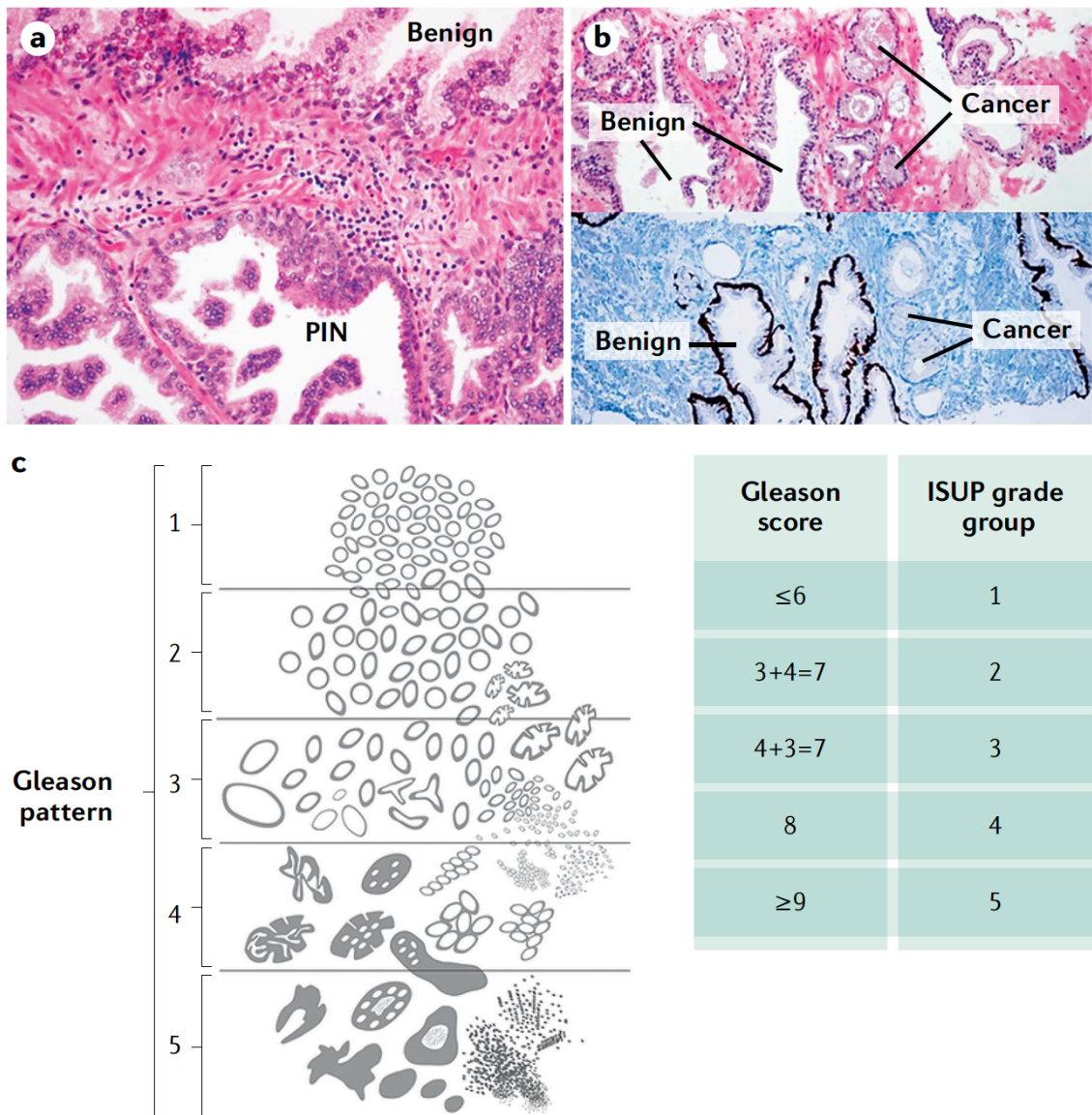


**Figure 3** – a) Histological representation of benign prostate tissue and intraepithelial neoplasia (PIN); b) Histological representation of benign prostate tissue and prostate cancer; c) Common Gleason patterns of prostate cancer with the derived International Society of Urological Pathology (ISUP) 2015 modified Gleason grading schematic diagram.

detect asymptomatic, early-stage tumors. Nevertheless, large PSA-screening campaigns also brought up the incidence of prostate cancer by increasing the detection of indolent tumors(24). Higher tumor incidence of indolent forms fomented the misuse of radical treatments and increased the burden of treatment-related morbidity(25). When this happened, the benefit of PSA-screening was outperformed by treatment-related complications leading to a disequilibrium between harms and benefits. In light of these considerations, the US Preventive Services Task Force (USPSTF), an independent, panel of national experts in disease prevention and evidence-based medicine, recommended against PSA-screening for men aged 75 years or older in 2008 and for all men in 2012(26,27). These recommendations were mainly driven by the negative results of the Prostate, Lung, Colorectal and Ovarian (PLCO) screening trial, which did not prove a survival benefit in the screened population after 13 years from initial accrual(28). Those recommendations were in conflict with the results of the European trials, and especially with the European Randomized Study of Screening for Prostate Cancer (ERSPC)(29), which showed lower rates of prostate cancer-specific death in the screened population. These conflicting results had a significant impact on many public health organizations worldwide, which differently reacted against to or in favor of PSA-screening. In the US, the USPSTF recommendations against PSA-screening generated a rebound of newly-diagnosed metastatic prostate cancer cases(30,31) (**Figure 4**). Thus, the USPSTF revised its guidelines in 2018, and it recommended PSA-screening based on informed decision-making for individuals aged 55-69 years(32). European countries, including Italy, follow the recommendations of the EAU, which supports the screening for prostate cancer only in well-informed individuals above the age of 50 and with a life expectancy of at least 10-15 years(33). Earlier screening can be initiated in specific high-risk groups, such as men with a family history of prostate cancer, African descent, or men carrying BRCA2 mutations(34). For other countries, the recommendations for prostate cancer screening may vary according to age thresholds and familiar risk factors, but generally, they all encourage the screening in subjects above the age of 50, unless other risk factors are present(16) (**Figure 5**).

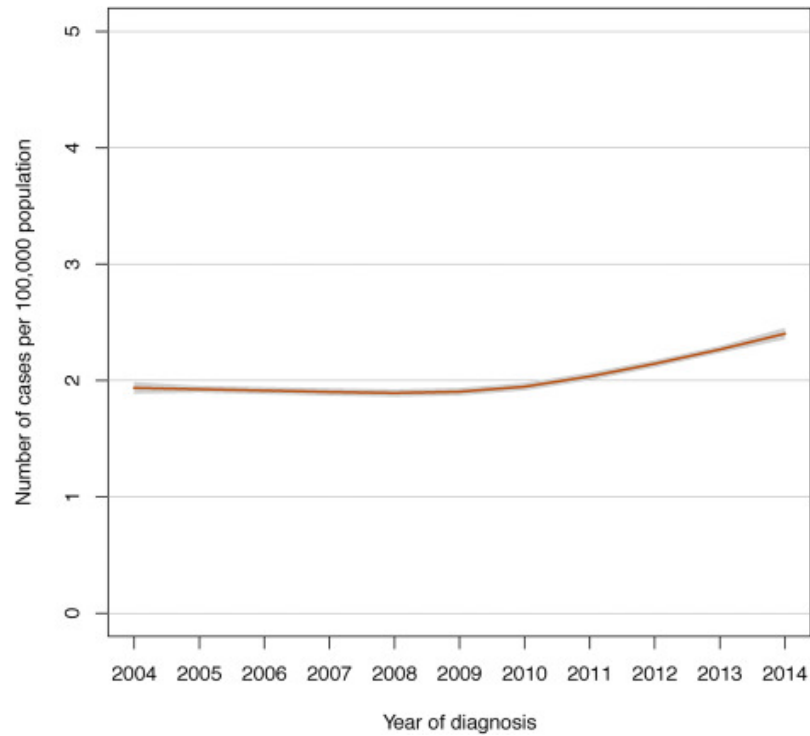


**Figure 4** – Age-adjusted temporal trends during 2004–2014 for newly diagnosed metastatic prostate cancer per 100 000 population (Reprinted from *European Urology Oncology*, Marco Bandini et al., “Increase in the Annual Rate of Newly Diagnosed Metastatic Prostate Cancer: A Contemporary Analysis of the Surveillance, Epidemiology and End Results Database”, ©2018, with permission from Elsevier).

Country/region	Recommendation			
	Without additional risk factors	Family history of any cancer	BRCA2 germline mutation carrier	African American ancestry
USA (USPSTF, AUA)	From age 55 to 69 years and if >10 years LE; stop at age 70 years	Individual decision-making before age 55 years	N/A	Individual decision-making before age 55 years
Canada (CUA)	From age 50 to 70 years and if >10 years LE	From age 45 years if >10 years LE	N/A	N/A
Europe (EAU, ESTRO, SIOG)	From age 50 years and only if >10 years LE	From age 45 years if >10 years LE	From age 40 years	From age 45 years if >10 years LE
Japan (JUA)	From age 50 years	From age 40 years	N/A	N/A

**Figure 5** – USA, Canada, European, and Japanese recommendations for PSA screening in the adult male population. Reprinted by permission from Springer Nature ("Springer Nature"), Nature Reviews Disease Primers, "Prostate cancer", Richard J. Rebello et al., ©2018

#### ***4.5 – Risk factors of prostate cancer***

The well-established leading causes of prostate cancer are older age, ethnicity, and family history (both paternal and maternal)(35). Men of African ancestry seems to be at higher risk of developing prostate cancer due to a certain genetic susceptibility(5,36). Indeed, prostate cancer occurs earlier and with more aggressive features in African or Caribbean descent living in the United States (US) as compared to Caucasians (two-fold higher relative risk)(37,38). By contrast, prostate cancer is less common in Asiatic men living in Asia as compared to Caucasian men living in the US. However, this geographical protective effect seems to disappear when the Asiatic population living in the US is compared to the Caucasian counterpart(39), suggesting a more relevant environmental effect driving these geographic variations. Family history of prostate cancer is present in up to 20% of men diagnosed with the disease(40). Prostate cancer can be defined as familial only when it occurs in at least three relatives, and when at least two of them developed the disease before 55 years of age. Accordingly, the risk of developing prostate cancer increase by 1.8-fold when a first-degree relative is diagnosed with the disease(41). Only 9% of men with prostate cancer present a truly hereditary disease, which is typically characterized by an earlier onset (6-7 years) compared to nonhereditary cases(42). The genetics behind family predisposition and hereditary cancer syndromes associated with prostate cancer is complex. Genome-wide association studies have identified over 100 common susceptibility loci increasing the risk of prostate cancer among families at high risk. Among those, *BRCA1*, *BRCA2*(43), *HOXB13*(44), *MSH2*(45), as well as germline pathogenic variants in DNA repair genes seem to confer an increased risk of developing the disease. Additionally, studies on genome-wide association identified over 170 single nucleotide polymorphisms (SNPs), which were associated with a higher risk of prostate cancer(46). These SNPs have been used to design genetic risk scores for the early detection of prostate cancer in subjects at risk. Although these scores did not demonstrate the ability to discriminate between clinically aggressive disease over indolent forms, their use is helpful to select individuals who can benefit from early screening(47). Among lifestyle factors, obesity, metabolic syndrome(48), alcohol intake(49), smoking(50), and high intake of protein(51) have been investigated as potential triggers of prostate cancer. Although some are associated with

an increased risk of the disease, there is still insufficient evidence to recommend lifestyle changes or a modified diet to significantly lower the risk of prostate cancer.

#### ***4.6 – Classification of the disease***

##### ***4.6.1 – the TNM classification system***

Prostate cancer can be stratified according to different classification systems. The Tumor, Node, Metastasis (TNM) staging system(52), a classification system provided by the American Joint Committee on Cancer (AJCC) for the majority of human tumors, identifies three different groups of prostate cancer: localized, locally advanced and metastatic. According to recently published data, 80% of men are diagnosed with organ-confined disease, 15% with locoregional metastases (i.e. regional lymph nodes) and 5% with distant metastases (i.e. non-regional nodes, bones, other organs) (53) (**Figure 6**). Given this assumption, the majority of patients with localized forms of prostate cancer. Life expectancy for men with localized prostate cancer can be as high as 99% over 10 years, if diagnosed at an early stage(54). Given the pick of incidence of this tumor in men with age 65 or older, many patients will die before any clinical signs of the disease. Thus, another classification of prostate cancer accounting for its clinical impact on patient health and survival is pivotal to defining any treatment recommendation.

##### ***4.6.2 – Classification according to clinical significance***

The use of the descriptors “*clinically significant*” and “*clinically insignificant*” is widely accepted to define the clinical behavior of newly-diagnosed prostate cancer. Accordingly, a clinically insignificant prostate cancer is defined as a localized disease with low potential of causing harm to the patient. Overtreatment is the only risk associated with clinically insignificant prostate cancer, where any form of treatment is associated with harmful side effects that exceed the benefits derived from the treatment itself. Whether a clinical definition of clinically significant and insignificant prostate cancer is advisable, its pathological designation remains less clear. According to the Gleason grading system and its adaptation by the 2014 ISUP classification(18), the aggressiveness of prostate cancer can be classified into five groups. Whether ISUP Gleason grade groups 2-5 are associated with non-negligible aggressiveness behavior, group 1 usually presents an indolent



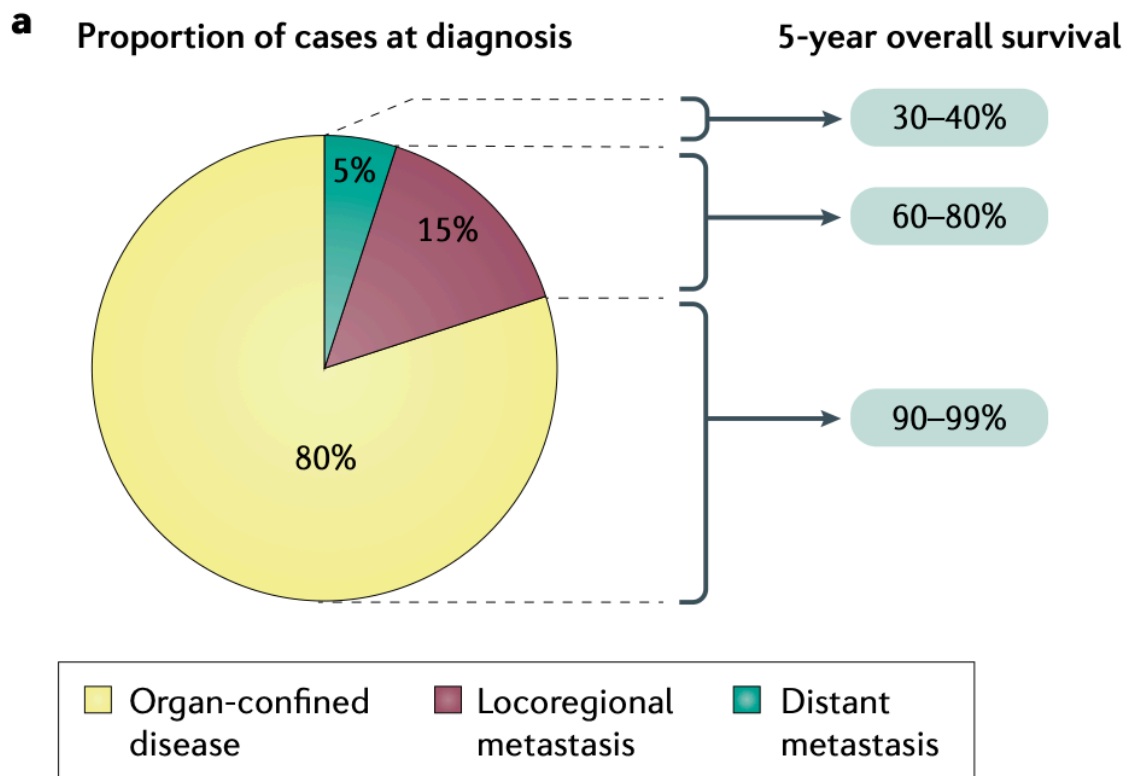


**Figure 6** – Proportion and corresponding 5-year overall survival of newly diagnosed prostate cancer according with the TNM staging groups. Reprinted by permission from Springer Nature ("Springer Nature"), Nature Reviews Disease Primers, "Prostate cancer", Richard J. Rebello et al., ©2018

evolution. Pathological studies on prostatectomy specimens of patients with ISUP group 1 tumors found that extraprostatic extension was very uncommon (0.28% of 2,502 cases) and seminal vesicle invasion or lymph node metastasis did not occur at all(55,56). Nevertheless, clinically insignificant prostate cancer (ISUP Gleason grade group 1) is usually detected by biopsy sampling, rather than after radical prostatectomy. Thus, management decision is influenced by biopsy inaccuracy. The widespread use of magnetic resonance imaging (MRI)-target biopsy has reduced diagnostic inaccuracy, but sampling error may still occur, especially when the initial MRI shows a suspicious lesion, but a Gleason grade groups 1 tumor is subsequently found at biopsy. Additionally, it is possible that Gleason grade group 1 can progress to higher grades over time, making the definition of insignificant prostate cancer uncertain and susceptible to modifications over time. On the contrary, clinically significant prostate cancers are tumors with a high potential of local and systemic progression over time, where curative treatments should be advocated to provide benefit to the patients, and where treatment related harm is justified by improved survival. To date, three large prospective randomized controlled trials have supported these assumptions. The SPCG-4(57), the PIVOT(58), and the Protec-T(59) trials helped to demark a line between clinically significant and insignificant prostate cancer, especially in terms of when and how curative treatments must be recommended. Those trials established that the clinical significance of prostate cancer should be defined according to pathological tumor characteristics (e.g., ISUP Gleason grade groups, T stage, and PSA), but also factoring in age expectancy, to better select candidates for curative treatments. Indeed, a minimum of 10 years of follow-up was necessary to observe any benefit from active treatments, while accounting for treatment complications and disease evolution. In other words, prostate cancer gains clinical significance only when the pathological features are relevant in terms of disease progression to account for treatment-related side effects, and the life expectancy of the patient is longer than 10 years. Indeed, 10 years is the minimum amount of time to account for the slow natural history of the disease, while appreciating the treatment benefits.

#### ***4.6.3 – The D’Amico risk groups***

Beside the classification of clinically significant and insignificant prostate cancer, a multitude of other risk classifications has been described to better stratify patients with

indolent or aggressive disease. Among those numerous classifications, The D'Amico classification represents one of the most commonly utilized (60). This classification was originally designed to predict the risk of recurrence following curative treatment (radiotherapy and radical prostatectomy) of localized forms of prostate cancer. The system categorizes patients into three groups (low, intermediate, and high risk) according to the intrinsic probability of recurrence. The risk score is calculated based on blood PSA levels, Gleason score, and tumor T stage. Using these references, patient's risk of recurrence is categorized as:

- Low risk: PSA less than or equal to 10, ISUP grade group equal to 1, and clinical stage T1-2a;
- Intermediate risk: PSA between 10 and 20ng/ml, ISUP grade group 2-3, or clinical stage T2b;
- High-risk: PSA more than 20ng/ml, ISUP grade group equal or higher than 4, or clinical stage T2c-3a.

The D'Amico classification has been endorsed, even with some modifications, by the National Comprehensive Cancer Network (NCCN) and EAU guidelines for tailoring treatment decision making in patients with localized prostate cancer.

#### ***4.6.4 – The novel EAU classification***

Recently, a novel risk stratification of patients with prostate cancer was designed to establish the probability of recurrence following radical treatments (61). The new classification is based on clinical, as well as preoperative MRI features, namely PSA, biopsy ISUP grade groups, MRI T stage, and the maximum diameter of the lesion at MRI. Similar to the D'Amico classification, the end-point for the EAU classifier is biochemical recurrence after radical treatment. Nevertheless, this new classification by Mazzone et al.(61), included only patients treated with radical prostatectomy, whereas the D'Amico's classification(60) was generated in a cohort of patients mainly treated with radiotherapy. The new classification identified four groups of patients: low, intermediate, high, and very-high risk of recurrence (**Figure 7**). In its external validation, the Mazzone classification showed higher accuracy as compared to the D'Amico classification(61).

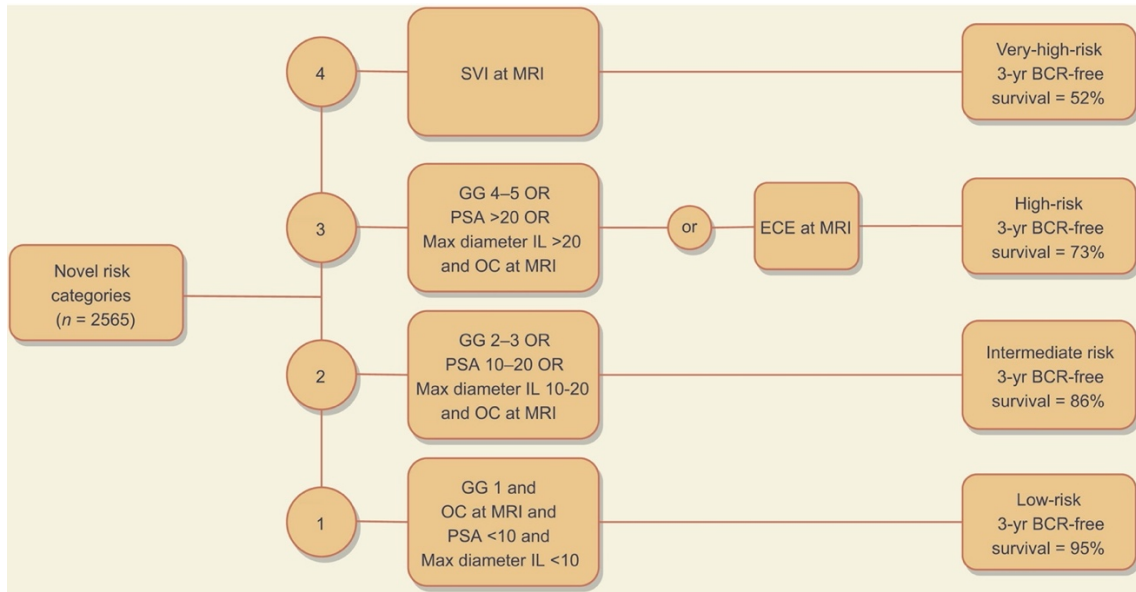


**Figure 7** – Novel risk classification stratifying patients into four categories according to grade group, T stage at MRI, maximum diameter of the index lesion at MRI, and preoperative PSA. BCR = biochemical recurrence; ECE = extracapsular extension; GG = grade group; IL = index lesion; MRI = magnetic resonance imaging; OC = organ confined; PSA = prostate-specific antigen; SVI = seminal vesicle invasion. (Reprinted from *European Urology*, Elio Mazzone et al., “Risk Stratification of Patients Candidate to Radical Prostatectomy Based on Clinical and Multiparametric Magnetic Resonance Imaging Parameters: Development and External Validation of Novel Risk Groups”, ©2022, with permission from Elsevier).

## ***4.7– Diagnosis***

### ***4.7.1 – Predictors of the disease***

Prostate cancer is suspected based on PSA blood values and/or digital rectal examination. Familiarity for prostate cancer, age, race, PSA kinetic, PSA density are also important for the clinical algorithm. However, only the histopathological verification of the disease via prostate biopsy can provide a definitive diagnosis of prostate cancer.

### ***4.7.2 – Prostate Cancer biopsy: from systematic biopsy to MRI-target approaches***

Historically, transrectal or transperineal TRUS-guided systematic prostate biopsy was the standard of care for the histopathological diagnosis of prostate cancer. Indeed, conventional imaging modalities, such as ultrasound and computer tomography (CT) scan, have never been able to correctly identify suspicious lesions within the prostate that could be targeted at the time of biopsy. Thus, prostate biopsy was usually performed random and in sextants (systematic) in order to uniformly sample the prostate (**Figure 8**). In the last ten years, the advent of the multi-parametric MRI (mp-MRI) has revolutionized the clinical management of localized prostate cancer and its diagnosis. Given the ability of mp-MRI to identify and target suspicious lesions of the prostate, mp-MRI target biopsy has progressively overtaken systematic sampling for the diagnosis of prostate cancer.

### ***4.7.3 – mp-MRI: methodological considerations***

mp-MRI is a method to obtain a three-dimensional (3D) prostate image by combining T2-weighted (T2WI), diffusion weighted (DWI), dynamic contrast enhanced (DCEI) and, if desired, magnetic resonance spectroscopy images (MRSI). Scientific evidence based upon radical prostatectomy specimens suggests that mpMRI has good sensitivity for the detection and localization of ISUP Gleason grade group 2-5 tumors, especially when their diameter is superior to 1cm(62). This important correlation was also proved in the biopsy setting. In a Cochrane meta-analysis(63), MRI-guided target biopsy was compared to TRUS-guided systematic biopsy for the detection of ISUP Gleason grade groups 2-5 and ISUP Gleason grade groups 3-5. Here, for ISUP grade 2-5 cancers, MRI-guided biopsy showed a pooled sensitivity of 0.80 (95% confidence interval: 0.60-0.87) and a pooled specificity of 0.94 (0.90-0.97) vs. 0.63 (0.19-0.93) and 1.00 (0.91-100) of the TRUS-guided biopsy. Additionally, mp-MRI showed to reduce the risk of identification of

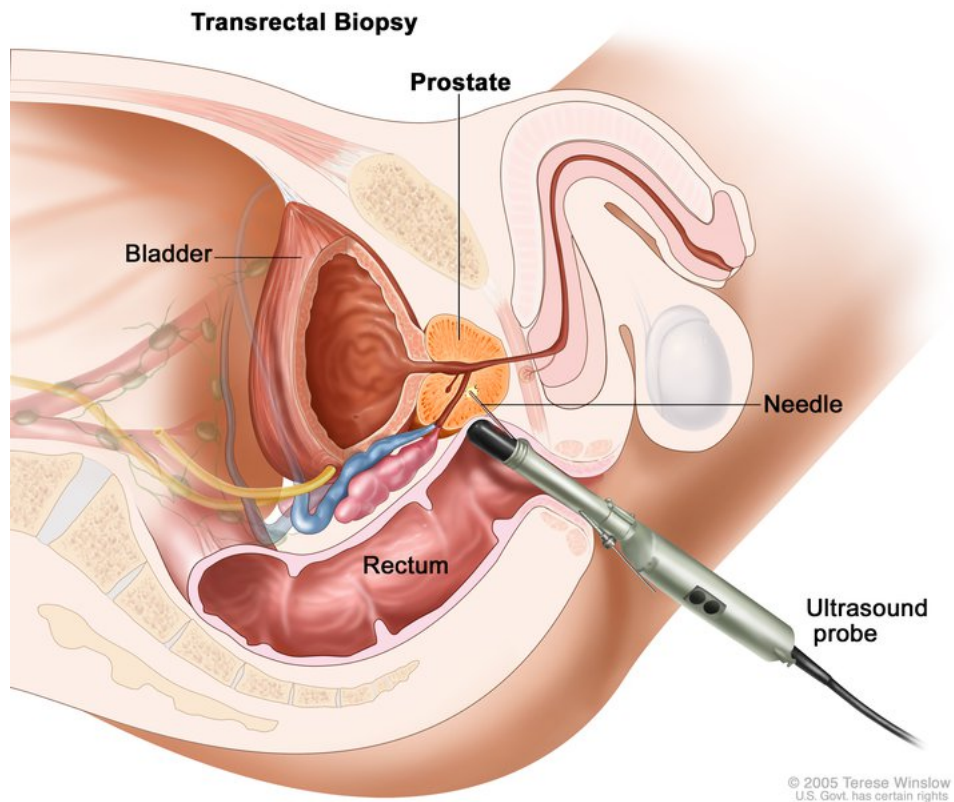


**Figure 8** – The transrectal biopsy. The probe is placed in the rectum facing upward. The needle is guided with the ultrasounds to sample the prostate. Reproduced with permission from Terese Winslow ([terese@teresewinslow.com](mailto:terese@teresewinslow.com)), © 2005 Terese Winslow LLC, U.S. Govt. has certain rights. Drawing available at <https://visualsonline.cancer.gov/details.cfm?imageid=7225>.

clinically insignificant cancer (ISUP Gleason grade group 1) with a pooled sensitivity of 0.70 (0.59-0.80) and pooled specificity of 0.27 (0.19-0.37) which compared favorably to TRUS-guided systematic biopsy that presented a pooled sensitivity of 0.55 (0.25-0.83) and pooled specificity of 0.99 (0.81-1.00).

#### ***4.7.4 – The PI-RADS score***

The likelihood of detecting significant prostate cancer at mp-MRI is calculated based on a structured scale known as Prostate Imaging Reporting and Data System (PI-RADS™). The PI-RADS is a score that spans from 1 (clinically significant cancer is highly unlikely to be present) to 5 (clinically significant cancer is highly likely to be present), with 3 (the presence of clinically significant cancer is equivocal) used as a threshold for triggering further assessments (e.g., target biopsy). The PI-RADS has been validated and updated multiple times since its introduction(64,65), with the 2019 version(66) being the current in use. **(Figure 9)**

#### ***4.7.5 – Evidences supporting mp-MRI target biopsy***

The superiority of mp-MRI-guided target biopsy over the conventional TRUS-guided systematic biopsy was established in three prospective multi-center trials, which compared the two techniques in patients who had never received a prostate biopsy before (biopsy naïve). The Prostate Evaluation for Clinically Important Disease: Sampling Using Image-guidance Or Not? (PRECISION) trial(67) randomized 500 biopsy-naïve patients to mp-MRI-guided target biopsy only vs. TRUS-guided systematic biopsy. It showed +12% higher rate of detection for ISUP grade 2-5 prostate cancers in the mp-MRI arm (detection ratio 1.46). The Assessment of Prostate MRI Before Prostate Biopsies (MRI-FIRST) trial(68) enrolled 251 biopsy-naïve patients who underwent TRUS-guided systematic biopsy and MRI-target biopsy. The two samplings were performed by different operators, where the operator performing the systematic biopsy was blinded to the MRI-findings. The mp-MRI target biopsy showed +4.8% detection rate of ISUP grade 3-5 prostate cancers (detection ratio: 1.32) as compared to systematic sampling. The Met Prostaat MRI Meer Mans (4M) trial(69) enrolled 626 biopsy-naïve patients. All patients received TRUS-guided systematic biopsy, and those with a positive mp-MRI (PI-RADS score of 3-5) underwent additional in-bore MRI-target biopsy (51%). The rate of

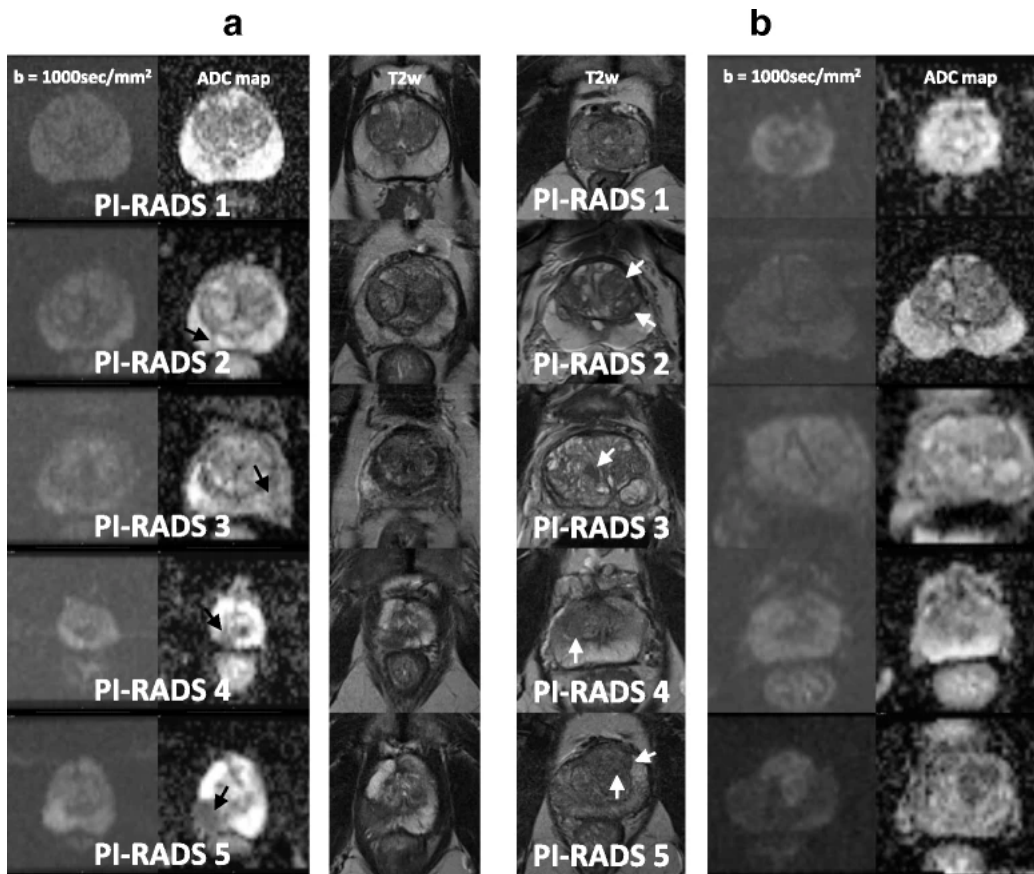


**Figure 9** – Radiological representation of the PI-RADS score according to MRI appearance in Apparent diffusion coefficient (ADC) and T2-weighted acquisitions. Reproduced from Philipp Steiger *et al*, “Prostate MRI based on PI-RADS version 2: how we review and report”, *Cancer Imaging*, Copyright © 2016, Steiger and Thoeny. (the original article is distributed under the terms of the Creative Commons CC-BY 4.0 license).



detection was +2% higher in those patients receiving additional mp-MRI-guided target biopsy for ISUP grade 2-5 prostate cancers, but similar for ISUP grade 3-5. The superiority of mp-MRI-guided target biopsy appears even stronger in the repeated biopsy setting. Here, the Target Biopsy Techniques Based on Magnetic Resonance Imaging in the Diagnosis of Prostate Cancer in Patients with Prior Negative Biopsies (FUTURE) randomized trial(70) showed that mp-MRI-guided target biopsy detected significantly more ISUP grade 2-5 cancers than TRUS-guided systematic biopsy (+18%, detection ratio: 2.1). According to those evidences, the EAU recommended the use of mp-MRI in the initial assessment of prostate cancer(71). For all patients with suspected prostate cancer, either biopsy naïve or after previous negative biopsy, the mp-MRI should be recommended, especially if not previously performed. In case of positive findings at the mp-MRI (PI-RADS 3-5), biopsy naïve patients should receive mp-MRI-guided target biopsy plus systematic sampling. Patients with previously negative biopsies should receive only mp-MRI-guided target biopsy, while avoiding systematic sampling. In case of negative findings at the mp-MRI (PI-RADS 1-2), biopsy naïve patients with low suspicion of prostate cancer (e.g. PSA density < 0.15 ng/mL) can avoid biopsy. Patients with previously negative prostate biopsy, but high clinical suspicion of prostate cancer, can repeat the systematic sampling. These recommendations were based on the results of the three aforementioned prospective trials and on the Cochrane meta-analyses(63) which included 18 studies on this topic. Accordingly, when the mp-MRI-guided target biopsy is added to systematic sampling in biopsy naïve patients, the number of ISUP grade 2-5 and ISUP grade 3-5 prostate cancers increase by approximately 20% and 30%, respectively. When the mp-MRI-guided target biopsy is added to systematic sampling in the repeat-biopsy setting, the number of ISUP grade 2-5 and ISUP grade 3-5 prostate cancers increases by approximately 40% and 50%, respectively. Conversely, when the systematic biopsy is omitted, ISUP grade 2-5 and ISUP grade 3-5 prostate cancer would be missed in approximately 16% and 18%, in biopsy-naïve patients, and in approximately 10% and 9% in the repeat-biopsy setting(72). Taken together, prostate biopsy should be recommended to patients based on PSA levels and kinetic, digital rectal examination and mp-MRI findings. Finally, age, potential co-morbidity and therapeutic consequences should also be considered and discussed beforehand, even in patients with clear indication for prostate biopsy(73).

#### ***4.7.6 – Biomarkers for initial diagnosis***

Blood and urine biomarkers have been largely investigated as potential predictors of prostate cancer, especially to avoid repeated biopsies. Commercially available tests rely on urine, blood or prostatic tissue from initial biopsy to estimate the probability of harboring prostate cancer. The biomarker kits that have reached the highest scientific interest are the Progens-PCA3(74) and the SelectMDX DRE(75) for urine samples, the serum four kallikrein (4K) score test(76) and Prostate Health Index (PHI)(77) test for blood samples, and the ConfirmMDx(78) for prostatic tissue samples. Nevertheless, no strong evidence supports the use of these biomarkers in clinical practice. For this reason, none of them is recommended by urological guidelines.

### ***4.8 – Conservative treatments***

#### ***4.8.1 – Expected survival in prostate cancer patients***

The life expectancy of more than 10 years is key before considering any active treatment in men with prostate cancer. Survival data on patients with prostate cancer who did not undergo active treatment show that cancer-specific survival rates at 10, 15, and 20 years are 82-87%, 58-80%, and 32-57%, respectively(79–84). The heterogeneity of these results is mainly related to different inclusion criteria among studies, including some released in the pre-PSA era. Nowadays, the majority of newly-diagnosed prostate cancer is detected in localized forms and mainly with ISUP grade groups 1-2. This screening effect has brought the mortality from these indolent forms of disease as low as 7% at 15 years(85). Thus, conservative management represents the best option to avoid invasive treatment-related morbidity and mortality in patients with a life expectancy lower than 10-year or in patients with a longer life expectancy that want to delay the treatment-related side effects, without impairing long-term survival. There are two distinct strategies of conservative management: i) watchful waiting; ii) active surveillance.

#### ***4.8.2 - Watchful waiting***

This option is reserved for men who are deemed unsuitable for curative treatments. Indeed, the reduced life expectancy dilutes any survival benefit derived from active treatments exposing the patients only to the side effects of the proposed cure. These patients are simply watched until they developed symptoms of the disease, and then are

treated with palliative intent, according to their symptoms, in order to maintain a reasonable quality of life. Three large prospective phase three studies have compared watchful waiting with active treatments in patients with prostate cancer. The Sweden SPCG-4 study(57) was conducted in the pre-PSA era, and it randomized 695 men to either watchful waiting or radical prostatectomy. The study found a benefit in favour of radical prostatectomy over watchful waiting only apparent after 10 years of follow-up supporting the conclusion that watchful waiting should be recommended in those patients with shorter life expectancy. Similarly, the PIVOT trial(86) compared radical prostatectomy and watchful waiting in 731 men with prostate cancer, but it was conducted in the early PSA era. Differently from the SPCG-4, it found little-to-no benefit for radical prostatectomy over watchful waiting after more than 15 years from randomization (median follow-up 18.6 years). The Veteran's Administration Cooperative Urological Research Group [VACURG] study(87) was the smallest among the three trials. The study randomized 111 men to either radical prostatectomy or watchful waiting. It was conducted in the pre-PSA era, and found no survival benefit for radical prostatectomy over watchful waiting, after 15 years of observation. The results of those three large prospective trials were pooled together in a meta-analysis conducted by Cochrane(88). Results showed that radical prostatectomy was associated with lower overall mortality (Hazard ratio: 0.79; 95% confidence interval: 0.70–0.90) and lower cancer-specific mortality (0.57; 0.44-0.73) compared to watchful waiting, within a time span of 29 years of follow-up. Radical prostatectomy was also associated with lower risk of progression (0.43; 0.35-0.54) and lower risk of metastatic disease (0.56; 0.46-0.70). However, radical prostatectomy was associated with higher rates of urinary incontinence (relative risk: 3.97; 95% confidence interval 2.34-6.74) and erectile dysfunction (2.67; 1.63-4.38) compared to no active treatment. In conclusion, the benefits derived from invasive treatment require more than 10 years from the procedure to emerge. Therefore, patients with a life expectancy below this threshold should be referred to watchful waiting.

#### ***4.8.3 – Active surveillance***

This option can be adopted in patients with life expectancy above 10 years, where the features of the tumor allow for a safe delay of any invasive treatment. Specifically, patients are actively followed in order to choose the correct timing of active intervention,

if needed. Patients under active surveillance do receive active observation with repeated prostatic biopsies, PSA tests, clinical examinations, and MRI imaging to monitor the natural history of the disease. Curative treatments are triggered when the tumor reaches pre-defined characteristics that are indicative of a potentially life-threatening condition, but still potentially curable, while considering individual life expectancy. There is still no formal randomized controlled trial comparing active surveillance to immediate curative treatments. Several cohort-based studies investigated active surveillance in patients with localized prostate cancer. A recent meta-analysis(89) of these studies showed that around one out of three men on active surveillance were reclassified during follow-up and the majority of these patients received active treatment thereafter. The largest study included in this meta-analysis enrolled 1298 men with very-low risk prostate cancer from the Johns Hopkins hospital (90). Very low-risk disease was defined as clinical stage T1c, PSA density less than 0.15 ng/mL, biopsy ISUP grade group 1, two or fewer positive biopsy cores, and a maximum of 50% involvement of any biopsy core with cancer. The surveillance protocol included PSA measurement and digital rectal examination every six months, as well as an annual prostate biopsy. Curative intervention was recommended in case of disease reclassification, defined as biopsy findings no longer meeting the inclusion criteria. The median follow-up of the cohort was 5 years. The cumulative incidence of grade reclassification was 26% at 10 years and 31% at 15 years. Cumulative incidence of curative intervention was 50% at 10 years and 57% at 15 years. Overall, these data support the use of active surveillance in patients with localized prostate cancer, with the aim of postponing active treatments only at the time of disease progression, if it occurs.

#### ***4.8.4 – The Protec-T trial***

The only randomized phase three study comparing active treatments with active monitoring in the post-PSA era is the Protec-T trial(59,91). The three treatment arms were radical prostatectomy, external beam radiotherapy, and active monitoring with the latter being halfway between active surveillance and watchful waiting. The active monitoring consisted of a systematic repeat biopsy for patients with a PSA rise higher than 50% in 12 months. Fifty-six percent of patients had D'Amico low-risk disease. Of those, 90% had PSA < 10 ng/mL, 77% ISUP grade 1 (20% ISUP grade 2-3), and 76% T1c. The

remaining patients presented tumors classified as D'Amico intermediate-risk disease. At ten-year follow-up, patients treated with active monitoring and invasive treatments showed similar cancer-specific survival (98.8% vs 99%, respectively) and overall survival. Active monitoring was associated with higher metastatic progression (6% vs 2.6%). Functional outcomes examined in the trial were urinary continence, bowel function and erectile function(91). Patients in the radical prostatectomy arm presented worse sexual function and urinary continence in the first six months as compared with the other two arms. Although there was some recovery, functional outcomes remained worse in the prostatectomy arm thereafter. Patients in the radiotherapy arm reported the worst outcomes for bowel function in the first six months. Sexual and urinary function declined gradually in the active-monitoring group. No significant differences were observed among the three trial cohorts in terms of anxiety, depression, or general health-related or cancer-related quality of life indicators. Data from this important trial emphasized, even more, the importance of treatment tailoring in patients with localized prostate cancer. Active treatments should be reserved for patients with clinically significant disease, acknowledging that survival benefits may require more than ten years to outweigh harms, while treatment-related side effects will impact on patient's life immediately.

#### ***4.9 – Active treatments***

##### ***4.9.1 – The EAU risk stratification for active treatment***

It is considered an active treatment any instrumental or pharmacological agent that aims to neutralize the growth of prostate cancer. Among the numerous options, radical prostatectomy, radiotherapy, and hormonal therapy represent the cornerstones of prostate cancer treatment. Other treatments, which are still experimental and mainly recommended for localized forms of cancer, include cryotherapy, high-intensity focused ultrasound, photodynamic therapy, electroporation, and focal radiotherapy. Importantly, different treatment modalities can be combined in a multi-modal approach to reach a curative intent, especially when dealing with aggressive forms of the disease. To this end, EAU guidelines recommend a risk-based approach to select the best treatment during patient counselling(71). The EAU risk group classification derived from the D'Amico classifications and it recognizes three groups for localized forms (**Figure 10**):

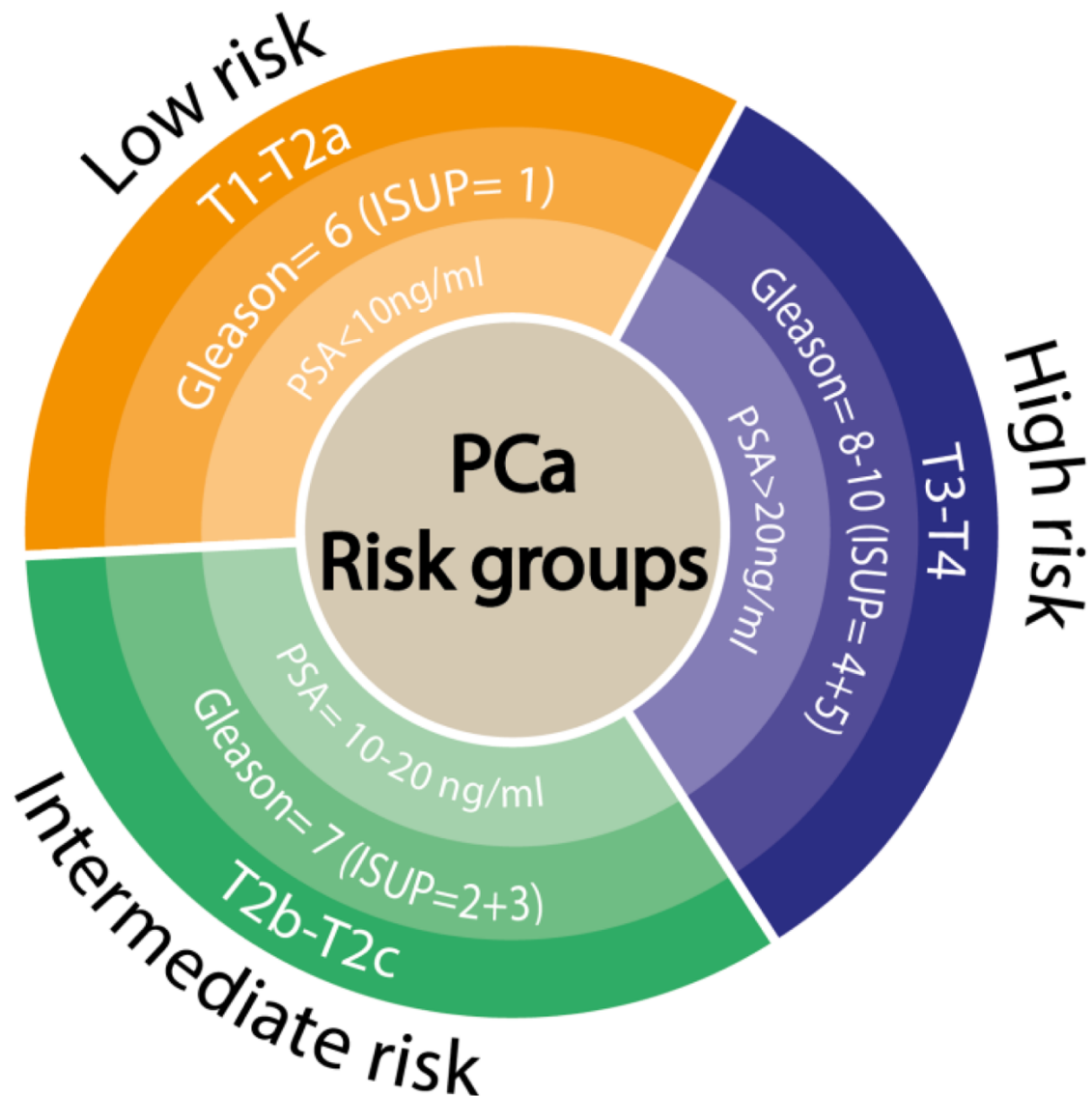


**Figure 10** – Prostate cancer risk groups classification for localized tumors, referring to biochemical recurrence according to European Association of Urology (EAU) Guidelines (2019). Reproduced from Munteanu et al., “MiRNA-Based Inspired Approach in Diagnosis of Prostate Cancer”, *Medicina* 2020, 56(2), 94 (the original article is distributed under the terms of the Creative Commons CC-BY 4.0 license).

- Low Risk: PSA < 10 ng/mL, ISUP grade group 1, and cT1-2a;
- Intermediate Risk: PSA 10-20 ng/mL, or ISUP grade group 2-3, or cT2b;
- High Risk: PSA > 20 ng/mL, or ISUP grade group 4-5, or cT2c;

and one group for locally advanced forms:

- Locally advanced: any PSA, any ISUP grade group, cT3-4 or cN+

#### ***4.9.2 – Treatment for Low-risk tumors***

In low-risk diseases, overtreatment is the main issue when choosing the best therapeutic approach. In this group, active surveillance represents the recommended treatment option since it successfully balances oncological safety and treatment side effects. Alternative options to active surveillance may include low-dose-rate brachytherapy or active treatments such as radical prostatectomy and external beam radiotherapy, for those patients who accept a trade-off between toxicity and prevention of disease progression. Conversely, hormonal therapy does not represent a valid alternative in these patients due to the lack of survival benefit over observation(92). As said, active surveillance represents the standard of care in low-risk patients although no randomized data has yet been published in support of this treatment modality. Cohort studies on active surveillance adopted different definitions of low-risk disease, as well as many surveillance strategies. Therefore, comparison among results is challenging using the available literature. Based on the results of a systematic review and meta-analysis(93) of these studies, the multi-society panel of the EAU-EANM-ESTRO-ESUR-SIOG Prostate Cancer Guideline developed a consensus statement to outline the best active surveillance strategy in low-risk disease. Based on the evidence of the DETECTIVE Study(94), the panel identified ISUP grade group 1, clinical stage cT1c or cT2a, PSA < 10 ng/mL and PSA-Density < 0.15 ng/mL/cc as the most commonly adopted criteria for active surveillance(95). The panel also examined the importance of mp-MRI imaging in patients under active surveillance. Here, the results of The Active Surveillance Magnetic Resonance Imaging Study (ASIST)(96) showed that the use of MRI may decrease the risk of failure of surveillance (19% vs. 35%,  $p = 0.017$ ) compared to no use, and it decreased also the number of patients progressing to ISUP grade group >2 (9.9% vs. 23%,  $p = 0.048$ ) during observation. The DETECTIVE panel(94) reached the consensus that MRI should be offered in patients eligible for active surveillance to reduce the risk of progression and

failure during observation. Whole gland treatments (cryotherapy, high-intensity focused ultrasound, etc.) or focal treatments were examined as alternative treatment options for low-risk tumors. For those, the panel suggested that given the lack of strong supporting evidence, they can be advised but only within a clinical trial setting or well-designed prospective cohort study.

#### ***4.9.3 – Treatment for Intermediate-risk tumors***

Active treatments, namely radical prostatectomy or external beam radiotherapy in combination with short-term androgen deprivation therapy (ADT) (4–6 months), are the recommended treatment options in patients with intermediate-risk disease, based on randomized trials(59). Active surveillance has been examined in intermediate-risk patients, who are motivated to avoid radical prostatectomy or radiotherapy as initial treatment options. The DETECTIVE Study consensus panel(93) recommended active surveillance in patients with intermediate-risk disease if they met specific characteristics such as low-volume ISUP grade group 2 tumors (defined as < 3 positive cores and < 50% core involvement by cancer) or another single element of the EAU intermediate-risk category (PSA 10-20 or cT2b stage) with the exception of ISUP 3 disease (i.e., favorable intermediate-risk disease). Radical prostatectomy is a valid treatment option in intermediate-risk patients as proved by randomized data from the SPCG-4(57), PIVOT(86) and Protec-T(59) trials. Nevertheless, survival benefit derived from radical prostatectomy was evident only after 10 years from randomization in all trials, thus precluding this option to patients with shorter life expectancy. Given the low, albeit non-negligible risk of lymph node metastases in intermediate-risk patients (3.7–20.1%)(97), extended pelvic lymph node dissection (ePLND) should be performed according to clinical risk tools(98). External beam radiotherapy (EBRT) is another valid option for intermediate-risk disease(99–103). Intensity-modulated RT (IMRT)(104) or volumetric arc radiation therapy (VMAT) with image-guided RT (IGRT) are two common techniques of EBRT(105). Patients suitable for hormonal therapy can receive IMRT/VMAT (with a dose of 76–78 Gy, or moderate hypofractionation with 20 fractions at 60 Gy each in 4 weeks, or 28 fractions at 70 Gy each in 6 weeks), with combined short-term ADT (4–6 months)(106–108). Adjuvant ADT seemed to be better than neoadjuvant or concurrent ADT(109), although trials testing EBRT combined with different ADT



protocols were heterogeneous in terms of patient characteristics, exact scheduling, and hormonal medications. Thus, ADT is still recommended either as neoadjuvant, concurrent or adjuvant to radiation. For patients who are ineligible to ADT (e.g., cardiac or other co-morbidities) or unwilling to accept ADT (e.g., to preserve their sexual function), the recommended treatment is IMRT/VMAT (76–78 Gy) or a combination of IMRT/VMAT and brachytherapy. Low-dose(110) or high-dose(111) brachytherapy boost can be offered in combination with IMRT/VMAT plus IGRT for intermediate-risk patients. Here, combination with short-term ADT (4–6 months) is also advised by the EAU guidelines(112). The urinary function should be assessed in all patients eligible for low-dose and high-dose brachytherapy boost since these treatments are associated with an increased risk of prolonged (5 years) genitourinary toxicity, as compared to EBRT alone(113). Whole-gland and focal treatments have been tested in patients with intermediate-risk prostate cancer with positive results(114). However, data supporting these treatment modalities came from uncontrolled case series and retrospective studies. Thus, the use of these alternative treatment modalities should be limited to clinical trials(115). Lastly, hormonal therapy was also tested as monotherapy in patients with intermediate-risk prostate cancer. Results were extracted from the EORTC 30891 trial, which compared immediate vs. deferred ADT in patients with T<sub>0-4</sub>N<sub>0-2</sub>M<sub>0</sub> disease. Immediate ADT was not associated with any survival benefit, giving the conclusion that hormonal therapy cannot be recommended in intermediate-risk patients, even when patients are not eligible for radical treatments(97).

#### ***4.9.4 – Treatment for High-risk tumors***

Radical prostatectomy with ePLND or EBRT with long-course ADT (at least 2-3 years) are the recommended treatment options in patients with high-risk prostate cancer. These patients should be advised preoperatively that radical prostatectomy may be part of multi-modal management, which includes EBRT and/or hormonal or systemic treatments. In this setting, surgery has been associated with long-term survival in retrospective series, with cancer-specific survival over 60% at 15 years(116,117). Hormonal therapy and/or EBRT should be considered after radical prostatectomy in case of documented or high risk of cancer progression (118,119). For high-risk patients, EBRT alone is not sufficient to achieve long-term cancer control. Numerous trials showed that long-term adjuvant

ADT is necessary to consolidate the effect of local radiation(102). Long-term adjuvant ADT is also superior to short-term neoadjuvant ADT(101,120). Given the significant risk of lymph node spread in high-risk disease, the prophylactic irradiation of the pelvis has been largely discussed. In this context, a well-designed albeit small randomized trial compared the effect of prostate-only vs. whole pelvic radiotherapy in patients with cN0, high-risk prostate cancer. Metastasis-free survival (95.9% vs. 89.2%, hazard ratio: 0.35, p = 0.01) and disease-free survival (89.5% vs.77.2%, p = 0.02) were in favour of whole pelvic radiotherapy. Nevertheless, whole pelvic radiotherapy was also associated with higher rate of late genitourinary toxicity (grade > 2, 17.7% vs. 7.5%, p = 0.02)(121,122). Brachytherapy boost can be added to EBRT plus ADT.

#### ***4.10 – Radical Prostatectomy***

##### ***4.10.1 – From open to robot-assisted radical prostatectomy***

The goal of radical prostatectomy is the eradication of cancer, while preserving pelvic organ function, mainly the urinary and sexual functions. The aim of the operation is to remove the prostate gland along with its capsule and the seminal vesicles, with or without the preservation of the neurovascular bundle, followed by vesico-urethral anastomosis. The technique of radical prostatectomy has evolved from the initial open procedure described by Hugh Hampton Young in 1904, who was credited for the first radical prostatectomy. The Young's technique of radical prostatectomy was via the perineum, but suffered from lack of access to the pelvic lymph nodes. Only in 1982, Patrick Wash described a new technique of radical prostatectomy via the retropubic or suprapubic space(123). This technique allowed for an easy access to the pelvic lymph nodes while removing the prostate. The presentation of this technique came along with the anatomical description of the neurovascular bundles, and the preservation of the cavernosal nerves during radical prostatectomy to allow a fast recovery of sexual function after the operation. Since its introduction, radical retropubic prostatectomy has become the standard of care for the surgical treatment of prostate cancer. Over the last forty years, this approach has evolved with the intent of reducing surgical morbidity, while improving functional outcomes, such as urinary continence and sexual function. In 1997, the first series of minimally invasive video-assisted laparoscopic radical prostatectomy was published by Schuessler(124), and subsequently by Guillonneau(125). Both techniques

followed the retropubic principles of Walsh. In 2002, Binder(126) reported the initial experience with the da Vinci Surgical System® for robot-assisted radical prostatectomy (RARP). This technology merged the minimally-invasive advantages of laparoscopic radical prostatectomy with improved surgeon ergonomics and easier suture reconstruction of the vesico-urethral anastomosis. Nowadays, RARP has overcome open radical prostatectomy as the most popular surgical approach for the treatment of prostate cancer, whenever both options are available(127). Its popularity has been facilitated by widespread of teaching-programs and modular training that accelerate the learning curve(128). Additionally, RARP proved non-inferiority to open radical prostatectomy in terms of oncological and surgical outcomes. Here, the strongest evidence came from a randomized controlled trial, which compared open radical prostatectomy with RARP in terms of early and late functional outcomes, as well as on cancer control outcomes(116). The trial recruited and randomized 326 men to either open or robotic prostatectomy. The results of this trial have been updated at 24 months(129). While the two approaches showed comparable results for oncological and functional (early and late) outcomes, RARP seemed superior in terms of reduced in-hospital stay and blood loss.

#### ***4.10.2 – Surgical techniques for robot-assisted radical prostatectomy***

Among several variations of the surgical technique of RARP, the extraperitoneal and the transperitoneal approaches represent the two main options. The extraperitoneal approach begins with the development of the space between the rectus abdominis and its posterior sheet. Then, the posterior sheet is incised to enter the extraperitoneal space, where a balloon is expanded to develop the space of Retzius(130). On the contrary, for the transperitoneal approach, the ports are placed in the peritoneal cavity. The transperitoneal approach can be further divided into two variations: the transperitoneal anterior and posterior routes. In the posterior route(131), a peritoneotomy is performed at the lower peritoneal fold; then the vasa deferens are identified and transected, the seminal vesicles are dissected free, and the prostatic base is demarked. The dissection is carried on with the incision of the Denonvilliers fascia and following the posterior aspect of the prostate from its base to the apex. Subsequently, the dissection moves anteriorly starting from the incision of the parietal peritoneum, which releases the bladder. Then, the Retzius space is developed, by clearing the fatty tissue around the prostate. The prostate is detached

from the bladder while trying to preserve the bladder neck. At this point, being the prostate detached from the incised Denonvilliers fascia, it is dissected on its lateral aspects until the apex. Finally, the prostatic pedicles and the dorsal venous complex are ligated and the urethra is transected. In the anterior route(132), the dissection starts with the incision of the parietal peritoneum lateral to the lateral umbilical ligaments. The bladder is released and the space of Retzius is developed. The bladder neck can be either preserved or sacrificed, then the dissection moves posteriorly. Here, the retrotrigonal space is developed to identify the seminal vesicles and the vasa deferentia. The Denonvilliers fascia is then incised and the remaining dissection is carried on following the same steps as those of the posterior route. For both routes, the preservation of the neurovascular bundles can be achieved in toto (intrafascial dissection), partly (interfascial dissection), or dissected completely (extra-fascial dissection)(133). Following the removal of the prostate, the continuity of the lower urinary tract is reconstructed. To achieve so, the bladder neck and the membranous urethra are joined together. The aim is to create a tension-free, watertight, precisely aligned and stricture-free anastomosis, that preserves the integrity of the intrinsic sphincter mechanism. For the bladder-urethral anastomosis, open and robot-assisted approaches have different techniques. The open approach uses a direct technique. Six interrupted sutures are placed circumferentially to construct a primary end-to-end inter-mucosal anastomosis between the bladder neck and the membranous urethra. For the robotic approach, the trend has been oriented towards a unidirectional barbed suture technique(134) using a continuous suturing(135). However, many other techniques for the vesico-urethral anastomosis have been described and data comparing these techniques did not show a clear superiority of one technique over the others.

#### ***4.11 – Pelvic lymph node dissection (PLND)***

The regional lymph nodes represent the most common site of initial dissemination in prostate cancer(136,137). Indeed, more than 30% of men with high-risk prostate cancer treated with radical prostatectomy and PLND may harbor lymph node metastases(138). The number of lymph node metastases and the lymph node metastatic burden depends on tumor characteristics, but also on the extent of PLND(139–146). Accordingly, the more extended the template of PLND, the higher the probability to detect lymph node

metastases, given the fact that disease spreading does not follow a predefined pathway (147). Thus, it is not uncommon that patients may harbor micrometastases in the distant (common iliac, sacral) lymph nodes, whereas more proximal (obturator, external iliac) nodes are free from the disease(148). This assumption raises the question of defining which is the most correct PLND template for the patient with intermediate- or high-risk prostate cancer. To date, Authors do not agree with the anatomical definition of limited and extended PLND. Touijer et al.(149) considered limited PLND the removal of external iliac nodes only, while Lestingi et al.(150) included only obturator nodes in the limited PLND template. Templates of extended PLND differ even more in terms of definitions. Some authors include in the definition of extended PLND the obturator, external iliac, and hypogastric nodes(142,149). Others include the pre-sacral nodes(141,151). Finally, other Authors include in the definition of extended PLND the common iliac nodes, at least up to the ureteric crossing(143,152). With super extended PLND Mattei et al.(153) included the removal of lymph nodes of the common iliac vessels, up to the aortic and caval bifurcation. Although removing the pelvic lymph node may provide useful staging and prognostic information, no clear survival benefit seems to emerge among patients who were treated with limited, extended or no PLND(154,155). Two randomized controlled trials failed to show a benefit of an extended approach vs. a limited PLND on early oncologic outcomes. In a single-center trial that randomized 1440 patients to limited (external iliac nodes) or extended (external iliac, obturator fossa and hypogastric nodes) PLND, Touijer et al.(149) found no differences in terms of biochemical recurrence between the two groups (hazard ratio 1.04, 95% confidence interval 0.93-1.15;  $p = 0.5$ ). Another single-center trial randomized 300 patients with intermediate or high-risk prostate cancer to limited (obturator nodes) or extended (obturator, external iliac, internal iliac, common iliac, and presacral nodes) PLNDs. The trial found no biochemical recurrence-free survival (hazard ratio 0.91, 95% confidence interval 0.63-1.32;  $p = 0.6$ ) and metastasis-free survival (hazard ratio 0.57, 95% confidence interval 0.17-1.8;  $p = 0.3$ ) differences among the two groups. Although PLND offers the most accurate staging in patients with localized prostate cancer, it is not devoid of complications, and these complications can significantly increase the morbidity of radical prostatectomy. A recent comprehensive systematic review and meta-analysis(156) summarized the impact of PLND on perioperative morbidity in patients receiving radical prostatectomy. A selection

of 84 studies including over 28 000 patients was analyzed. The authors classified the complications into two groups, namely intraoperative and post-operative complications. Complications were also classified into three categories according to the likelihood of being associated with PLND (strongly PLND-related, likely PLND-related, unlikely PLND-related). Among intraoperative complications, external iliac artery injury, internal iliac vein injury, and obturator nerve injury were labeled as strongly PLND-related; bleeding and ureteric injury were labeled as likely PLND-related; subcutaneous emphysema, bladder injury, small bowel and colon injury, inferior epigastric vessel injury, and rectal injury were labeled as unlikely PLND-related. Among the postoperative complications, lymphatic fistula, chronic lymphedema, lymphorrhagia, and lymphocele were labeled as strongly PLND-related; pelvic hematoma, infected pelvic collection, muscle vein thrombosis, obturator nerve palsy, edema/swelling of the groin, scrotum, penis, lower extremities, pulmonary thromboembolism, and deep vein thrombosis were labeled as likely PLND-related; finally, wound complications, infective complications, and complications involving the genitourinary, gastrointestinal, cardio-vascular, and pulmonary systems were labeled as unlikely PLND-related. The Authors found that 1.8% of patients presented one or more intraoperative complications related to PLND. Postoperative complications were more common, being present in 14.1% of treated patients, and the most reported postoperative complication was lymphocele (90.6%). The definition of the template of PLND was provided by the Authors, who classified limited PLND as including obturator nodes only, standard PLND as including obturator and external iliac nodes, extended PLND as including obturator, external, and internal iliac nodes, super-extended PLND as including the template of extended PLND plus common iliac, presacral, and/or other nodes. According with these definitions, limited PLND or standard PLND were associated with lower risk of any intraoperative complication (risk ratio: 0.55;  $p = 0.01$ ), postoperative complications strongly related to PLND (risk ratio: 0.46;  $p \leq 0.00001$ ), lymphocele formation (risk ratio: 0.52;  $p = 0.0003$ ), and thromboembolic events (risk ratio: 0.59;  $p = 0.008$ ), as compared to extended/super-extended PLND. The extent of PLND was an independent predictor of lymphocele formation (risk ratio: 1.77;  $p < 0.00001$ ). Of note, this meta-analysis did not include the only two randomized trials on PLND. Comparative data on perioperative complications after limited and extended PLND were available only in one randomized trial(149). Here,

grade 2 and 3 complications were similar among templates (7.3% for limited vs. 6.4% for extended PLND).

#### ***4.12 – How to select candidates for PLND***

##### ***4.12.1 – Prevalence of LNI according with the D’Amico risk group classification***

Real-world data showed that the prevalence of lymph node metastases in patients with D’Amico low-risk prostate cancer is between 0.5 and 0.7%(157–159). The risk of lymph node metastases changes when D’Amico intermediate-risk patients are considered. Here, the risk of having positive nodes is between 3.7-20.1%(97). Lastly, D’Amico high-risk patients report the highest risk of lymph node invasion (LNI) ranging from 10% to 57%(160) or even 100% according to sub-categories of this group(161). Given those figures, the EAU guidelines do not recommend PLND in low-risk patients when radical prostatectomy is performed. Conversely, ePLND is recommended in D’Amico high-risk patients to properly assess the tumor staging. The intermediate-risk group represents the “grey” category, where the risk of LNI does not always justify the aggressiveness of ePLND. For this group of patients, the use of non-invasive diagnostic modalities has been investigated to facilitate the decision to perform or avoid ePLND.

##### ***4.12.2 – Predicting ability of different imaging tools***

Conventional imaging modalities such as abdominal CT scan and T1-T2 weighted MRI scan showed low diagnostic performances. These diagnostic tools assess the status of the regional lymph nodes based on the diameter and morphology of the nodes. However, the size of non-metastatic lymph nodes may vary considerably, overlapping the size of metastatic lymph nodes. This said, pooled data quantified the sensitivity of CT and MRI for the detection of lymph node metastases as low as 40%(162,163). In particular, the ability to detect microscopic LNI by CT scan was < 1% in patients with ISUP grade group < 4, PSA < 20 ng/mL, or localised disease(164–166). Given these figures, the EAU guidelines give no role to CT-scan and MRI-scan for the preoperative assessment of lymph node metastases in patients with intermediate-risk prostate cancer. Whole-body positron emission tomography/CT (PET/CT) with [(11)C]- and [(18)F]-labeled choline has been proposed as an alternative to conventional imaging modalities for the staging of prostate cancer. In a meta-analysis of 609 patients, (11)C- and (18)F-choline PET/CT

showed a pooled sensitivity and specificity of 62% (95% confidence interval: 51-66%) and 92% (89-94%) for pelvic lymph node metastases, respectively(167). However, the predictive ability of choline PET/CT is heavily affected by the characteristic of the primary tumor, being reliable for locally advanced disease, but losing sensibility in localized tumors. In a prospective trial including 75 patients with intermediate-risk disease, the sensitivity of (11)C-choline PET/CT was only 8.2% at region-based analysis and 18.9% at patient-based analysis(168). These figures cannot justify any clinical use of choline PET/CT in intermediate-risk disease. Lately, prostate-specific membrane antigen (PSMA) positron-emission tomography (PET)/CT emerged as a possible game changer in prostate cancer management. Its use has been tested in primary prostate cancer staging. A prospective, multi-centre study addressed the use of 68Ga-PSMA PET/CT in patients with newly diagnosed prostate cancer. The per-patient-based sensitivity and specificity were 41.5% (26.7-57.8) and 90.9% (79.3-96.6)(169). Similarly, another prospective multi-centre trial reported a sensitivity of 41.2% (19.4-66.5%) for the assessment of lymph node metastases with 18fluorine-labelled PSMA PET/CT scan in newly diagnosed prostate cancer(170). A review and meta-analysis including 37 articles evaluated the sensitivity and specificity of preoperative PSMA PET/CT in patients with prostate cancer receiving subsequent radical prostatectomy with ePLND. The per-patient-based sensitivity and specificity were 77% and 97%. The per-lesion-based sensitivity and specificity were 75% and 99%. These preliminary results suggest that PSMA-based PET/CT imaging cannot yet replace diagnostic extended PLND, but truly represents the most promising tool for this task. Until the reliability of PSMA-based PET/CT or other new potential alternatives will be confirmed, the decision to perform or avoid ePLND in prostate cancer is based on the risk of lymph node metastasis derived from clinical features. This risk is also known as risk of LNI, and it is calculated using preoperative tumor characteristics derived from physical examination, blood samples, and prostate biopsy.

#### ***4.12.3 – LNI predicting models***

Among the numerous risk-assessment tools, the EAU guidelines recommend the Roach formula, the Briganti nomogram, the Partin tables, and the MSKCC nomogram. Differently from other risk assessment tools, these four were validated in numerous



patient cohorts(171–174) confirming their predicting abilities to discriminate between patients in whom ePLND is recommended or in whom ePLND might be avoided. The Roach formula calculates the risk of LNI using the equation:  $LNI = 2/3(PSA) + (Gleason\ score - 6) \times 10$ , where PSA is the pre-treatment PSA value and Gleason score is derived from the diagnostic systematic biopsy. The Partin tables rely on a multivariable logistic regression, where known preoperative predictors such as PSA, Gleason score, and clinical T stage are used to calculate the risk of LNI. Finally, the Briganti and the MSKCC are two nomograms that rely on patient and tumor factors to elaborate the risk of LNI. Originally, these two nomograms were based on preoperative PSA, systematic biopsy Gleason score and clinical T stage to calculate the risk of LNI(175,176). In the last fifteen years, several updates of the two nomograms have incorporated new predictors increasing the accuracy of the models. Using dynamic statistical formulas, the MSKCC nomogram draws on data from more than 10,000 prostate cancer patients treated at the Memorial Sloan Kettering Cancer Center. Updated predictors include age, PSA, biopsy Gleason grade group, and clinical T stage. The MSKCC is constantly updated, and it is freely available on the MSKCC web-page(177,178). The first version of the Briganti nomogram was published in 2007 (**Figure 11**). It was generated from a cohort of 602 consecutive patients treated at a single Italian institution and it included only three predictors: PSA, clinical T stage, and biopsy Gleason score. In 2012, this version was updated (**Figure 12**) with the inclusion of another predictor: the percentage of positive cores at systematic biopsy(179). In 2017, the third updated version of Briganti nomogram (**Figure 13**) was released(180). Here, the number of predictors was increased to five, including PSA, clinical T stage, biopsy Gleason grade group, percentage of cores with highest-grade prostate cancer, and percentage of cores with lower-grade disease. All these nomograms and predicting models were developed in the pre-MRI era, and all were based on systematic random biopsy. For all of them, a risk of LNI over 5% could be used to select candidates for ePLND during radical prostatectomy. According to this threshold, the 2011 Briganti nomogram allows for sparing ePLND in more than 60% of men while missing LNI in only 1% of the population. Unfortunately, it is still sub-optimal for two main reasons: i) High but not perfect sensitivity: a certain number of nodal lesions are still missed using a 5% cut-off. ii) Low specificity: roughly 80% of men with LNI risk above

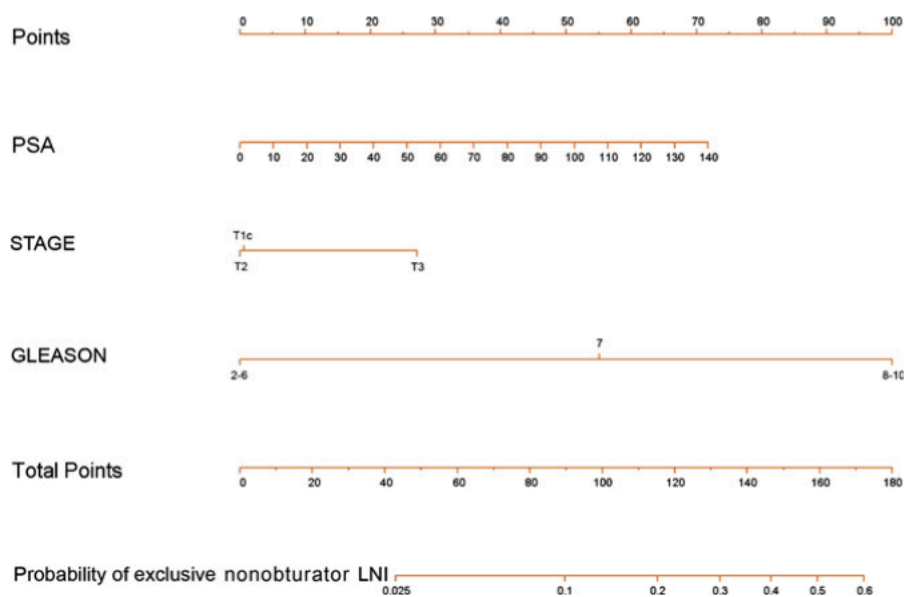


**Figure 11** – The first (2007) version of the Briganti nomogram. PSA = prostate specific antigen; Stage = clinical T stage at digital rectal examination; Gleason = Gleason score at systematic biopsy; (Reprinted from European Urology, Alberto Briganti et al., “A nomogram for staging of exclusive nonobturator lymph node metastases in men with localized prostate cancer”, ©2007, with permission from Elsevier).

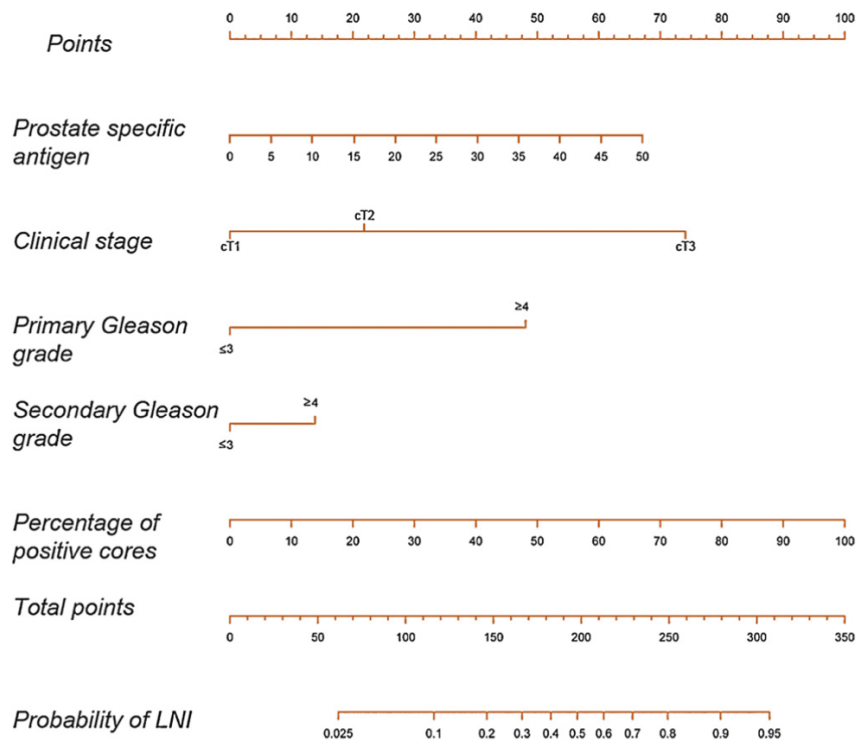


**Figure 12** – The revised (2012) version of the Briganti nomogram; (Reprinted from European Urology, Alberto Briganti et al., “Updated nomogram predicting lymph node invasion in patients with prostate cancer undergoing extended pelvic lymph node dissection: the essential importance of percentage of positive cores”, ©2012, with permission from Elsevier).

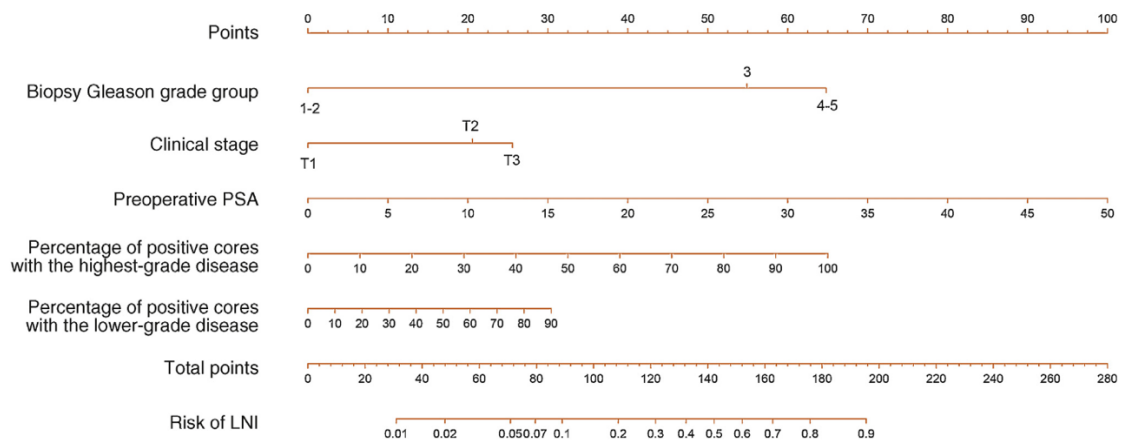


**Figure 13** – The 2017 version of the Briganti nomogram; (Reprinted from European Urology, Giorgio Gandaglia et al., “Development and Internal Validation of a Novel Model to Identify the Candidates for Extended Pelvic Lymph Node Dissection in Prostate Cancer”, ©2017, with permission from Elsevier).

the 5% cut-off are treated with ePLND without nodal metastases. The latter consideration is crucial since many men are still exposed to unnecessary ePLNDs, which is a time-consuming approach associated with possible complications. In more recent times, mp-MRI has become more and more preponderant in clinical practice. MRI may provide useful information on intraprostatic tumor extension and it may significantly increase the accuracy of prostate biopsy when guiding the biopsy sampling. Based on these premises, a new generation of predicting models has been designed incorporating mp-MRI in the preoperative workout of patients with localized disease. The 2019 version of Briganti nomogram (**Figure 14**) was the result of the integration of mp-MRI in the determination of LNI risk in patients eligible for radical prostatectomy(98). This new update was generated from a multi-institutional cohort of 497 patients with prostate cancer diagnosed via MRI-target biopsies and treated with radical prostatectomy plus ePLND. The model included preoperative PSA, MRI-derived clinical T stage, the maximum diameter of the index lesion at the mpMRI, Gleason grade group derived from mpMRI-target biopsy, and the percentage of clinically significant prostate cancer on concomitant systematic biopsy. According to this new nomogram, a risk up to 7% is acceptable to spare patients from ePLND, which would result in missing only 1.5% of patients with nodal invasion. Indeed, the 7% cut-off, derived from this MRI-based nomogram, was comparable with the 5% cut-off of the previous models designed in cohorts of patients diagnosed with systematic biopsy alone(181).

#### ***4.12.4 – DNA methylation and LNI prediction***

Abnormal gene expression is one of the hallmarks of cancer development and progression. Abnormal gene expression is not always an expression of changes in the nucleotide sequences of the DNA double-strand, but it can also be related to disturbances in epigenetic mechanisms. Indeed, the DNA structure and its encoding ability can be modified by post-replication modification of the DNA, and/or post-translational modification of proteins associated with the DNA. These epigenetic changes include aberrant DNA methylation (hypermethylation or hypomethylation), modifications of histones, chromatin remodeling and changes in gene expression caused by non-coding RNAs. Consequences of these epigenetic alterations may lead to genomic instability and

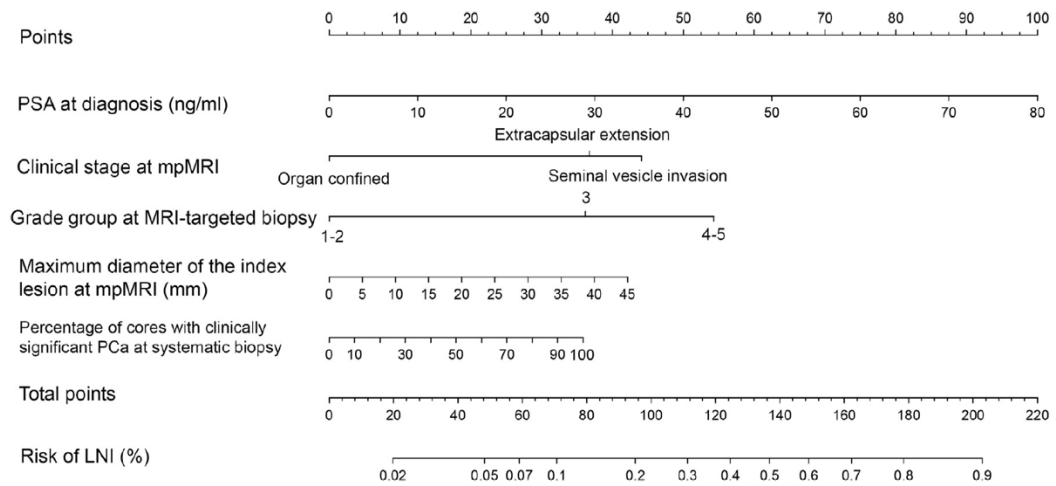


**Figure 14** – The 2019 version of the Briganti nomogram; (Reprinted from European Urology, Giorgio Gandaglia et al., “A Novel Nomogram to Identify Candidates for Extended Pelvic Lymph Node Dissection Among Patients with Clinically Localized Prostate Cancer Diagnosed with Magnetic Resonance Imaging-targeted and Systematic Biopsies”, ©2019, with permission from Elsevier).

inappropriate gene expression, which ultimately facilitates cancer initiation and progression(182,183). Indeed, DNA replication, recombination and repair are deeply controlled by DNA methylation. The methylation of the double strand of DNA occurs at the level of CpG dinucleotide sequences, where a methyl group is added to the 5'-carbon of the cytosine (**Figure 15**). Certain areas of the DNA, called CpG islands, are rich in CpG dinucleotide sequences. CpG islands extend from 200bp to several kilobases, and they are usually located near the promoters of highly expressed genes. These CpGs islands are common sites of impaired methylation in human tumors, including prostate cancer. The methylation or demethylation of the CpG islands in promoter regions may result in the inhibition or activation of gene transcription. For instance, the hypermethylation of cytosines 5' in CpG islands within the regulatory (promoter) region of suppressor genes may result in gene silencing. In contrast, the hypomethylation of cytosines 5' in the same region of oncogenes may reactivate the transcription. Localized prostate cancers exhibit varying degrees of changes in hyper- or hypo- methylation of promoters that regulate gene expression(184). From a post-radical prostatectomy cohort of patients with prostate cancer, Geybels et al.(185) explored methylation differences among tumor and adjacent benign prostatic tissue obtained from formalin-fixed, paraffin-embedded (FFPE) cores. They identified 2,040 differentially methylated CpG sites. The majority of differentially methylated CpG were hypermethylated (n = 1,946; 95%), and among them the *SCGB3A1*, *HIF3A*, and *AOXI* were the top-ranked differentially methylated genes. Similarly, Patel et al(186). Compared the methylation of 15 CpGs loci among prostate cancer and benign prostatic tissues in over 1300 prostatectomy samples. They identified three genes, *GAS6*, *GSTP1*, and *HAPLN3*, whose DNA methylation status was capable to distinguish between prostate cancer and benign tissue. In a setting of patients at risk of prostate cancer with prior negative biopsy, Stewart and colleagues(187) developed an epigenetic assay to predict the risk of cancer detection at re-biopsy. Within a sample of 498 patients, hypermethylation of CpG islands in the promoter regions of *GSTP1*, *APC*, and *RASSF1* of normal cells in the human prostate and in benign prostatic hyperplasia came to be correlated with a higher risk of a diagnosis of prostate cancer at repeated biopsy. This phenomenon was explained by the probability of having cancerous cells in the contiguity of those healthy cells with hypermethylated and thus silenced *GSTP1*, *APC*, and *RASSF1* genes. In the US, this assay is now

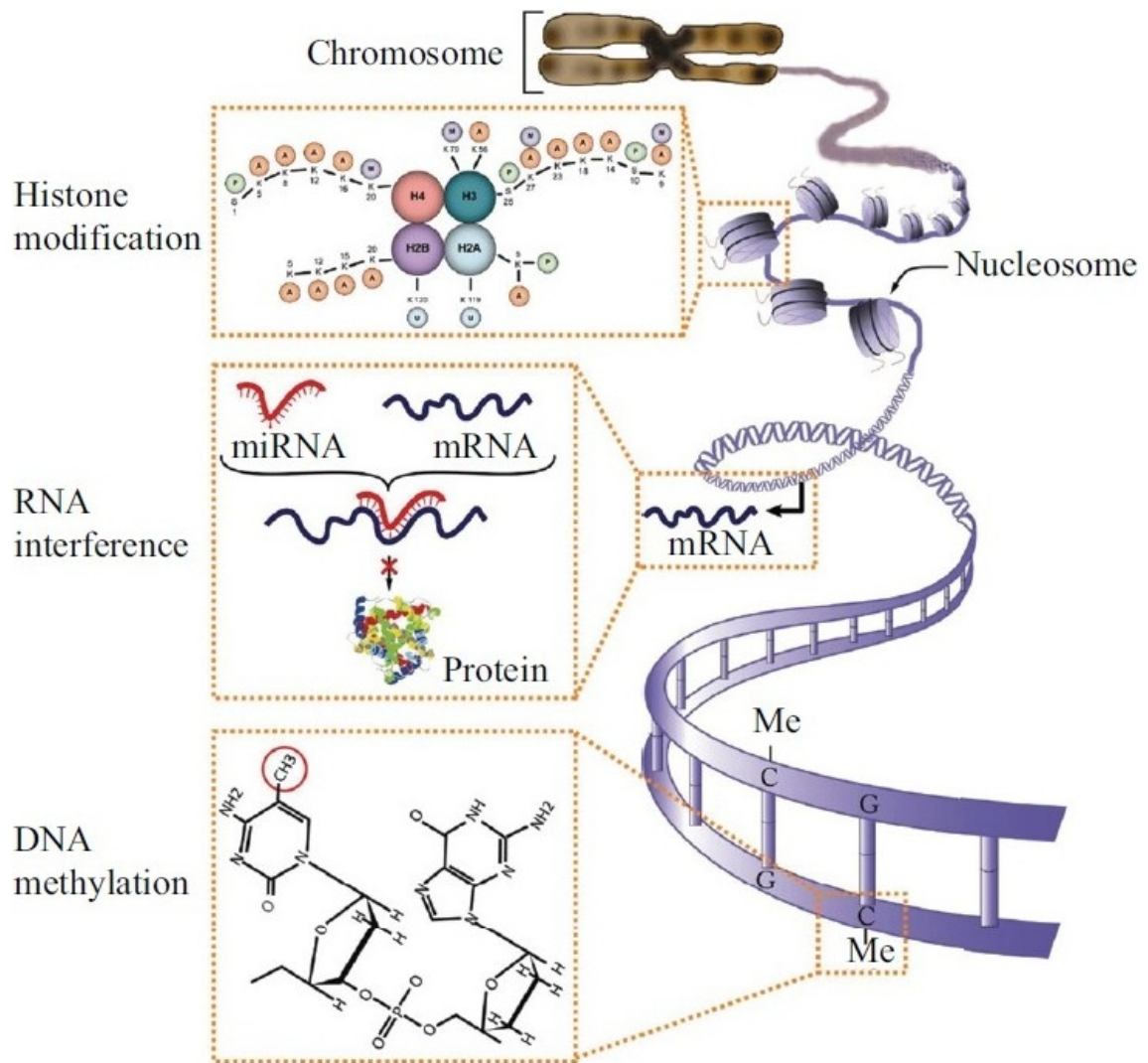


**Figure 15** – Graphical representation of the double strand of the human DNA and its methylation and transcription. Reproduced from Kim et al., “Epigenetic Mechanisms of Pulmonary Hypertension”, *Pulm Circ.* 2011 Jul-Sep;1(3):347-56 (the original article is distributed under the terms of the Creative Commons CC BY-NC-SA 3.0 license).



commercialized with the name of ConfirmMDx®, which is reimbursed by Medicare and recommended by NCCN Early Detection for Prostate Cancer Guidelines(188). Epigenetic changes are constantly involved in cancer progression. For prostate cancer, the relation between hyper/hypomethylated CpG sites and the occurrence of lethal metastatic progression has been investigated. Relying on a cohort of 430 patients with surgically resected prostate cancer, Zhao et al.(189) identified eight differentially methylated CpGs in 5 genes (*ALKBH5*, *ATP11A*, *FHAD1*, *KLHL8*, and *PII5*) and 3 intergenic regions that were able to predict metastatic-lethal progression. These findings were subsequently validated in two independent cohorts of respectively 344 and 80 patients. The score demonstrated better prediction performance (area under the curve [AUC] = 0.91; p = 0.037) compare to Gleason score alone (AUC = 0.87; p = 0.025)(190). Similar studies, which relied on smaller cohorts, have elucidated the correlation between epigenetic alterations in localized disease. Henrique et al.(191) found hypermethylation of APC as a predictor of worse disease-specific survival in a series of 83 consecutive prostate biopsy specimens harboring prostate carcinoma. Richiardi and colleagues (192) analyzed a cohort of 459 consecutive patients diagnosed with prostate cancer after systematic biopsy, trans-urethral prostatic resection, or radical prostatectomy, in a pre-PSA screening era, and found that among three pre-defined genes (*APC*, *RUNX3*, and *GSTP1*), methylation of the *APC* promoter was associated with higher prostate cancer-specific mortality. Rosenbaum et al.(193) demonstrated that hypermethylation of *GSTP1* and hypermethylation of *APC* were correlated with cancer progression in a cohort of 37 patients with Gleason grade group 2 and treated with radical prostatectomy. Lastly, Vasiljević and colleagues(194) found that methylation of genes *HSPB1*, *CCND2* and *DPYS* was correlated to prostate cancer death in 367 patients with a diagnosis of prostate cancer after transurethral prostate resection. The correlation between aberrant DNA methylation and lymph node metastases was also previously investigated. In a set of 14 patients with multifocal prostate cancer, Mundbjerg et al.(195) developed a classifier to assess epigenetic similarities among lymph node metastases and primary prostatic disease. The development cohort consisted in patients with multifocal prostate cancer disease who underwent radical prostatectomy and ePLND. All patients harbored lymph node metastases at the time of radical prostatectomy. The FFPE samples were retrieved from both the prostate and the lymph nodes. For each patient, the Authors analyzed

samples from the lymph node metastases, different foci of adenocarcinoma of the prostate, prostatic intraepithelial neoplasia (PIN), adjacent-normal prostatic tissues, and non-metastatic nodes. The aim was to identify an epigenetic correlation between primary prostatic tumor foci and lymph node metastases. The Authors identified 25 CpGs sites that were highly correlated between lymph node metastases and isolated prostatic tumor foci. This 25-CpG position signature still waits for prospective validation in large cohorts, as well as a validation in FFPE biopsy tumor samples which are taken upfront radical prostatectomy. The latter will be clinically more relevant given that prostate cancer is diagnosed through the biopsy and upfront radical prostatectomy. Thus, the Mundbjerg score, as well as any other epigenomic classifier, should demonstrate their clinical utility in predicting the risk of LNI when applied to the biopsy tissue. The latter is generally more technically demanding to be examined, as well as less informative than prostatectomy samples. Indeed, biopsy cores provide a lower amount of tissue than prostatectomy specimens, being also less representative of the true extent of the primary tumor and its characteristics. In summary, genomic methylation holds relevant information about the clonal origin of prostate cancer spread. This is suggested by the evidence that nodal metastasis and primary foci share a common epigenetic profile(195). These findings show that epigenetics may describe the biological behaviour and relationship between nodal metastasis and primary tumor foci. Therefore, epigenetic signatures are worthwhile being investigated further and possibly assessed on prostate biopsy tissue to predict LNI upfront radical prostatectomy.

## 5. Aims of the research project

The presence of lymph node metastases is an adverse prognostic factor associated with a higher risk of prostate cancer recurrence and decreased long-term survival(196). Management of men with LNI requires post-operative therapies, such as androgen deprivation therapy (ADT) and/or radiotherapy, which have been shown to improve survival in these patients(197). Thus, pathological assessment of LNI is crucial for treatment planning and post-surgical follow-up. On the other hand, accurate extent of LNI can only be documented after extended PLND, but extended PLND is not devoid of complications(198) and it should be performed only in patients more likely to harbor LNI. In order to balance the benefit of more accurate disease staging with the side effects related to this surgical approach, efforts should be made to improve preoperative prediction of LNI in men suitable for surgical intervention. To date, the decision to remove regional lymph nodes is guided by the individual risk of LNI that can be estimated using preoperative models such as Briganti nomograms(174,199). These predictive tools are based on clinical and biopsy features only. Although Briganti nomogram is the most accurate tool, it is still associated with imperfect sensitivity and low specificity, given that many patients without LNI may receive extended PLND as per nomogram's prediction. This exposes a significant number of patients to PLND-related complications without any proven benefit on staging and oncological outcomes. These limitations have not been completely overcome even in the latest version of Briganti nomogram(98,181), where mpMRI features have been integrated into the model increasing its accuracy. Recent evidence demonstrated that DNA methylation features may improve patient stratification to identify men at risk of LNI(195). We then hypothesized that integration of clinical, imaging, and epigenetic features may improve our abilities to predict LNI at extended PLND. Therefore, the significance of this study is to improve preoperative LNI prediction in patients at risk of LNI by integrating clinical, radiologic, and epigenomic data to better identify patients suitable for extended PLND and to reduce the number of unnecessary PLND. To achieve this goal, the current study is articulated into four main aims:

**Specific aim 1:** To provide an epigenetic profiling of FFPE biopsy specimens from patients with localized (cTanyN0M0) prostate cancer in whom PLND, at the time of radical prostatectomy, was recommended due to their pre-surgical risk of LNI above 5%, according to the 2012 Briganti nomogram.

**Specific aim 2:** To validate the recently published Mundbjerg's signature, consisting of 25 DNA methylation probes, to predict the risk of LNI. This classifier represents the only available genomic tool specifically designed to predict LNI in localized prostate cancer by using only epigenetic features.

**Specific aim 3:** To identify the most clinically relevant CpGs sites and related genes which are differentially methylated among patients with and without LNI. We aim to develop two epigenetic signatures to predict LNI in localized prostate cancer: i) a signature including relevant CpGs sites that emerge from the analysis of target samples; ii) another signature including relevant CpGs sites that emerge from the analysis of systematic samples.

**Specific aim 4:** To integrate the developed epigenetic signatures with clinical and mp-MRI-derived features in a combined predictive linear model to predict LNI. The model aims to outperform previous predicting tools that are based only on clinical and/or mp-MRI features.

## 6. Results

### 6.1 – Characteristics of the study population

The present study enrolled 172 patients with a histological diagnosis of prostate cancer. Tumor diagnosis was achieved via transperineal prostate fusion biopsy with combined targeted and systematic sampling. Prostate biopsy was recommended based on suspicious findings on mp-MRI (PI-RADS 3-5 area/s) of the prostate. All included patients presented at least two cores with prostate cancer involvement that were respectively obtained from i) target (PI-RADS 3-5 area/s) and ii) systematic sampling. Moreover, all patients underwent radical prostatectomy and extended PLND based on a calculated risk of LNI above 5%, according to the 2012 version of Briganti nomogram.

#### 6.1.1 – Clinical characteristics

The median (interquartile range [IQR]) age of the patient population, at the time of prostate biopsy, was 66 years (63-71). The median pre-biopsy PSA value was 7 ng/ml. Digital rectal examination was positive (T2 or higher) in 55 (32%) patients at the time of biopsy (**Table 1**).

**Table 1** – Clinical characteristics of the 172 included patients.

Variables	Values (IQR)
Median age (yrs)	66 (63-71)
Median PSA (ng/ml)	7 (5-10)
cT stage	
T1c	117 (68%)
T2	44 (26%)
T3	11 (6%)

#### 6.1.2 – mpMRI features

Median (IQR) prostatic volume at mp-MRI was 43.7 cc. Overall, we identified 243 mp-MRI positive lesions (PI-RADS 3-5) in our cohort. Specifically, 115 (67%) patients presented only one mp-MRI positive lesion, 45 (26%) presented two mp-MRI positive lesions, 12 (7%) presented more than two mp-MRI positive lesions. PI-RADS 5 was detected in 53 (31%) patients, PI-RADS 4 in 86 (50%) patients, and PI-RADS 3 in 33 (19%) patients. The median (IQR) diameter of mpMRI positive (PI-RADS 3-5) lesions was 13mm (9-18) (**Table 2**).

**Table 2** – mpMRI characteristics of the 172 included patients.

<b>Variables</b>		<b>Values (IQR)</b>
Prostate volume (cc)		43.7 (34-59)
Index lesions diameter		13 (9-18)
Highest PI-RADS		
	3	33 (19%)
	4	86 (50%)
	5	53 (31%)
N of PI-RADS 3-5		
	1	115 (67%)
	2	45 (26%)
	>2	12 (7%)
mp-MRI T stage		
	Organ confined	136 (79.0%)
	Extra capsular extension	23 (13.4%)
	Seminal vesicle invasion	13 (7.6)

### 6.1.3 – Biopsy sampling data

The median (IQR) number of collected cores per patient was 15 (13-16). Of these, the median number of target (PI-RADS 3-5) cores was 3 (3-5) and the median number of systematic cores was 12 (8-13). The target sampling had higher rates of positive cores as compared to the systematic sampling (median 100% vs. 37.5%,  $p < 0.001$ ) (**Table 3**). The ISUP grade groups derived from the target sampling were compared with the ISUP Gleason grade groups derived from the systematic sampling and resulted in higher, similar, or lower in 19%, 71%, and 10% of patients, respectively.

**Table 3** – Biopsy features of the 172 recruited patients.

<b>Variables</b>	<b>Overall</b>	<b>Systematic</b>	<b>Targeted</b>	<b>P values</b>
Median (IQR) N cores	15 (13-16)	12 (8-13)	3 (3-5)	<0.001
Median (IQR) N positive cores	7 (5-9)	4 (2-6)	3 (2-4)	<0.001
Percentage (IQR) of positive cores	50 (33-62)	37.5 (21.4-50)	100 (66.6-100)	<0.001
ISUP Gleason grade groups (%)				
	1	12 (7)	6 (3)	0.01
	2	56 (33)	48 (28)	
	3	51 (30)	54 (31)	
	4	27 (16)	36 (21)	
	5	26 (15)	29 (17)	

The ISUP Gleason grade groups for the overall cohort of patients is presented in **Table 4**. Results are stratified according to the type of sampling (overall, target, systematic) and the highest PI-RADS score.

**Table 4** – ISUP Gleason grade grouping according to the highest PI-RADS score.

<b>Variables</b>	<b>PI-RADS 3 (%)</b>	<b>PI-RADS 4 (%)</b>	<b>PI-RADS 5 (%)</b>
ISUP 1			
Overall	0 (0)	4 (4.7)	1 (1.9)
Systematic	2 (6.1)	8 (9.3)	2 (3.8)
Target	2 (6.1)	3 (3.5)	1 (1.9)
ISUP 2			
Overall	13 (39)	30 (35)	5 (9.4)
Systematic	13 (39)	35 (41)	8 (15)
Target	13 (39)	32 (37)	5 (9.4)
ISUP 3			
Overall	11 (33)	25 (29)	18 (34)
Systematic	10 (30)	25 (29)	16(30)
Target	10 (30)	28 (33)	20 (38)
ISUP 4			
Overall	5 (15)	19 (22)	12 (23)
Systematic	4 (12)	12 (14)	11 (21)
Target	4 (12)	16 (19)	13 (25)
ISUP 5			
Overall	4 (12)	8 (9.3)	17 (32)
Systematic	4 (12)	6 (7)	16 (30)
Target	4 (12)	7 (8.1)	14 (26)

Among 129 patients with unilateral mp-MRI visible lesion and available data on positive core laterality, 61(47%) patients presented absolute concordant laterality, defined as positive core/s from the same prostatic lobe and no positive core from the other lobe, for either the target and systematic sampling. Of all patients, 59 (46%) presented partial concordant laterality, defined as positive core/s from the same prostatic lobe for either the target and systematic sampling, with also positive systematic core/s on the other lobe. Only 9 (7%) patients presented discordant laterality, defined as positive core/s from different prostatic lobes and no positive cores on the same lobe, for the target and systematic sampling (**Table 5**).

**Table 5** – Concordance among target and systematic sampling in terms of core positivity by side.

<b>Variables</b>	<b>Overall (129)</b>	<b>PI-RADS 3 28 (22%)</b>	<b>PI-RADS 4 66 (51%)</b>	<b>PI-RADS 5 35 (27%)</b>
Absolute concordant laterality (%)	61 (47)	10 (36)	34 (52)	17 (49)
Partial concordant laterality (%)	59 (46)	17 (61)	25 (38)	17 (49)
Discordant laterality (%)	9 (7)	1 (3)	7 (11)	1 (2%)

#### **6.1.4 – Risk classification grouping**

According to the D’Amico risk classification, we enrolled 3 (2%) low, 95 (55%) intermediate, and 74 (43%) high-risk patients. According to the 2012 Briganti nomogram, the median calculated-risk value of LNI was 9%. For 172 and 133 patients the risk of LNI according with the 2017 and 2019 Briganti nomograms was calculated and it was 13% and 10%, respectively (**Table 6**).

**Table 6** – Nomogram’s derived risk of LNI.

<b>Variables</b>	<b>Briganti-2012*</b>	<b>Briganti-2017 *</b>	<b>Briganti-2019**</b>
LNI risk; median (IQR)	9% (5-8%)	13% (4-30%)	10% (3-23%)

\*172 patients; \*\*133 patients

#### **6.1.5 – Pathological features from radical prostatectomy specimens**

The pathological characteristics of the 172 patients are summarized in **Table 7**. Overall, 37 (21.5%) patients had LNI. The median (IQR) number of metastatic nodes among pN1 patients was 2 (1-4). ISUP Gleason score upgrading from biopsy to radical prostatectomy specimens was reported in 45 (26%) patients. Conversely, ISUP Gleason score downgrading was reported in 25 (15%) patients.



**Table 7 – Radical prostatectomy features of the recruited 172 patients.**

Variables	Overall 172	pN1 37 (21.5)	pN0 135 (78.5)	P values
pT				
pT2	50 (29)	2 (5)	48 (36)	<0.001
pT3a	90 (52)	11 (30)	79 (59)	
pT3b	32 (19)	24 (65)	8 (5)	
ISUP grade group				
1	1 (1)	0 (0)	1 (0.7)	<0.001
2	43 (25)	1 (2.8)	42 (31)	
3	66 (39)	7 (19)	59 (44)	
4	17 (10)	4 (11)	13 (9.7)	
5	43 (25)	24 (67)	19 (14)	
Positive margins	39 (23)	17 (46)	22 (16)	<0.001
Type of surgery				
Open	20 (12)	4 (11)	16 (12)	0.8
Laparoscopic	3 (1.7)	1 (2.7)	2 (1.5)	
Robotic	149 (87)	32 (86)	117 (87)	
Removed lymph nodes	18 (13-24)	22 (16-30)	17 (12-23)	0.002

### ***6.1.6 – Follow-up and oncological outcomes***

Among the 152 patients with available follow-up, the median (IQR) follow-up time calculated from the date of prostate biopsy to the 31<sup>st</sup> August 2022 with the inverse-Kaplan-Meier method, was 36 months (22-48). Salvage or adjuvant radiotherapy was administered in 9 (6%) and 8 (5.3%) patients, respectively. Androgen deprivation therapy (ADT) was given along with salvage and adjuvant radiotherapy in 4 (2.6%) and 14 (9.2%) patients, respectively. ADT alone was given in five (3.2%) patients. Only one patient died, due to other causes. Overall, 23 had biochemical progression (BCR) and 10 clinical recurrence, as per Response Evaluation Criteria in Solid Tumors (RECIST) criteria. Finally, 2-yr BCR-free survival and clinical recurrence-free survival were 89.1% (95% CI: 83.8-94.7) and 96.2% (95% CI: 93-99.6), respectively.

## ***6.2 – Epigenetic analysis***

### ***6.2.1 – Cohort definition***

From the 172 recruited patients, we processed 347 samples, which included 332 biopsy cores (166 target and 166 systematic cores) and 15 metastatic lymph node samples. Twelve core samples were excluded due to the low amount of extracted DNA (<10ng).

Bisulfite conversion failed in 7 core samples (conversion rate < 85% on unmethylated spike in). One additional core sample with low coverage was excluded (less than 5 reads on each cytosine). The final cohort included 339 samples, which were accounting for 161 target cores, 163 systematic cores, and 15 lymph node metastases, respectively (**Table 8**). Patients with both target and systematic samples available and processed were 157. Patients with target, systematic, and lymph node samples available and processed were 8.

**Table 8** – Number of processed samples by type and according with LNI status.

Type of samples	Overall	LNI –	LNI +
Target cores	161	129	32
Systematic cores	163	132	31
Lymph node mets	15/37	0	15

### 6.2.2 – Validation of the *Mundbjerg* signature

The *Mundbjerg* signature is a genomic classifier based on 25 DNA methylation probes that can predict the aggressiveness of prostate cancer in terms of its ability to metastasize to the regional lymph nodes. Each of the 25 probes corresponds to 3 nucleotides, and together identify 75 genomic positions of the human DNA. These 75 genomic positions were annotated in each of our 339 samples according to the human reference genome HG38. Among the 25 probes, only 6 were consistently measured across samples, 14 were measured only in few samples, and 5 probes were not covered at all. Overall, only 8 samples did not match any of the probes. The heatmap for each of the *Mundbjerg* probes across the 339 samples is shown in **Figure 16**. The average methylation status of the 75 genomic positions is reported in **Figure 17**. Here, the average methylation status according to i) LNI status (LNI+ vs. LNI-), and ii) sample type (target vs. systematic vs. lymph node metastases) was calculated with Wilcoxon test. We found no statistically significant differences among LNI+ and LNI- groups (pval=0.54), as well as among target vs. systematic vs. lymph node metastases (target vs. systematic: pval=0.5, FDR=0.53; target vs. metastases: pval=0.52, FDR=0.53; systematic vs. metastases: pval=0.39, FDR=0.53) groups. The comparison of methylation status for each individual probe

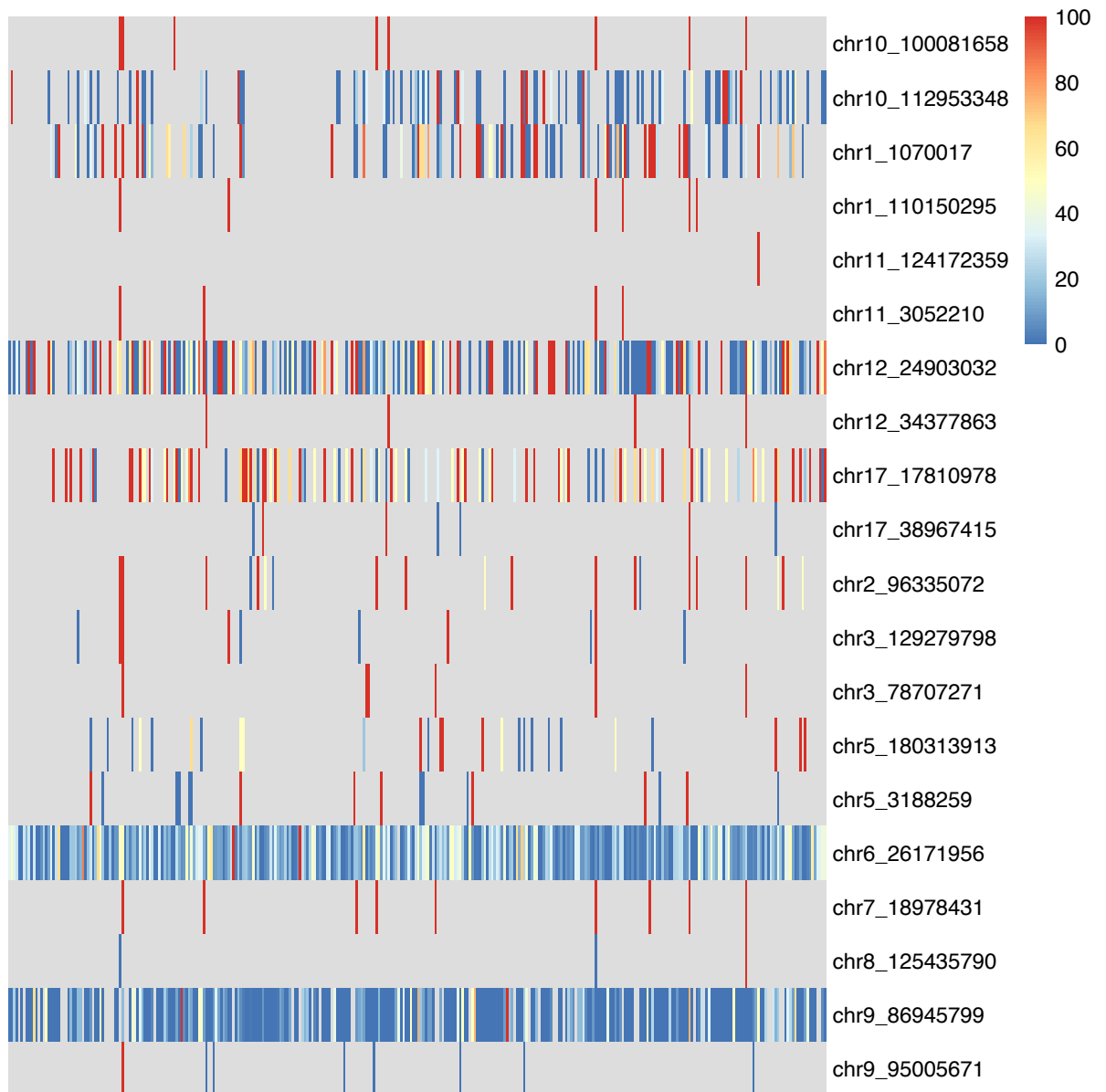


**Figure 16** –Heatmap of the tested Mundbjerg probes within our 339 samples. 8 samples were excluded because no probe was measured. The color gradient refers to the hypo (blue) or hyper (red) methylation status of the CpG position for that specific probe. Among all 25 probes, only 6 were constantly represented among all samples (higher number of colored lines), 5 probes were not covered by any read (not reported in the figure).

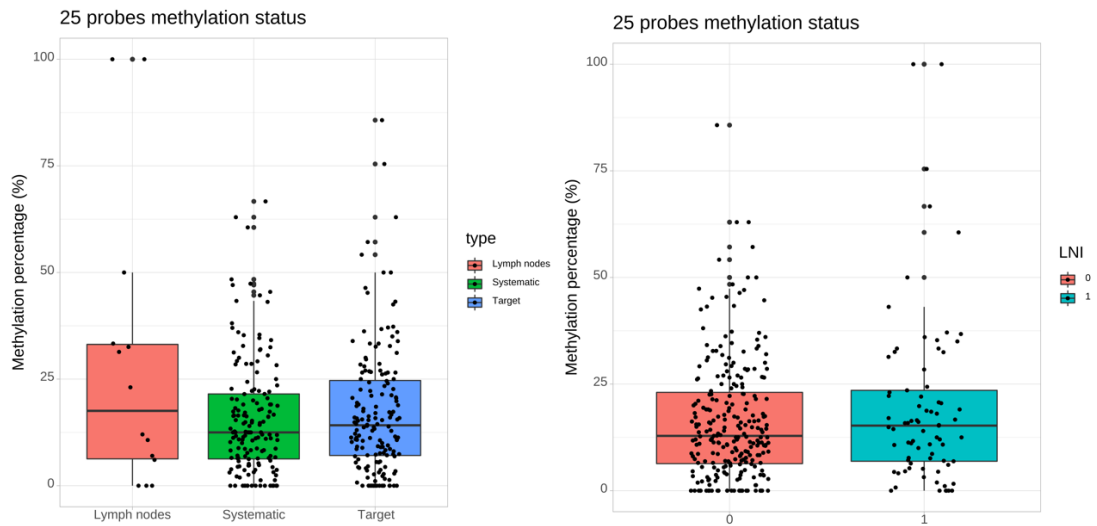


**Figure 17** – Comparison of the average methylation status for the 25 probes (each dot represents a sample) according to a) sample type (target vs. systematic vs. lymph node metastases) and b) LNI status (LNI+ vs. LNI-). The Wilcoxon test was used for the two-by-two comparison. No statistically significant differences emerged among the groups.

according to i) LNI status (LNI+ vs. LNI-), and ii) sample type (target vs. systematic vs. lymph node metastases) is depicted in **Figure 18**. Two-by-two comparison revealed that no probe was significantly hyper or hypomethylated among target vs. systematic samples. Here, 9 probes were evaluated for comparison given that were measured in at least 5 samples per group (see methods). For the two comparisons between target vs. lymph node metastases and systematic vs. lymph node metastases, only the probe *chr17:17810978* resulted hypermethylated in the lymph node samples when compared to the target (p=0.025) and systematic (p=0.031) samples, respectively. The adjusted significance level in both comparisons was poor (false discovery rate [FDR]=0.124 and 0.158 respectively). For this analysis, 5 probes were evaluated for comparison given that were measured in at least 3 samples per group (see methods). The genomic position of the probe *chr17:17810978* is located on the *RAI1* gene. Lastly, the average methylation status of the 324 core samples showed that no probe was significantly hyper or hypomethylated among samples derived from patients with LNI+ vs. LNI-. Here, 8 probes were evaluated for comparison given that were measured in at least 3 samples per group (see methods).

### **6.2.3 – Differential Methylation analysis**

Differential methylation analyses were performed three times on i) all core samples combined (N=324), but also on ii) target (N=161) and iii) systematic (N=163) core samples, independently. Then, the results of these three sets of analyses were overlapped to identify genes and gene pathways in common.

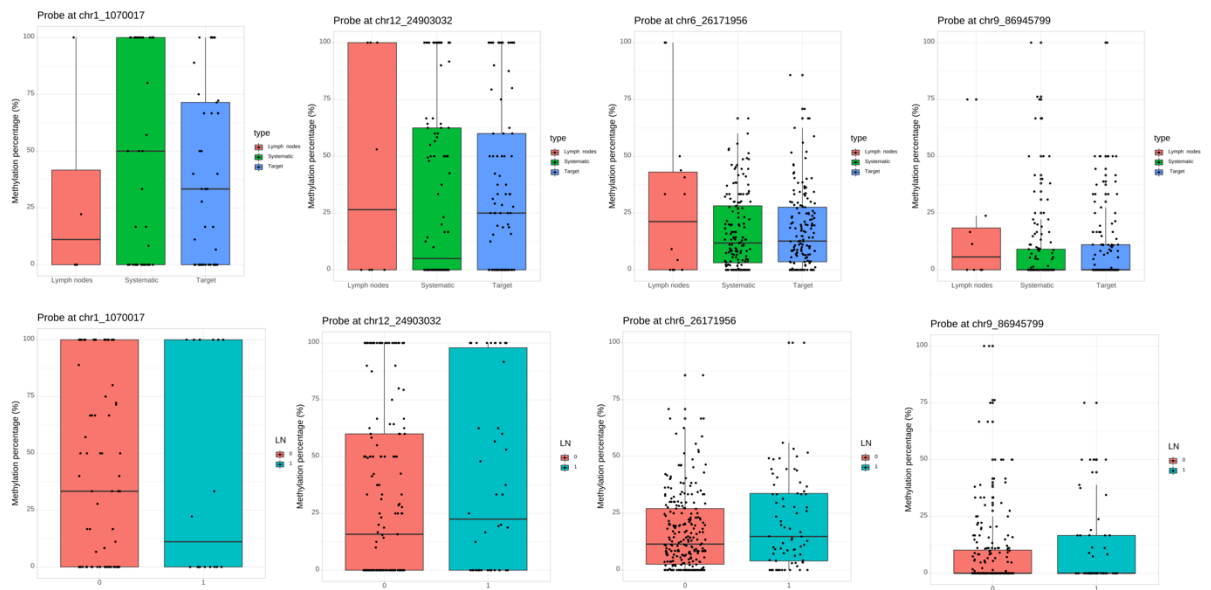


**Figure 18** – Comparison of methylation status for each individual probe according to i) LNI status (LNI+ vs. LNI-), and ii) sample type (target vs. systematic vs lymph node metastases). The results of only 4 probes are depicted. The remaining comparisons can be found at the following link:

[https://www.dropbox.com/s/0a9ww9d2abvm9hh/25probes\\_methyl\\_percent.each\\_boxplot.pdf?dl=0](https://www.dropbox.com/s/0a9ww9d2abvm9hh/25probes_methyl_percent.each_boxplot.pdf?dl=0).

Methylation percentages of each sample according to the 25 Mundbjerg’s probes can be found at the present link:

[https://www.dropbox.com/scl/fi/cdha6fzyriz00tqf1bwzv/25probes\\_aggregated\\_all.xlsx?dl=0&rlkey=mmmj1wmy1qatbgpsj9eerd2c5](https://www.dropbox.com/scl/fi/cdha6fzyriz00tqf1bwzv/25probes_aggregated_all.xlsx?dl=0&rlkey=mmmj1wmy1qatbgpsj9eerd2c5).

### ***6.2.3.1 – Differential Methylation analysis for the combined (target and systematic cores) sample cohort***

The sample size was 324 cores, including either target (N=161) and systematic (N=163) biopsy cores. Histograms of coverage showed similar profiles across samples. The histograms of the methylation status showed that unmethylated CpGs were more common than the methylated counterpart, but there were exemptions among samples (129\_C, 16\_B, 21\_F, 34\_B, 40\_E, 49\_E, 69\_B).

Coverage of target samples:

[https://www.dropbox.com/s/k6gk0rgiqgizlcy/coverageStats\\_histogram.Target.pdf?dl=0](https://www.dropbox.com/s/k6gk0rgiqgizlcy/coverageStats_histogram.Target.pdf?dl=0),

Coverage of systematic samples:

[https://www.dropbox.com/s/ac3ld9fmxdsq5kt/coverageStats\\_histogram.OffTarget.pdf?dl=0](https://www.dropbox.com/s/ac3ld9fmxdsq5kt/coverageStats_histogram.OffTarget.pdf?dl=0)

Methylation of target samples:

[https://www.dropbox.com/s/mjkoeabqb3jelr9/methylationStats\\_histogram.Target.pdf?dl=0](https://www.dropbox.com/s/mjkoeabqb3jelr9/methylationStats_histogram.Target.pdf?dl=0), Methylation of systematic samples:

[https://www.dropbox.com/s/hgzcmnswfzw4r3d/methylationStats\\_histogram.OffTarget.pdf?dl=0](https://www.dropbox.com/s/hgzcmnswfzw4r3d/methylationStats_histogram.OffTarget.pdf?dl=0)

Given the filter on coverage of at least 5 reads per CpGs in at least 12 samples per group (LNI+ and LNI-), we identified 17.3 millions of CpGs positions. To reduce the number of examined CpGs, 10% and 25% average methylation differences were used as cut-offs to exclude insignificant CpGs, and focus the analyses only on the most differentiated CpGs positions (see methods). The number of CpGs with a percent methylation difference larger than 10% and FDR<0.01 was 512 643 (2.97% of all the tested cytosines). The number of CpGs with a percent methylation difference larger than 25% and FDR<0.01 was 10 036 (0.058% of all the tested cytosines). The distribution of all tested CpGs (17.3M) across chromosomes is presented as bar plots in **Figure 19**. The distribution of all differentially methylated CpGs (for 10% and 25% cut-offs) across chromosomes is presented as bar plots in **Figure 19**. According to these figures, chromosomes 16, 17, 19, in spite of their shorter lengths, were enriched in differentially methylated CpGs. However, this enrichment mirrored a higher number of measured CpGs on these chromosomes. Conversely, chromosome 8 showed a real enrichment of differentially methylated cytosines, but most of these cytosines were located outside of

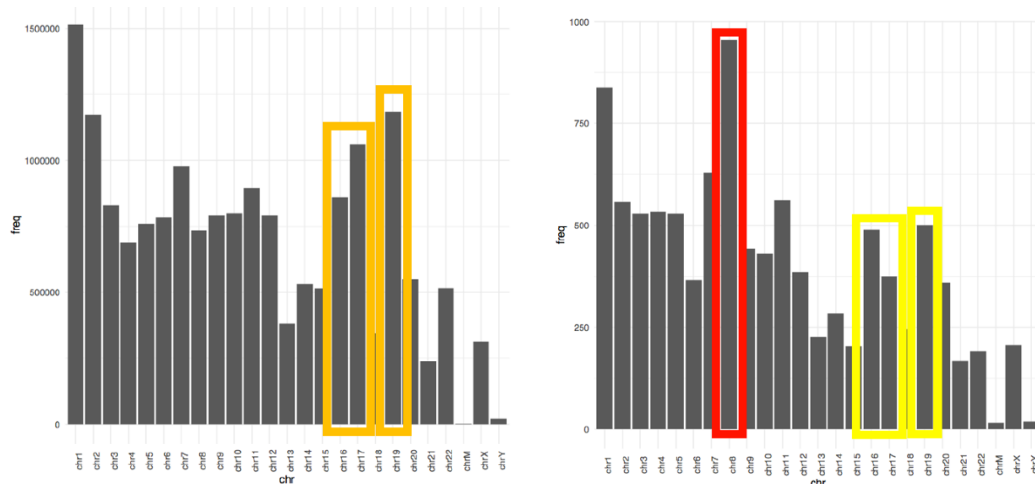


**Figure 19** – a) Bar plot of the distribution of all tested CpGs (17.3M) across chromosomes; b) bar plot of the distribution of all differentially methylated CpGs (Cut-off 10%) across chromosomes.

Figure for Cut-off 25% is available at this link:

[https://www.dropbox.com/s/t9bt50jlz4h3qpx/chr\\_distribution\\_diff\\_methyl.AllTumors.FDR\\_01\\_diff\\_25.pdf?dl=0](https://www.dropbox.com/s/t9bt50jlz4h3qpx/chr_distribution_diff_methyl.AllTumors.FDR_01_diff_25.pdf?dl=0)



CpG islands. When the analyses were stratified according to hyper- and hypomethylated CpGs, there was an overall abundance of hypo-methylated cytosines, compared to the hyper-methylated ones, when considering the 10% cutoff. Instead, the distribution of differentially methylated cytosines on chromosomes was similar between hyper- and hypo-methylated regions according to the 25% cutoff, except for a peak of hypo-methylated cytosines observed on chromosome 8 (**Figure 20**). The distribution of all and differentially methylated (with both cut-offs 10% and 25%) CpGs is depicted in cake plots in **Figure 21**. Promoters seemed to host the highest number of all covered CpGs. However, these figures decreased when only CpGs with differential methylation higher than 10% and 25% were considered. Here, the portions of the genome with the highest coverage of differentiated CpGs were introns and intergenic parts. When the analyses were stratified according to hyper- and hypomethylated CpGs, the hyper-methylated cytosines, compared to the hypo-methylated counterparts, were enriched within genes' promoters and depleted on intergenic regions. These differences were much more evident when considering the 25% cutoff (**Figure 22**). Annotations of the differentially methylated CpGs on the HG38 were performed independently for the CpGs that were identified with cut-off 10% and 25%. The 512 643 CpGs derived from the use of 10% cut-off, were overlapping 13 280 CpG islands and 12 929 associated genes. However, when we considered only those CpGs islands containing at least 100, 50, and 30 differentially methylated CpGs, the numbers of corresponding CpGs islands were 6, 209, and 988 and the overlapping genes were 13, 312, and 1339, respectively. The 10 036 CpGs derived from the use of 25% cut-off, overlapped 641 CpGs islands and 753 associated genes. However, when we considered only those CpGs islands containing at least 30, 20, and 10 differentially methylated CpGs, the number of corresponding CpGs islands were 0, 6 and 15 and the overlapping genes were 0, 9, and 21, respectively. The results of the enrichment analysis for the 312 genes derived from the use of 10% cut-off, and located within those 209 CpG islands with at least 50 differentially methylated CpGs can be found at this link:

[https://www.dropbox.com/scl/fi/foxpexsc377e3x5ylevx9l/diff\\_methyl.AllTumors.FDR\\_01\\_diff\\_10.CpGi\\_ENST.genes\\_50.enrichR.xlsx?dl=0&rlkey=7adpzzm26rr8f79ke6w0msx0j](https://www.dropbox.com/scl/fi/foxpexsc377e3x5ylevx9l/diff_methyl.AllTumors.FDR_01_diff_10.CpGi_ENST.genes_50.enrichR.xlsx?dl=0&rlkey=7adpzzm26rr8f79ke6w0msx0j)

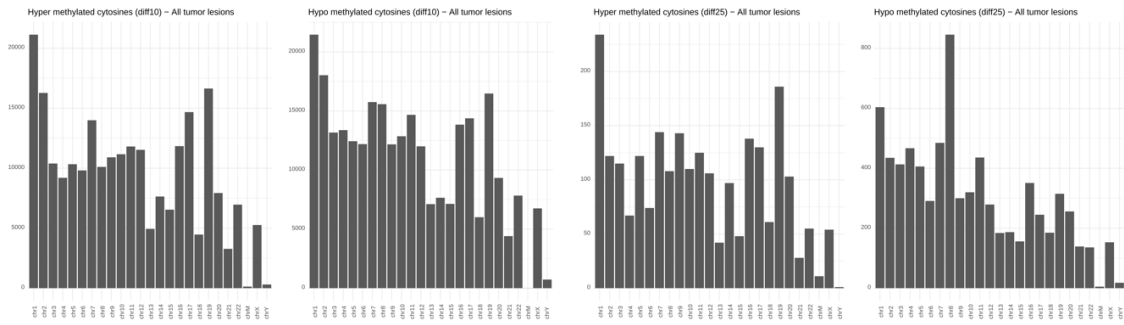


**Figure 20** – Bar plot of the distribution of differentially (cut-off 10%) hyper-methylated CpGs (237 272 CpGs) across chromosomes; a2) Bar plot of the distribution of differentially (cut-off 10%) hypo-methylated CpGs (275 371 CpGs) across chromosomes; b1) Bar plot of the distribution of differentially (cut-off 25%) hyper-methylated CpGs (2 424 CpGs) across chromosomes; b2) Bar plot of the distribution of differentially (cut-off 25%) hypo-methylated CpGs (7 612 CpGs) across chromosomes.

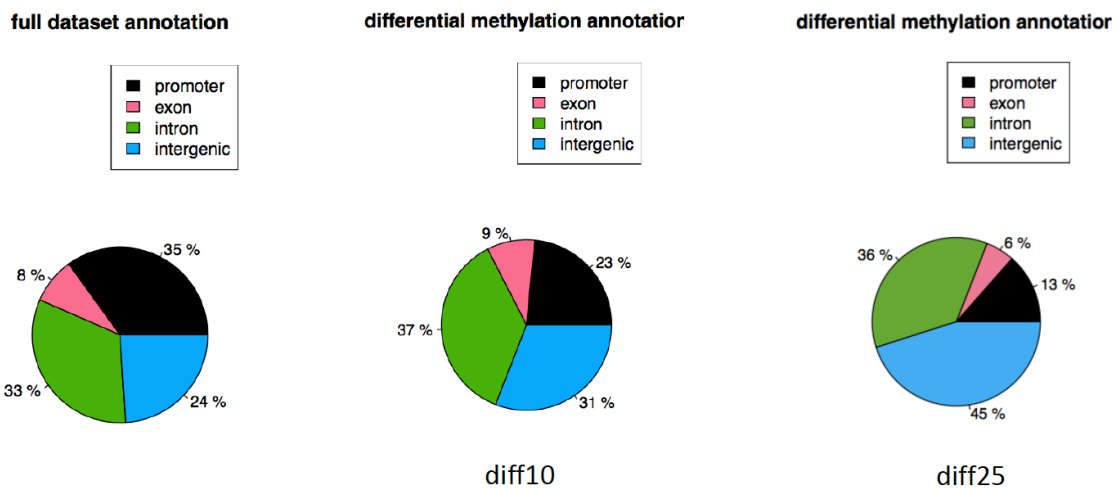


**Figure 21** –Distribution of all and differentially methylated (with both cut-offs 10% and 25%) CpGs in all samples.

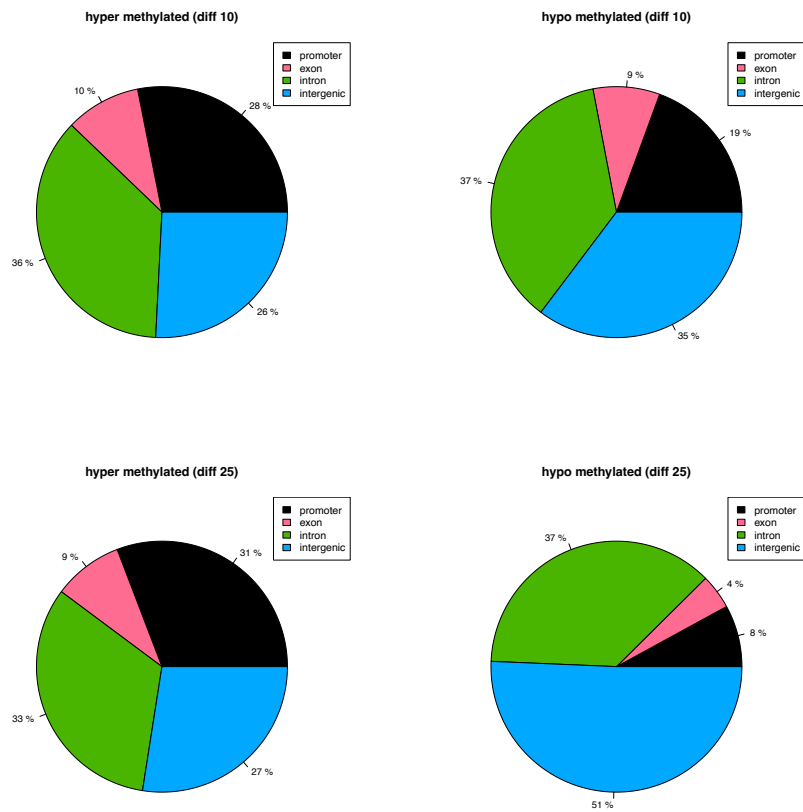


**Figure 22** – Top left) cake plot of the distribution of differentially hyper-methylated (cut-off 10%) CpGs in all samples; Top right) cake plot of the distribution of differentially hypo-methylated (cut-off 10%) CpGs in all samples; Bottom left) cake plot of the distribution of differentially hyper-methylated (cut-off 25%) CpGs in all samples; Bottom right) cake plot of the distribution of differentially hypo-methylated (cut-off 25%) CpGs in all samples.

The results of the enrichment analysis for the 21 genes derived from the use of 25% cut-off, and located within those 15 CpG islands with at least 10 differentially methylated CpGs can be found at this link:

[https://www.dropbox.com/scl/fi/7etly13xzuql5518ovffj/diff\\_methyl.AllTumors.FDR\\_01\\_diff\\_25.CpGi\\_ENST.genes\\_10.enrichR.xlsx?dl=0&rlkey=lcigcp3indvx5lfb5p81f2ab7](https://www.dropbox.com/scl/fi/7etly13xzuql5518ovffj/diff_methyl.AllTumors.FDR_01_diff_25.CpGi_ENST.genes_10.enrichR.xlsx?dl=0&rlkey=lcigcp3indvx5lfb5p81f2ab7)

The enrichment analyses were achieved after matching the identified list of genes with the tested collections, namely Gene Ontologies (GO\_BP, GO\_CC, GO\_MF); WikiPathways; Kegg; Biocarta; Reactome; Hallmarks; TF Perturbations Followed by Expression (from NCBI-GEO). After adjustment for multiple testing (FDR), only few pathways reached statistical significance (FDR <0.005), and only when the 10% cut-off was applied to select the genes. The most significant gene pathways are presented in **Figure 23**. No significant enrichment was reached with the list of genes that were selected using the 25% cut-off. Analyses were stratified according to hyper- and hypo-methylated CpGs, but only with the 10% cut-offs, we reached statistically significant results. We found 237 272 differentially hyper-methylated cytosines, which overlapped 9 172 CpGs islands and 9 698 genes. When only CpGs islands with at least 50 differentially hyper-methylated cytosines were considered, the number of selected genes was 108, within 69 islands. Enrichment results for these 108 genes can be found at this link:

[https://www.dropbox.com/scl/fi/ocpxfbja3znoxgcznmzko/diff\\_methyl.AllTumors.FDR\\_01\\_diff\\_10\\_hyper.CpGi\\_ENST.genes\\_50.enrichR.xlsx?dl=0&rlkey=yImqig8hz1ycedyx87egw43i5](https://www.dropbox.com/scl/fi/ocpxfbja3znoxgcznmzko/diff_methyl.AllTumors.FDR_01_diff_10_hyper.CpGi_ENST.genes_50.enrichR.xlsx?dl=0&rlkey=yImqig8hz1ycedyx87egw43i5)

The most significant gene pathways for genes with hyper-methylated cytosines are showed in **Figure 24**. Moreover, we found 275 371 differentially hypo-methylated cytosines, which overlapped 9 712 CpGs islands and 8 745 genes. When only CpGs islands with at least 50 differentially hyper-methylated cytosines were considered, the number of selected genes was 48, within 34 islands. Enrichment results for these 48 genes can be found at this link:

[https://www.dropbox.com/scl/fi/jzsyf4nrl052luause7ep/diff\\_methyl.AllTumors.FDR\\_01\\_diff\\_10\\_hypo.CpGi\\_ENST.genes\\_50.enrichR.xlsx?dl=0&rlkey=terim15mrgnausd2iyi94x6eo](https://www.dropbox.com/scl/fi/jzsyf4nrl052luause7ep/diff_methyl.AllTumors.FDR_01_diff_10_hypo.CpGi_ENST.genes_50.enrichR.xlsx?dl=0&rlkey=terim15mrgnausd2iyi94x6eo)

The most significant gene pathways for genes with hypo-methylated cytosines are showed in **Figure 25**.

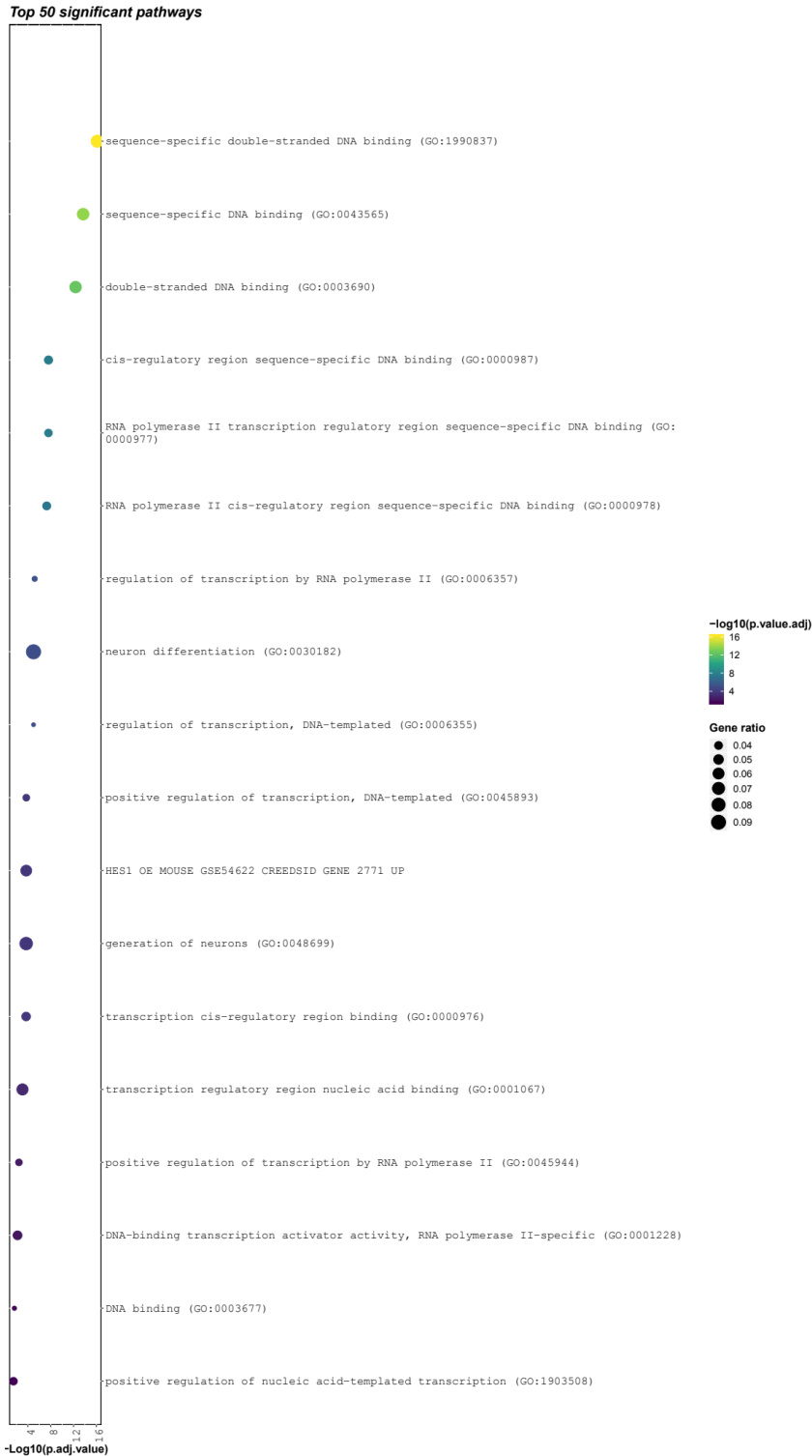


**Figure 23** – Summary of the most significant results ( $FDR < 0.005$ ) from the enrichment analysis when the cut-off of 10% (percent methylation difference) was used. The dimension of the dots is proportional to the number of overlapping genes with the pathway. The color gradient expresses the statistical significance.

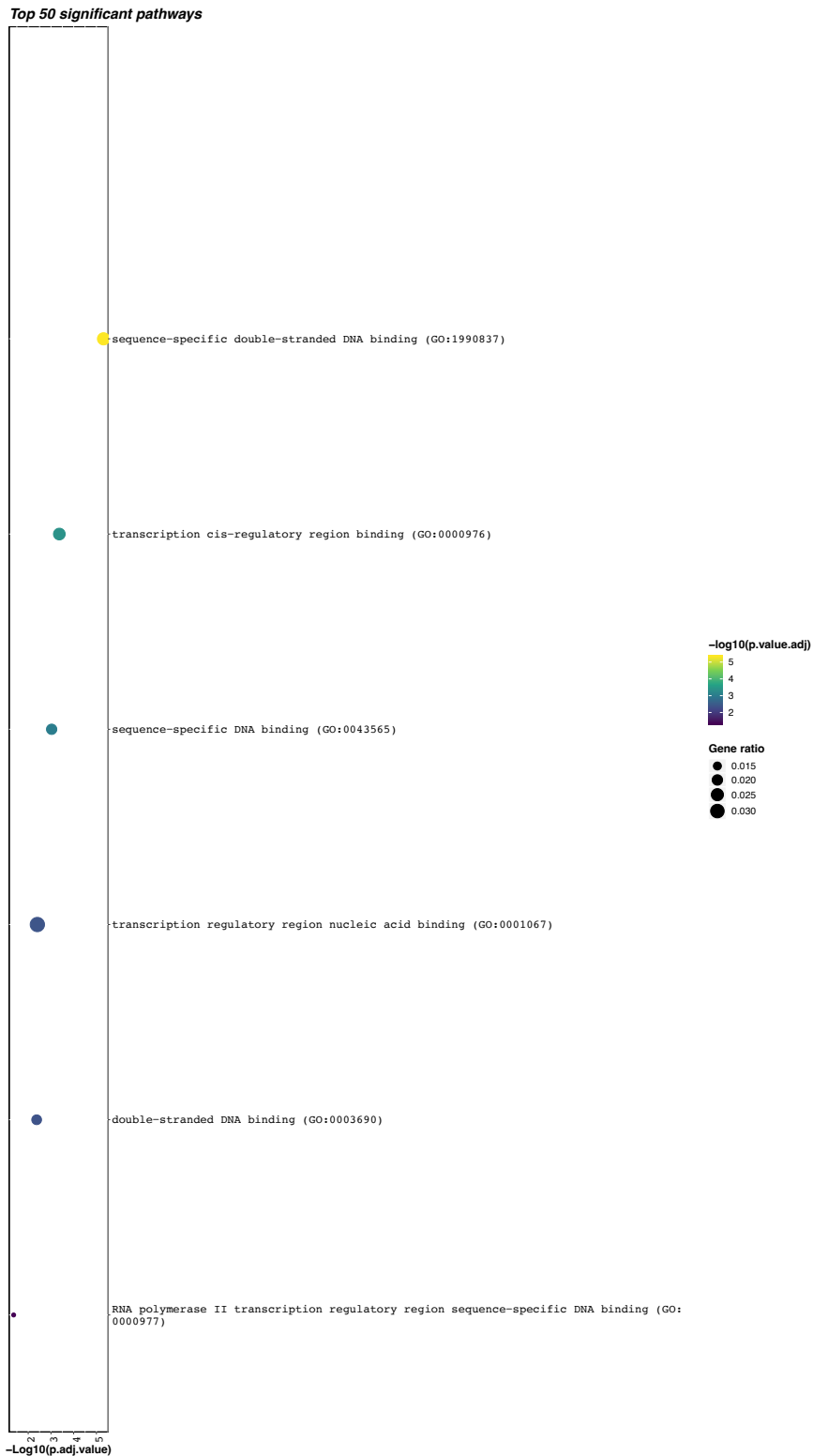


**Figure 24** – Summary of the most significant results (FDR<0.005) from the enrichment analysis when the cut-off of 10% (percent methylation difference) was used. Here, only hyper-methylated CpGs were considered.

**Top 50 significant pathways**

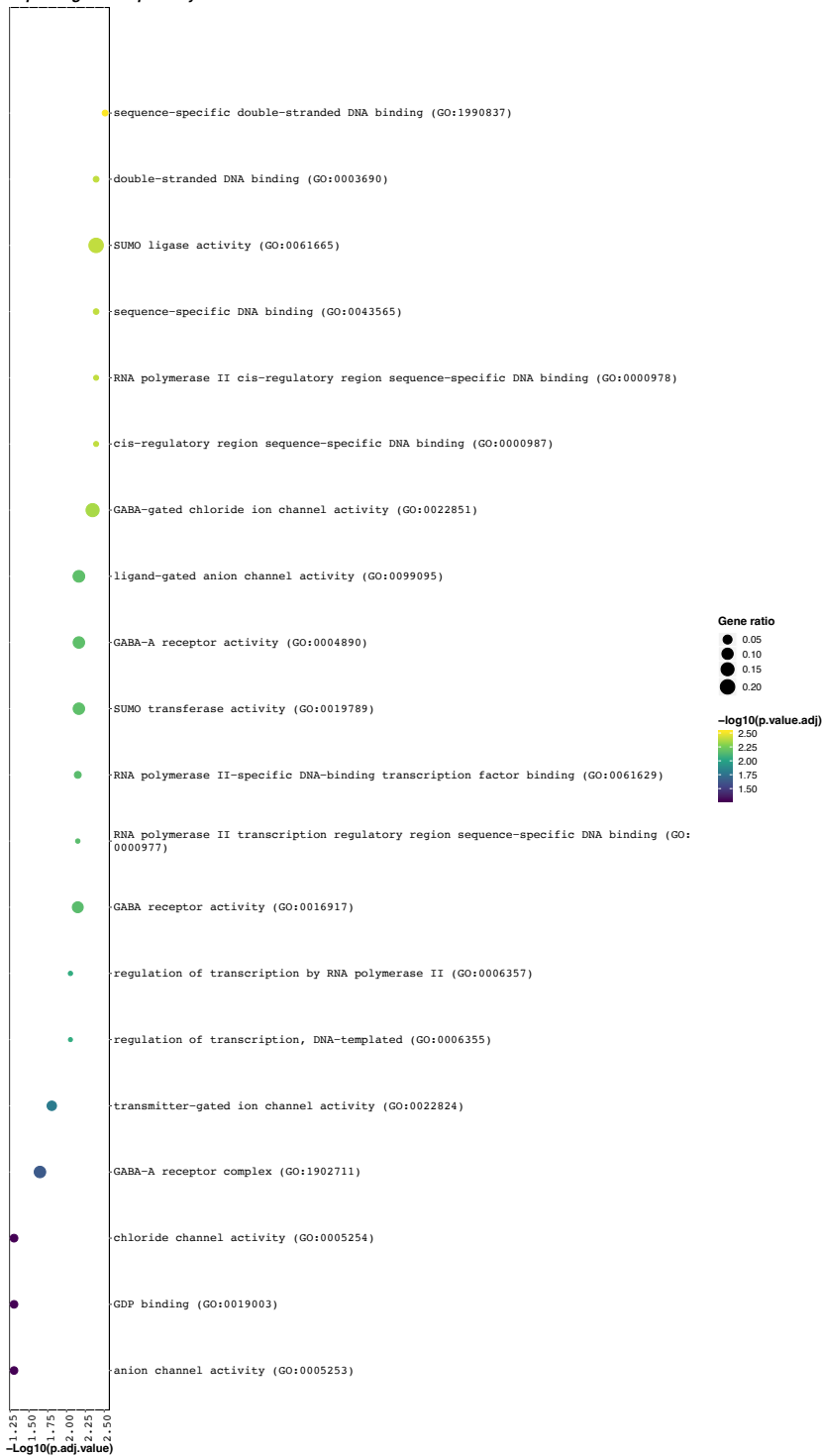


**Figure 25** – Summary of the most significant results ( $FDR < 0.005$ ) from the enrichment analysis when the cut-off of 10% (percent methylation difference) was used. Here, only hypo-methylated CpGs were considered.

### **6.2.3.2 – Differential methylation analysis of the target core samples**

The sample size was 161 cores. Given the filter on coverage of at least 5 reads per CpGs in at least 6 samples per group (32 LNI+ and 129 LNI-), we identified 19.5M of CpGs positions. The number of CpGs with percent methylation difference larger than 10% and  $FDR < 0.01$  was 1.362M (6.99% of all the tested cytosines). The number of CpGs with percent methylation difference larger than 25% and  $FDR < 0.01$  was 70 365 (0.17% of all the tested cytosines). The distribution of all tested CpGs (19.5M) across chromosomes is presented as bar plots in **Figure 26**. The distribution of all differentially methylated CpGs across chromosomes is presented as bar plots in **Figure 26**. Results were similar to those of the combined sample analysis, with chromosomes 16, 17, 19, being the most represented for either all and differentially methylated CpGs positions. When the analyses were stratified according to hyper- and hypomethylated CpGs, the distribution of differentially methylated cytosines on chromosomes was similar between hyper- and hypo-methylated regions. An abundance of hypo-methylated cytosines was observed again on chromosome 8, according to the 25% cutoff (**Figure 27**). The distribution of all and differentially methylated (with both cut-offs 10% and 25%) CpGs is depicted in cake plots in **Figure 28**. Here, promoters seemed to host the highest number of all covered CpGs. However, these figures decreased when only CpGs with differential methylation higher than 10% and 25% were considered. Here, the portions of the genome with the highest coverage of differentiated CpGs were introns and intergenic parts. When the analyses were stratified according to hyper- and hypo-methylated CpGs, the hyper-methylated cytosines, compared to the hypo-methylated counterparts, were enriched within genes' promoters and depleted on intergenic regions. These differences were much more evident when considering the 25% cutoff (**Figure 29**). Annotations of the differentially methylated CpGs on the HG38 were performed independently for the CpGs that were identified with cut-off 10% and 25%. The 1.362M CpGs derived from the use of 10% cut-off, were overlapping 18 401 CpG islands and 17 321 corresponding genes. However, when we considered only those CpGs islands containing at least 100 and 50 differentially methylated CpGs, the numbers of corresponding CpGs islands were 170 and 1 416, and the overlapping genes were 261 and 1 895, respectively. The results of the enrichment analysis for the 1 895 genes derived from the use of 10% cut-off, and located within those 1416 CpG islands with at least 50 differentially methylated CpGs can be



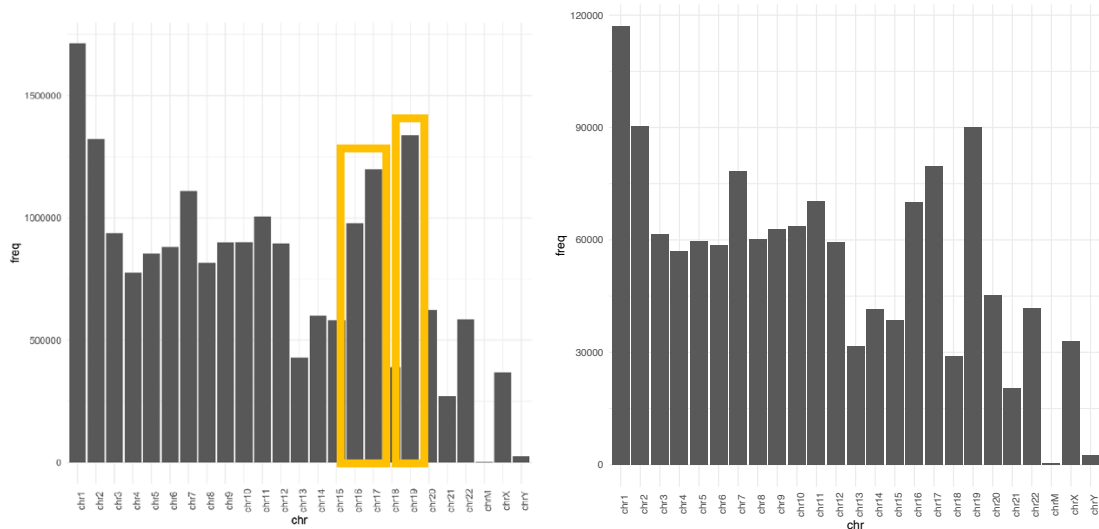


**Figure 26** – a) Bar plot of the distribution of all tested CpGs (19.5M) across chromosomes; b) bar plot of the distribution of all differentially methylated CpGs (cut-offs 10%) across chromosomes. Including only target samples. Figure for Cut-off 25% is available at this link:

[https://www.dropbox.com/s/n5xu8j1atfdgsj1/chr\\_distribution\\_diff\\_methyl.Target.FDR\\_01\\_diff\\_25.pdf?dl=0](https://www.dropbox.com/s/n5xu8j1atfdgsj1/chr_distribution_diff_methyl.Target.FDR_01_diff_25.pdf?dl=0).

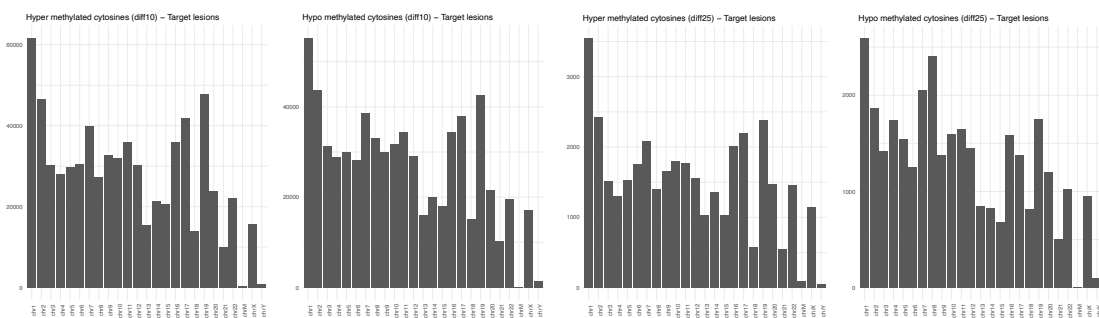


**Figure 27** – Left) Bar plot of the distribution of differentially (cut-off 10%) hyper-methylated CpGs (695 100) across chromosomes; Mid-left) Bar plot of the distribution of differentially (cut-off 10%) hypo-methylated CpGs (667 893) across chromosomes; Mid-right) Bar plot of the distribution of differentially (cut-off 25%) hyper-methylated CpGs (37741) across chromosomes; Right) Bar plot of the distribution of differentially (cut-off 25%) hypo-methylated CpGs (32 624) across chromosomes. Including only target samples.

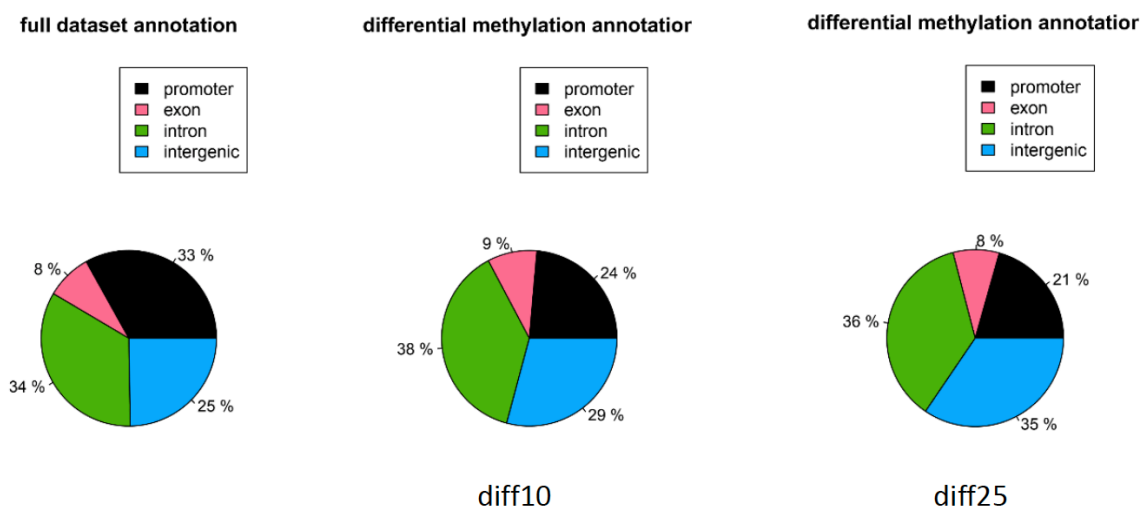


**Figure 28** – Cake plots of the distribution of all and differentially methylated (with both cut-offs 10% and 25%) CpGs in target samples.

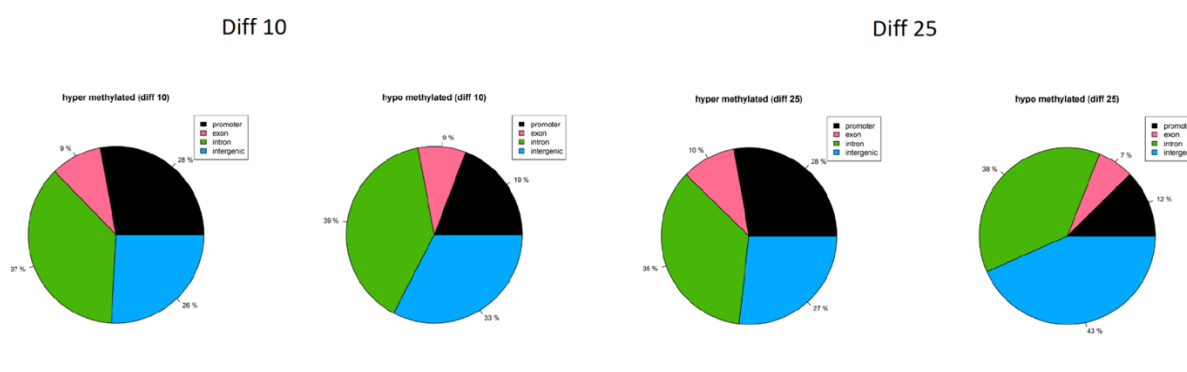


**Figure 29** – Left) cake plot of the distribution of differentially hyper-methylated (cut-off 10%) CpGs in target samples; Mid-left) cake plot of the distribution of differentially hypo-methylated (cut-off 10%) CpGs in target samples; Mid-right) cake plot of the distribution of differentially hyper-methylated (cut-off 25%) CpGs in target samples; Right) cake plot of the distribution of differentially hypo-methylated (cut-off 25%) CpGs in target samples.

found at this link:

[https://www.dropbox.com/scl/fi/fqvog0ue3qq6eh2kxv4v9/diff\\_methyl.Target.FDR\\_01\\_diff\\_10.CpGi\\_ENST.genes\\_50.enrichR.xlsx?dl=0&rlkey=zi6bj2zuc4akgk1pgn9gll4jr](https://www.dropbox.com/scl/fi/fqvog0ue3qq6eh2kxv4v9/diff_methyl.Target.FDR_01_diff_10.CpGi_ENST.genes_50.enrichR.xlsx?dl=0&rlkey=zi6bj2zuc4akgk1pgn9gll4jr).

After adjustment for multiple testing (FDR), only few pathways reached statistical significance (FDR <0.005), and only when the 10% cut-off was applied to select the genes. The most significant gene pathways are presented in **Figure 30**. The 70 365 CpGs derived from the use of 25% cut-off, were overlapping 3971 CpGs islands and 4401 associated genes. However, when we considered only those CpGs islands containing at least 30 and 10 differentially methylated CpGs, the numbers of corresponding CpGs islands were 37 and 361, and the overlapping genes were 53 and 474, respectively. The results of the enrichment analysis for the 474 genes derived from the use of 25% cut-off, and located within those 361 CpG islands with at least 10 differentially methylated CpGs can be found at this link:

[https://www.dropbox.com/scl/fi/7po7yonlyh2hl4yb0a79r3/diff\\_methyl.Target.FDR\\_01\\_diff\\_25.CpGi\\_ENST.genes\\_10.enrichR.xlsx?dl=0&rlkey=spimmyj0rn8zh3hrcgpy59r8g](https://www.dropbox.com/scl/fi/7po7yonlyh2hl4yb0a79r3/diff_methyl.Target.FDR_01_diff_25.CpGi_ENST.genes_10.enrichR.xlsx?dl=0&rlkey=spimmyj0rn8zh3hrcgpy59r8g)

No significant enrichment was reached with the list of genes that were selected using the 25% cut-off. Analyses were stratified according to hyper- and hypo-methylated CpGs. Here, only with the 10% cut-off, we reached statistically significant results. We found 695 100 differentially hyper-methylated cytosines, which overlapped 15 013 CpGs islands and 14974 genes. When only CpGs islands with at least 50 differentially hyper-methylated cytosines were considered, the number of selected genes was 891 within 629 islands. Enrichment results for these 891 genes can be found at this link:

[https://www.dropbox.com/scl/fi/tq87h4xjejown9n04oxed/diff\\_methyl.Target.FDR\\_01\\_diff\\_10\\_hyper.CpGi\\_ENST.genes\\_50.enrichR.xlsx?dl=0&rlkey=7v6va9z8gdji3z6pr1chr8t43](https://www.dropbox.com/scl/fi/tq87h4xjejown9n04oxed/diff_methyl.Target.FDR_01_diff_10_hyper.CpGi_ENST.genes_50.enrichR.xlsx?dl=0&rlkey=7v6va9z8gdji3z6pr1chr8t43).

The most significant gene pathways for genes with hyper-methylated cytosines are showed in **Figure 31**. Moreover, we found 667 893 differentially hypo-methylated cytosines, which overlapped 12 987 CpGs islands and 12 692 genes. When only CpGs islands with at least 50 differentially hyper-methylated cytosines were considered, the number of selected genes was 251 within 189 islands. Enrichment results for these 251 genes can be found at this link:

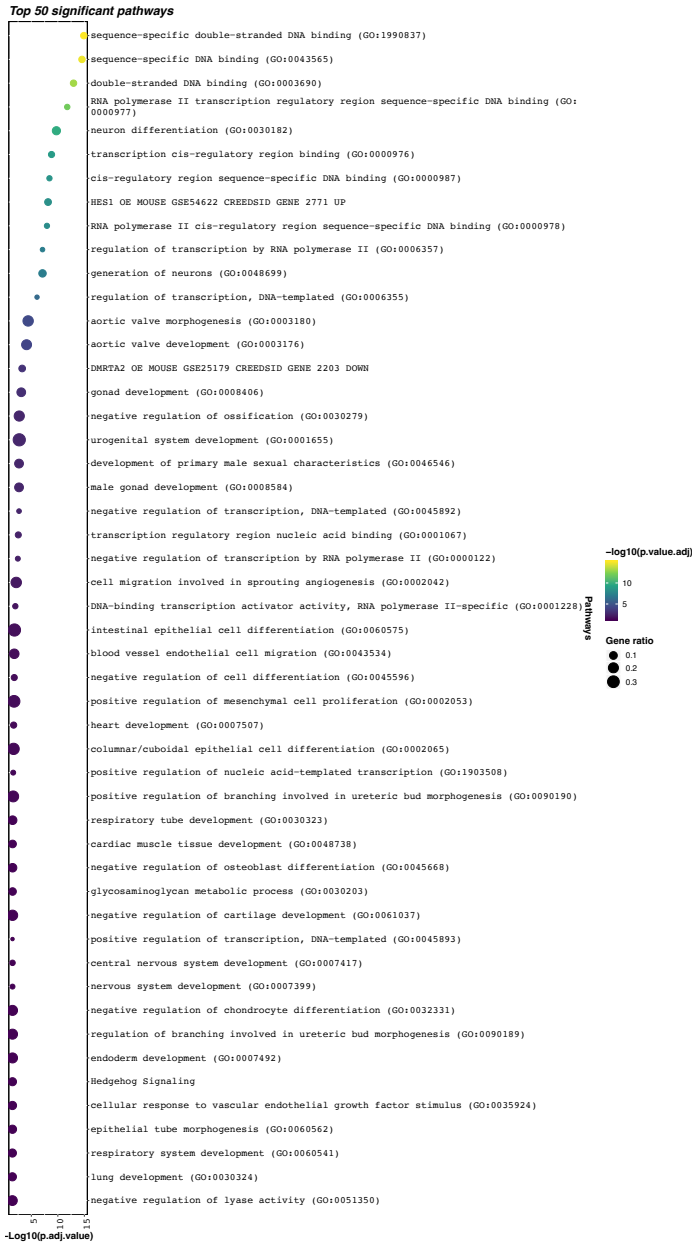


**Figure 30** – Summary of the most significant results ( $FDR < 0.005$ ) from the enrichment analysis when the cut-off of 10% (percent methylation difference) was used. Only target samples were included.

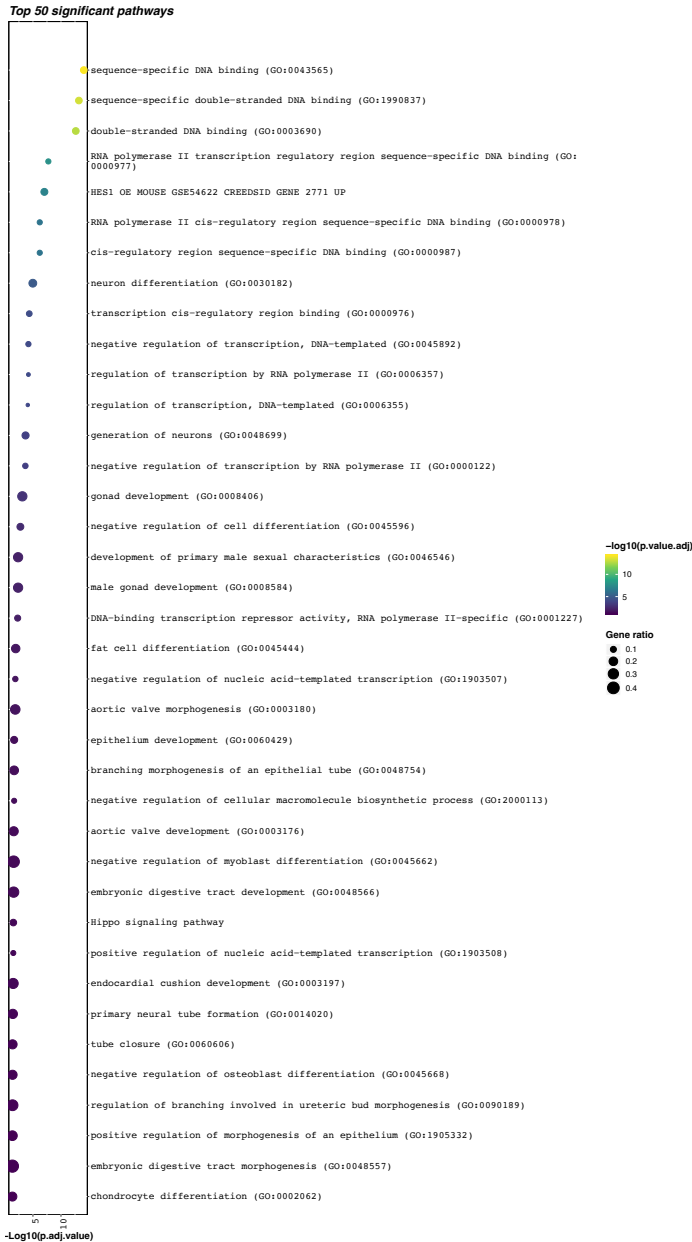


**Figure 31** – Summary of the most significant results (FDR<0.005) from the enrichment analysis when the cut-off of 10% (percent methylation difference) was used. Here, only hyper-methylated CpGs from target samples were considered.

[https://www.dropbox.com/scl/fi/tz9vpsvrk8v3ba2rminx9/diff\\_methyl.Target.FDR\\_01\\_diff\\_10\\_hypo.CpGi\\_ENST.genes\\_50.enrichR.xlsx?dl=0&rlkey=mdcn8rlk3wbrfpd42tstu15o4](https://www.dropbox.com/scl/fi/tz9vpsvrk8v3ba2rminx9/diff_methyl.Target.FDR_01_diff_10_hypo.CpGi_ENST.genes_50.enrichR.xlsx?dl=0&rlkey=mdcn8rlk3wbrfpd42tstu15o4).

The most significant gene pathways for genes with hypo-methylated cytosines are shown in **Figure 32**.

### **6.2.3.3 – Differential Methylation analysis of the systematic core samples**

The sample size was 163 cores. Given the filter on coverage of at least 5 reads per CpGs in at least 6 samples per group (31 LNI+ and 132 LNI-), we identified 15.8M of CpGs positions. The number of CpGs with percent methylation difference larger than 10% and FDR<0.01 was 1.254M (7.93% of all the tested cytosines). The number of CpGs with percent methylation difference larger than 25% and FDR<0.01 was 62 976 (0.4% of all the tested cytosines). The distribution of all tested CpGs (15.8M) across chromosomes is presented as bar plots in **Figure 33**. The distribution of all differentially methylated CpGs (for both cut-offs) across chromosomes is presented as bar plots in **Figure 33**. Results were similar to those of the combined and target sample analyses, with chromosomes 16, 17, 19, being the most represented for either all and differentially methylated CpGs positions. When the analyses were stratified according to hyper- and hypomethylated CpGs, there was an overall abundance of hypo-methylated cytosines, compared to the hyper-methylated counterpart. A peak of hypo-methylated cytosines was observed on chromosome 8, according to the 25% cutoff (**Figure 34**). The distribution of all and differentially methylated (with both cut-offs 10% and 25%) CpGs is depicted in cake plots in **Figure 35**. Here, promoters seemed to host the highest number of all covered CpGs. However, these figures decreased when only CpGs with differential methylation higher than 10% and 25% were considered. Here, the portions of the genome with the highest coverage of differentiated CpGs were introns and intergenic parts. When the analyses were stratified according to hyper- and hypomethylated CpGs, the distributions of hyper- and hypo-methylated cytosines across gene parts were similar when considering the 10% cutoff. At the same time, the hyper-methylated cytosines, compared to the hypo-methylated ones, were enriched within genes' promoters, and depleted on intergenic regions, when considering the 25% cutoff. (**Figure 36**). Annotations of the differentially methylated CpGs on the HG38 were performed independently for the CpGs that were

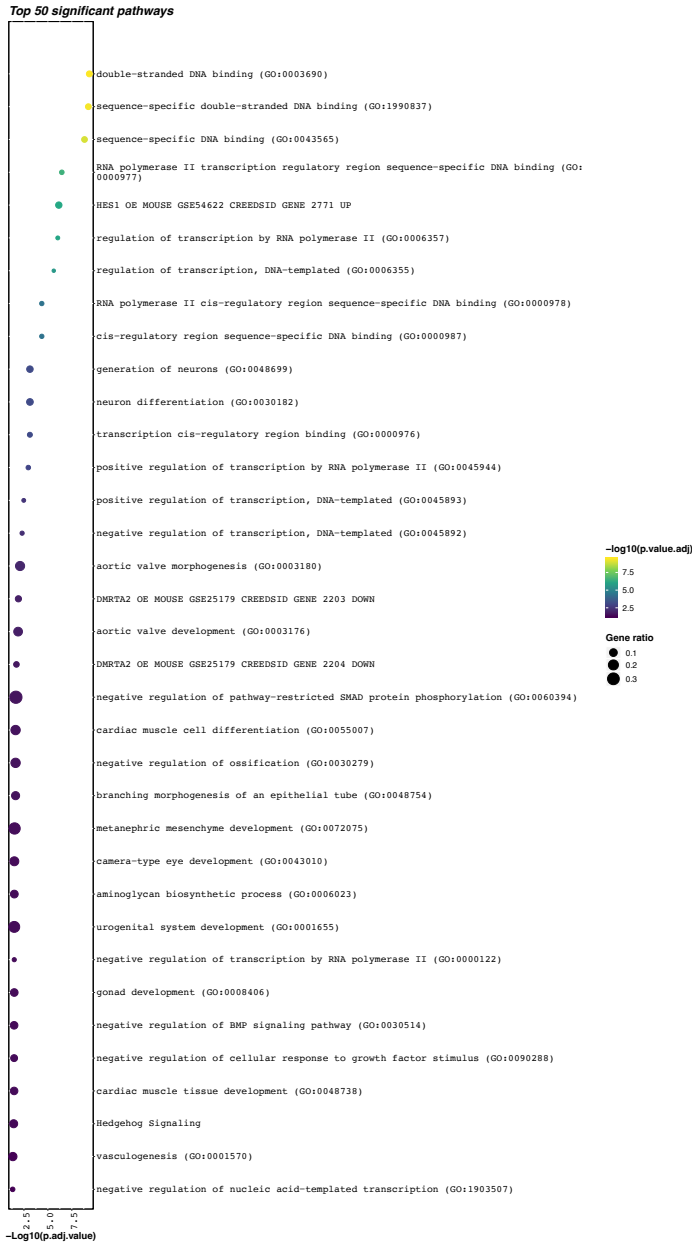


**Figure 32** – Summary of the most significant results ( $FDR < 0.005$ ) from the enrichment analysis when the cut-off of 10% (percent methylation difference) was used. Here, only hypo-methylated CpGs from target samples were considered.

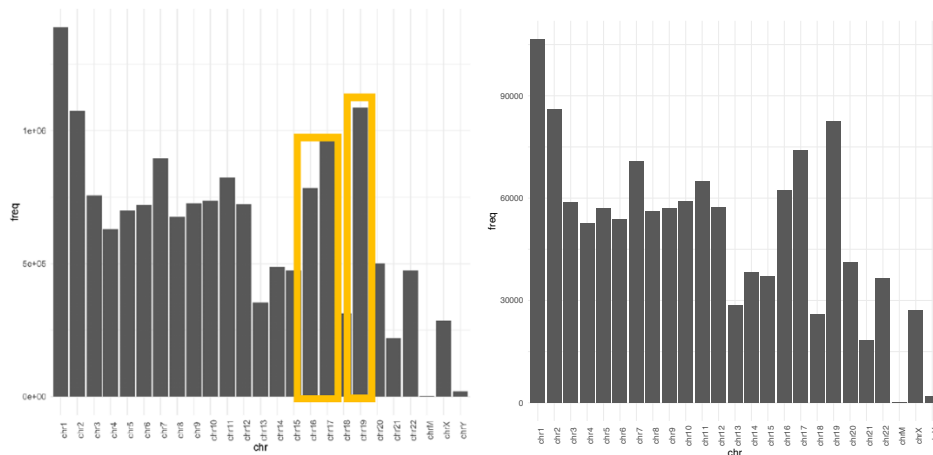


**Figure 33** – a) Bar plot of the distribution of all tested CpGs (15.8M) across chromosomes; b) bar plot of the distribution of all differentially methylated CpGs (cut-offs 10%) across chromosomes. Including only systematic samples. Figure for Cut-off 25% is available at this link:

[https://www.dropbox.com/s/te3kusqjg2izqbp/chr\\_distribution\\_diff\\_methyl.OffTarget.FDR\\_01\\_diff\\_25.pdf?dl=0](https://www.dropbox.com/s/te3kusqjg2izqbp/chr_distribution_diff_methyl.OffTarget.FDR_01_diff_25.pdf?dl=0)

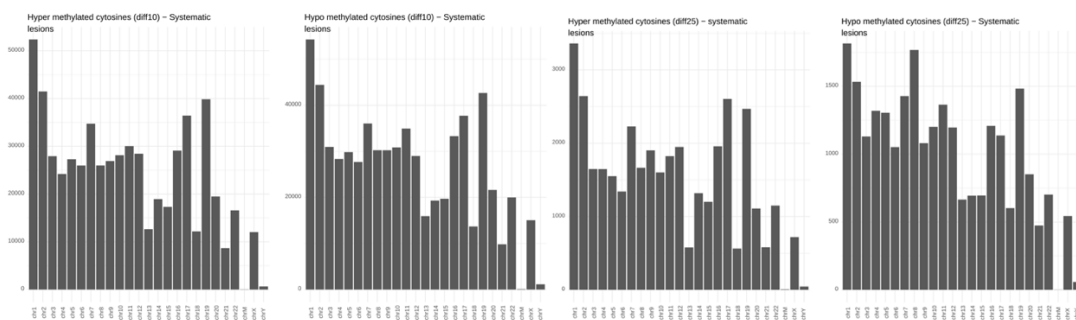


**Figure 34** – Left) Bar plot of the distribution of differentially (cut-off 10%) hyper-methylated CpGs (597250) across chromosomes; Mid-Left) Bar plot of the distribution of differentially (cut-off 10%) hypo-methylated CpGs (656833) across chromosomes; Mid-Right) Bar plot of the distribution of differentially (cut-off 25%) hyper-methylated CpGs (37670) across chromosomes; Right) Bar plot of the distribution of differentially (cut-off 25%) hypo-methylated CpGs (25306) across chromosomes. Including only systematic samples.



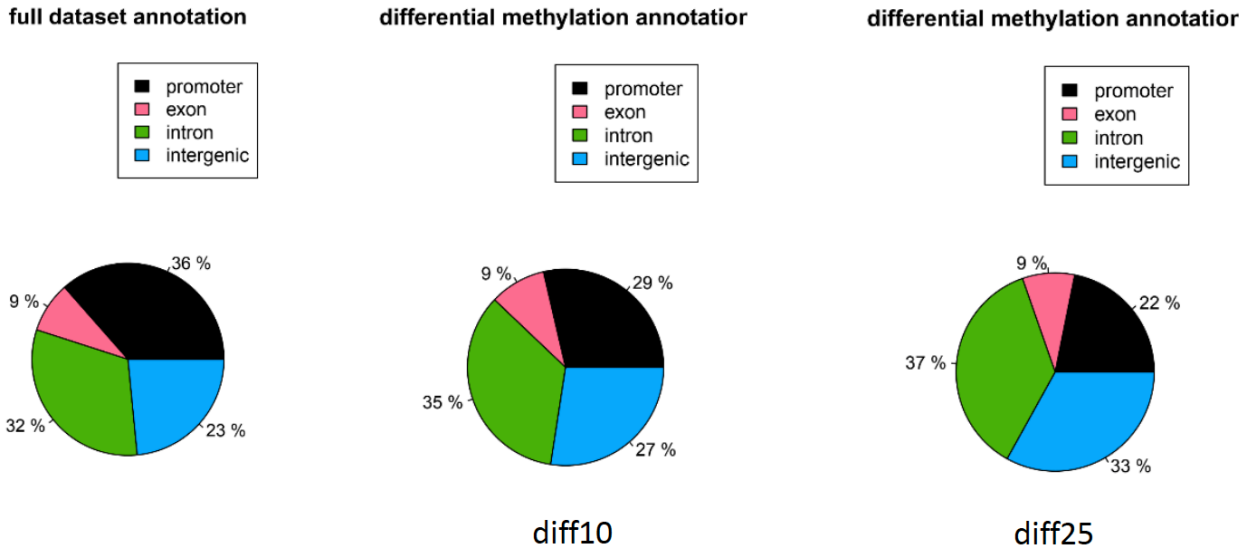


**Figure 35** – Cake plots of the distribution of all and differentially methylated (with both cut-offs 10% and 25%) CpGs in systematic samples.

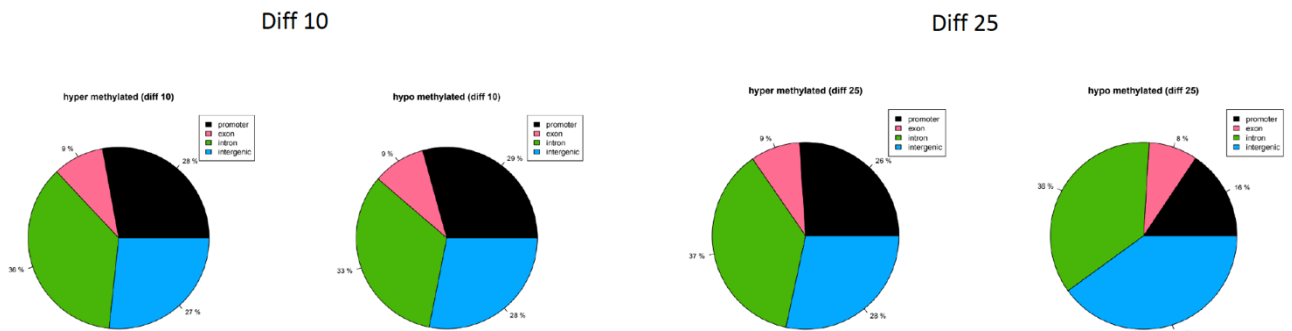


**Figure 36** – Left) cake plot of the distribution of differentially hyper-methylated (cut-off 10%) CpGs in target samples; Mid-Left) cake plot of the distribution of differentially hypo-methylated (cut-off 10%) CpGs in target samples; Mid-Right) cake plot of the distribution of differentially hyper-methylated (cut-off 25%) CpGs in target samples; Right) cake plot of the distribution of differentially hypo-methylated (cut-off 25%) CpGs in systematic samples.

identified with cut-off 10% and 25%. The 1.254M CpGs derived from the use of 10% cut-off, were overlapping 18 502 CpG islands and 17 501 associated genes. However, when we considered only those CpGs islands containing at least 100 and 50 differentially methylated CpGs, the number of corresponding CpGs islands were 243 and 1 749 and the overlapping genes were 359 and 2 379, respectively. The results of the enrichment analysis for the 2379 genes derived from the use of 10% cut-off, and located within those 1 749 CpG islands with at least 50 differentially methylated CpGs can be found at this link:

[https://www.dropbox.com/scl/fi/0h285sbdxclsv76051hx8/diff\\_methyl.OffTarget.FDR\\_01\\_diff\\_10.CpGi\\_ENST.genes\\_50.enrichR.xlsx?dl=0&rlkey=5nd1x5zc0oyx7dnb9ca6p289u](https://www.dropbox.com/scl/fi/0h285sbdxclsv76051hx8/diff_methyl.OffTarget.FDR_01_diff_10.CpGi_ENST.genes_50.enrichR.xlsx?dl=0&rlkey=5nd1x5zc0oyx7dnb9ca6p289u).

After adjustment for multiple testing (FDR), only few pathways reached the statistical significance (FDR <0.005), and only when the 10% cut-off was applied to select the genes. The most significant gene pathways are presented in **Figure 37**. The 62 976 CpGs derived from the use of 25% cut-off, were overlapping 3 862 CpGs islands and 4 409 associated genes. However, when we considered only those CpGs islands containing at least 30 and 10 differentially methylated CpGs, the number of corresponding CpGs islands were 37 and 329 and the overlapping genes were 51 and 446, respectively. The results of the enrichment analyses for the 446 genes derived from the use of 25% cut-off, and located within those 329 CpG islands with at least 10 differentially methylated CpGs can be found at this link:

[https://www.dropbox.com/scl/fi/1dgdda128dy284q15kxco/diff\\_methyl.OffTarget.FDR\\_01\\_diff\\_25.CpGi\\_ENST.genes\\_10.enrichR.xlsx?dl=0&rlkey=xc6gsqzwcgkce5qosgryt4ykr](https://www.dropbox.com/scl/fi/1dgdda128dy284q15kxco/diff_methyl.OffTarget.FDR_01_diff_25.CpGi_ENST.genes_10.enrichR.xlsx?dl=0&rlkey=xc6gsqzwcgkce5qosgryt4ykr).

No significant enrichment was reached with the list of genes that were selected using the 25% cut-off. Analyses were stratified according to hyper- and hypo-methylated CpGs. Here, only with the 10% cut-off we reached statistically significant results. We found 597 250 differentially hyper-methylated cytosines, which overlapped 13 571 CpGs islands and 13 909 genes. When only CpGs islands with at least 50 differentially hyper-methylated cytosines were considered, the number of selected genes was 571 within 400 islands. Enrichment results for these 571 genes can be found at this link:

[https://www.dropbox.com/scl/fi/uxnnc84gm4e5jlc3iieeo/diff\\_methyl.OffTarget.FDR\\_01\\_diff\\_10\\_hyper.CpGi\\_ENST.genes\\_50.enrichR.xlsx?dl=0&rlkey=qp2rxtghr12g2aoivn078x5g8](https://www.dropbox.com/scl/fi/uxnnc84gm4e5jlc3iieeo/diff_methyl.OffTarget.FDR_01_diff_10_hyper.CpGi_ENST.genes_50.enrichR.xlsx?dl=0&rlkey=qp2rxtghr12g2aoivn078x5g8).

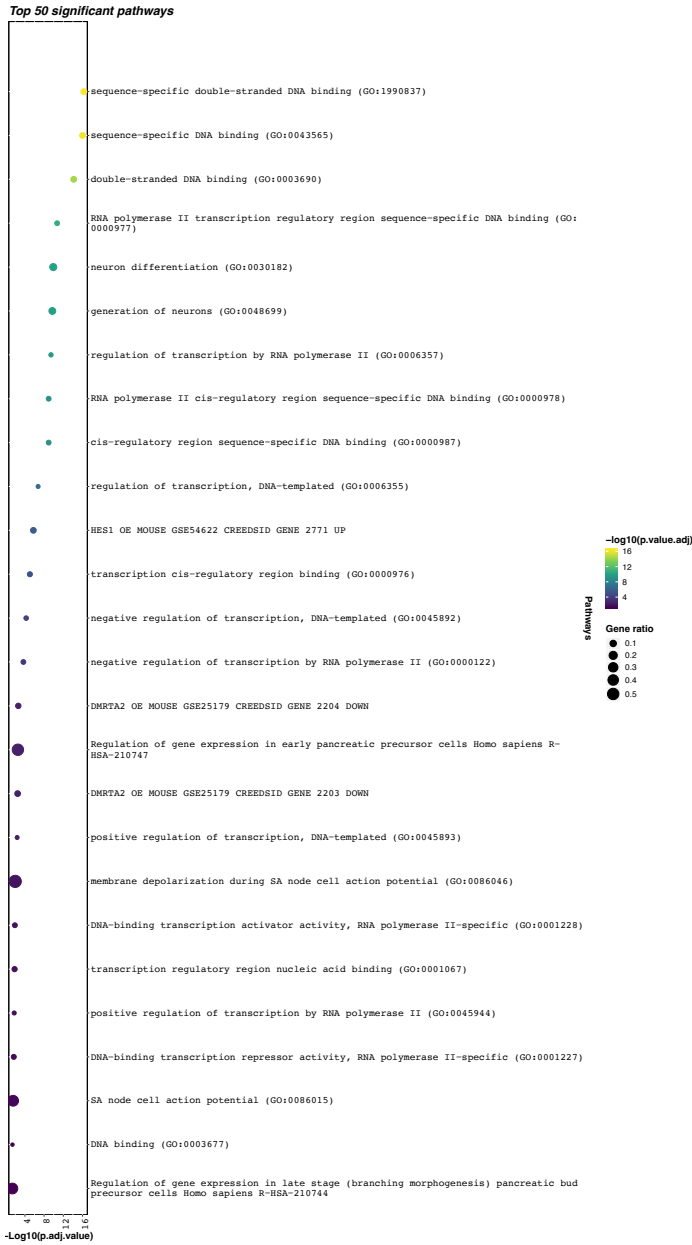


**Figure 37** – Summary of the most significant results (FDR<0.005) from the enrichment analysis when the cut-off of 10% (percent methylation difference) was used. Only systematic samples were included.

The most significant gene pathways for genes with hyper-methylated cytosines are shown in **Figure 38**. Moreover, we found 656 833 differentially hypo-methylated cytosines, which overlapped 15 101 CpGs islands and 14 783 genes. When only CpGs islands with at least 50 differentially hypo-methylated cytosines were considered, the number of selected genes was 858 within 577 islands. Enrichment results for these 858 genes can be found at this link:

[https://www.dropbox.com/scl/fi/lb3mf2f2uow2usio0w2pa/diff\\_methyl.OffTarget.FDR\\_01\\_diff\\_10\\_hypo.CpGi\\_ENST.genes\\_50.enrichR.xlsx?dl=0&rlkey=ejsrlqpf8sd8xp3x0x5mclibp](https://www.dropbox.com/scl/fi/lb3mf2f2uow2usio0w2pa/diff_methyl.OffTarget.FDR_01_diff_10_hypo.CpGi_ENST.genes_50.enrichR.xlsx?dl=0&rlkey=ejsrlqpf8sd8xp3x0x5mclibp).

The most significant gene pathways for genes with hypo-methylated cytosines are shown in **Figure 39**.

#### ***6.2.3.4 – Overlap among differential methylation analyses of target, systematic, and combined samples using different cut-offs***

The number of overlapping genes among those identified in the three group analyses, when 10% cut-off and at least 50 differentially methylated CpGs per island were considered, is shown in **Figure 40**. Here, 233 genes were in common among the three group analyses and they are listed at this link:

([https://www.dropbox.com/scl/fi/d0dwxelh2ta7sson3jfy/common\\_genes\\_diff10\\_genes\\_50.xlsx?dl=0&rlkey=ttqh2uljybk39ukvvse840ikg](https://www.dropbox.com/scl/fi/d0dwxelh2ta7sson3jfy/common_genes_diff10_genes_50.xlsx?dl=0&rlkey=ttqh2uljybk39ukvvse840ikg)). The number of overlapping genes among those identified in the three group analyses, when 25% cut-off and at least 10 differentially methylated CpGs per island were considered, is shown in **Figure 41**. Here, 6 genes were in common among the three groups of analysis and they were *CBX4*, *CHD5*, *ENSG00000285629*, *ENSG00000287655*, *RNF126*, *SHTN1*.

#### ***6.2.3.5 – Overlapping results of the enrichment analyses***

The top 15 highly significant genomic pathways for the three enrichment analyses of combined, target, and systematic samples are graphically reported in **Figure 42**. Results are reported also for hyper and hypomethylated genomic pathways, independently (**Figure 43** and **Figure 44**). The pathways reaching higher statistical significance across all groups were: sequence-specific double-stranded DNA binding (GO:1990837), sequence-specific DNA binding (GO:0043565), double-stranded DNA binding

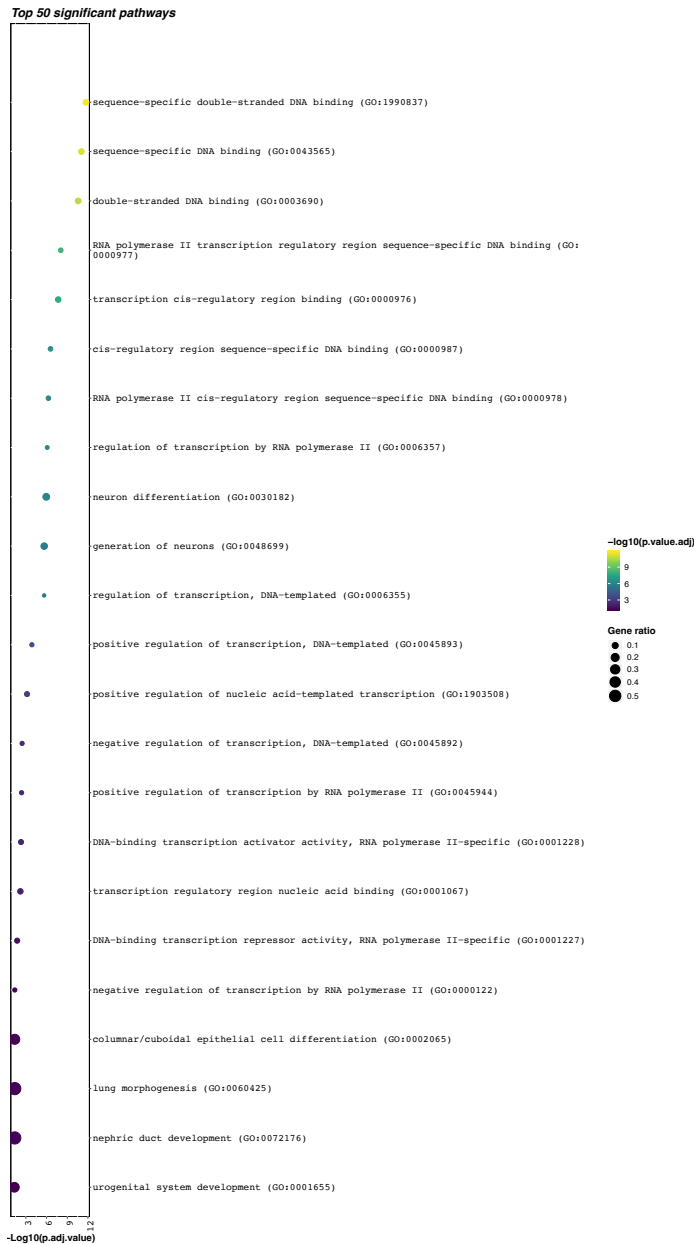


**Figure 38** – Summary of the most significant results ( $FDR < 0.005$ ) from the enrichment analysis when the cut-off of 10% (percent methylation difference) was used. Here, only hyper-methylated CpGs from systematic samples were considered.

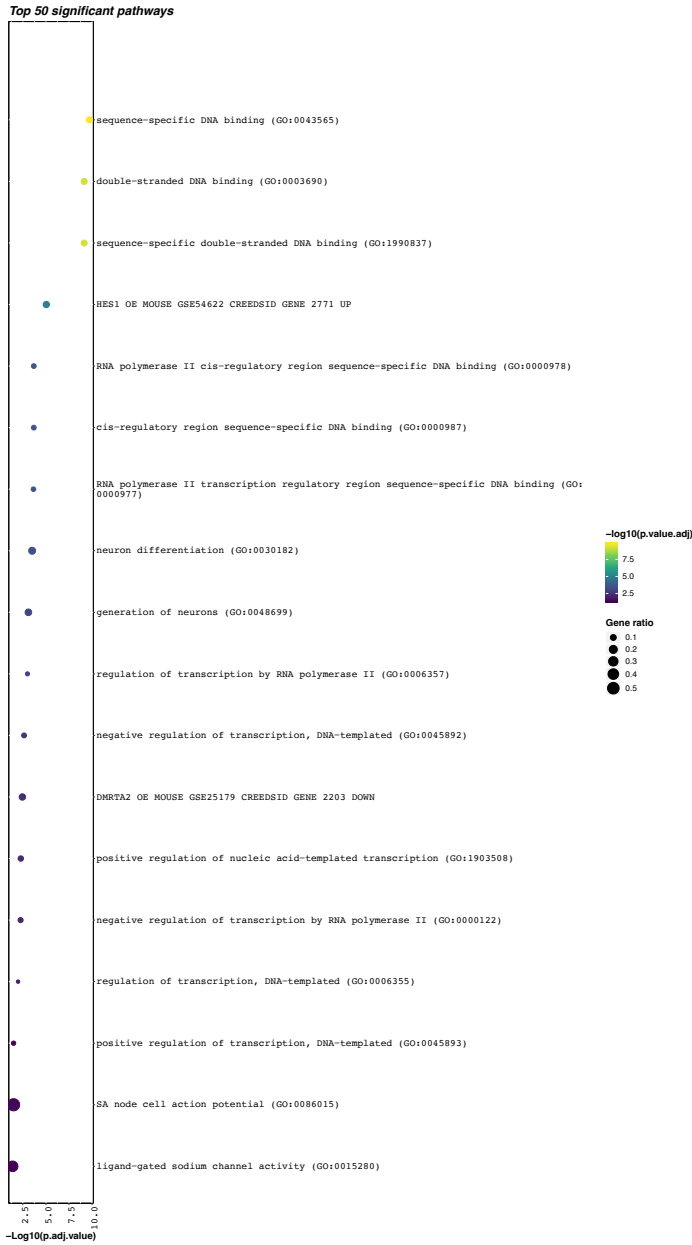


**Figure 39** – Summary of the most significant results ( $FDR < 0.005$ ) from the enrichment analysis when the cut-off of 10% (percent methylation difference) was used. Here, only hypo-methylated CpGs from systematic samples were considered.

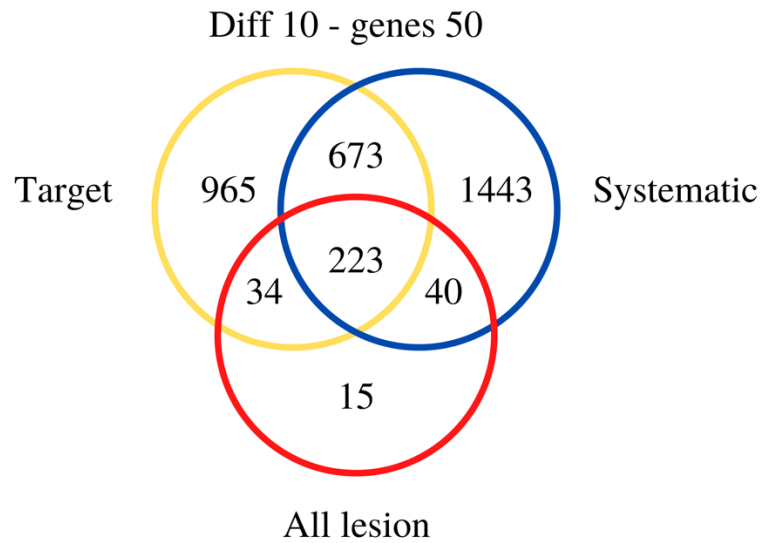


**Figure 40**– Overlapping genes among combined, target, and systematic samples when the 10% cut-off and at least 50 differentially methylated CpGs per island were considered. The list of the 223 common genes is available at this link: [https://www.dropbox.com/scl/fi/d0dwxelh2ta7ssson3jfy/common\\_genes\\_diff10\\_genes50.xlsx?dl=0&rlkey=ttqh2uljybk39ukvvse840ikg](https://www.dropbox.com/scl/fi/d0dwxelh2ta7ssson3jfy/common_genes_diff10_genes50.xlsx?dl=0&rlkey=ttqh2uljybk39ukvvse840ikg)

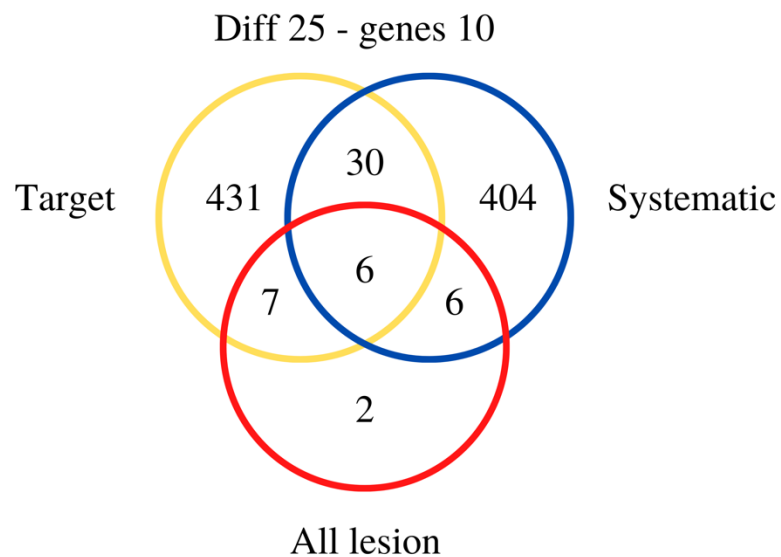


**Figure 41** – Overlapping genes among combined, target, and systematic samples when the 25% cut-off and at least 10 differentially methylated CpGs per island were considered.

Overall	Target	Systematic
sequence-specific double-stranded DNA binding (GO:1990837)	sequence-specific DNA binding (GO:0043565)	sequence-specific DNA binding (GO:0043565)
sequence-specific DNA binding (GO:0043565)	sequence-specific double-stranded DNA binding (GO:1990837)	sequence-specific double-stranded DNA binding (GO:1990837)
double-stranded DNA binding (GO:0003690)	double-stranded DNA binding (GO:0003690)	double-stranded DNA binding (GO:0003690)
cis-regulatory region sequence-specific DNA binding (GO:0000987)	HES1 OE MOUSE GSE54622 CREEDSID GENE 2771 UP	neuron differentiation (GO:0030182)
RNA polymerase II transcription regulatory region sequence-specific DNA binding (GO:0000977)	neuron differentiation (GO:0030182)	generation of neurons (GO:0048699)
RNA polymerase II cis-regulatory region sequence-specific DNA binding (GO:0000978)	RNA polymerase II transcription regulatory region sequence-specific DNA binding (GO:0000977)	positive regulation of nucleic acid-templated transcription (GO:1903508)
regulation of transcription by RNA polymerase II (GO:0006357)	RNA polymerase II cis-regulatory region sequence-specific DNA binding (GO:0000978)	transcription cis-regulatory region binding (GO:0000976)
neuron differentiation (GO:0030182)	cis-regulatory region sequence-specific DNA binding (GO:0000987)	RNA polymerase II transcription regulatory region sequence-specific DNA binding (GO:0000977)
regulation of transcription, DNA-templated (GO:0006355)	regulation of transcription, DNA-templated (GO:0006355)	cis-regulatory region sequence-specific DNA binding (GO:0000987)
positive regulation of transcription, DNA-templated (GO:0045893)	generation of neurons (GO:0048699)	RNA polymerase II cis-regulatory region sequence-specific DNA binding (GO:0000978)
HES1 OE MOUSE GSE54622 CREEDSID GENE 2771 UP	regulation of transcription by RNA polymerase II (GO:0006357)	cis-regulatory region sequence-specific DNA binding (GO:0000987)
generation of neurons (GO:0048699)	transcription cis-regulatory region binding (GO:0000976)	nervous system development (GO:0007399)
transcription cis-regulatory region binding (GO:0000976)	EOMES OE HUMAN GSE43805 CREEDSID GENE 92 UP	regulation of transcription by RNA polymerase II (GO:0006357)
transcription regulatory region nucleic acid binding (GO:0001067)	negative regulation of transcription, DNA-templated (GO:0045892)	positive regulation of transcription, DNA-templated (GO:0045893)
positive regulation of transcription by RNA polymerase II (GO:0045944)	negative regulation of cell differentiation (GO:0045596)	regulation of transcription, DNA-templated (GO:0006355)

**Figure 42** – Top 15 highly significant genomic pathways for overall, target, and systematic samples. Similar pathways among the three groups are identified with the same colors.



Overall	Target	Systematic
sequence-specific double-stranded DNA binding (GO:1990837)	sequence-specific DNA binding (GO:0043565)	sequence-specific double-stranded DNA binding (GO:1990837)
transcription cis-regulatory region binding (GO:0000976)	sequence-specific double-stranded DNA binding (GO:1990837)	sequence-specific DNA binding (GO:0043565)
sequence-specific DNA binding (GO:0043565)	double-stranded DNA binding (GO:0003690)	double-stranded DNA binding (GO:0003690)
transcription regulatory region nucleic acid binding (GO:0001067)	RNA polymerase II transcription regulatory region sequence-specific DNA binding (GO:0000977)	RNA polymerase II transcription regulatory region sequence-specific DNA binding (GO:0000977)
double-stranded DNA binding (GO:0003690)	HES1 OE MOUSE GSE54622 CREEDSID GENE 2771 UP	transcription cis-regulatory region binding (GO:0000976)
RNA polymerase II transcription regulatory region sequence-specific DNA binding (GO:0000977)	RNA polymerase II cis-regulatory region sequence-specific DNA binding (GO:0000978)	cis-regulatory region sequence-specific DNA binding (GO:0000987)

**Figure 43** – Top 6 highly significant genomic pathways considering hypermethylated CpGs for overall, target, and systematic samples. Similar pathways among the three groups are identified with the same colors. Here, only 6 pathways were considered given that the overall sample analysis only identified only 6 significant pathways (FDR<0.05)

Overall	Target	Systematic
sequence-specific double-stranded DNA binding (GO:1990837)	double-stranded DNA binding (GO:0003690)	sequence-specific DNA binding (GO:0043565)
double-stranded DNA binding (GO:0003690)	sequence-specific double-stranded DNA binding (GO:1990837)	double-stranded DNA binding (GO:0003690)
SUMO ligase activity (GO:0061665)	sequence-specific DNA binding (GO:0043565)	sequence-specific double-stranded DNA binding (GO:1990837)
sequence-specific DNA binding (GO:0043565)	RNA polymerase II transcription regulatory region sequence-specific DNA binding (GO:0000977)	HES1 OE MOUSE GSE54622 CREEDSID GENE 2771 UP
RNA polymerase II cis-regulatory region sequence-specific DNA binding (GO:0000978)	HES1 OE MOUSE GSE54622 CREEDSID GENE 2771 UP	RNA polymerase II cis-regulatory region sequence-specific DNA binding (GO:0000978)
cis-regulatory region sequence-specific DNA binding (GO:0000987)	regulation of transcription by RNA polymerase II (GO:0006357)	cis-regulatory region sequence-specific DNA binding (GO:0000987)
GABA-gated chloride ion channel activity (GO:0022851)	regulation of transcription, DNA-templated (GO:0006355)	RNA polymerase II transcription regulatory region sequence-specific DNA binding (GO:0000977)
ligand-gated anion channel activity (GO:0099095)	RNA polymerase II cis-regulatory region sequence-specific DNA binding (GO:0000978)	neuron differentiation (GO:0030182)
GABA-A receptor activity (GO:0004890)	cis-regulatory region sequence-specific DNA binding (GO:0000987)	generation of neurons (GO:0048699)
SUMO transferase activity (GO:0019789)	generation of neurons (GO:0048699)	regulation of transcription by RNA polymerase II (GO:0006357)
RNA polymerase II-specific DNA-binding transcription factor binding (GO:0061629)	neuron differentiation (GO:0030182)	negative regulation of transcription, DNA-templated (GO:0045892)
RNA polymerase II transcription regulatory region sequence-specific DNA binding (GO:0000977)	transcription cis-regulatory region binding (GO:0000976)	DMRTA2 OE MOUSE GSE25179 CREEDSID GENE 2203 DOWN
GABA receptor activity (GO:0016917)	positive regulation of transcription by RNA polymerase II (GO:0045944)	positive regulation of nucleic acid-templated transcription (GO:1903508)
regulation of transcription by RNA polymerase II (GO:0006357)	positive regulation of transcription, DNA-templated (GO:0045893)	negative regulation of transcription by RNA polymerase II (GO:0000122)
regulation of transcription, DNA-templated (GO:0006355)	negative regulation of transcription, DNA-templated (GO:0045892)	regulation of transcription, DNA-templated (GO:0006355)

**Figure 44** – Top 15 highly significant genomic pathways considering hypomethylated CpGs for overall, target, and systematic samples. Similar pathways among the three groups are identified with the same colors.

(GO:0003690), and RNA polymerase II transcription regulatory region sequence-specific DNA binding (GO:0000977). Among pathways that were not associated with the regulation of DNA transcription, neuron differentiation (GO:0030182) reached the highest statistical significance in combined, target, and systematic samples.

#### **6.2.4 – Developing models integrating epigenetic, clinical and mp-MRI features**

##### **6.2.4.1 – Identification of highly differentially methylated CpGs sites**

Imposing a cut-off of 50% for absolute change in methylation status and FDR<0.01, we reached a list of 508 highly differentially methylated CpGs sites for target samples and 551 for systematic samples. None of the identified CpGs were commonly shared among target and systematic samples. The number of corresponding CpG islands and genes of the target CpG positions were 68 and 360, respectively. The number of corresponding CpG islands and genes for systematic CpG positions were 106 and 411, respectively. Even with no site-specific CpGs positions in common, 18 genes were commonly shared among target and systematic samples: *ANO2*, *CDH4*, *CSMD1*, *CSMD3*, *DPP10*, *LINC01166*, *LINGO2*, *MIR3667HG*, *RAI1*, *RBFOX1*, *RIMBP2*, *SBNO2*, *SCAMP5*, *SEMA3A*, *TMEM132C*, *TP73*, *TSPEAR*, *WSCD2*. The full list of highly differentially methylated CpGs and corresponding CpGs islands and genes is available, for either target and systematic samples, at this link:

[https://www.dropbox.com/scl/fi/j9mv2cy03lgbkime4975m/diff\\_methyl.Target.FDR\\_01\\_diff\\_50.xlsx?dl=0&rlkey=v9l15v76pc1ez6x8yzjn1fz87](https://www.dropbox.com/scl/fi/j9mv2cy03lgbkime4975m/diff_methyl.Target.FDR_01_diff_50.xlsx?dl=0&rlkey=v9l15v76pc1ez6x8yzjn1fz87) (Target).

[https://www.dropbox.com/scl/fi/eoy8rf6q85k1rbu65ox3b/diff\\_methyl.OffTarget.FDR\\_01\\_diff\\_50.xlsx?dl=0&rlkey=w0u0v7usbtxwy0vsjg8y3dcpy](https://www.dropbox.com/scl/fi/eoy8rf6q85k1rbu65ox3b/diff_methyl.OffTarget.FDR_01_diff_50.xlsx?dl=0&rlkey=w0u0v7usbtxwy0vsjg8y3dcpy) (Systematic).

The genomic distribution of highly differentially methylated CpGs for target and systematic samples is reported in **Figure 45**. Enrichment analysis of highly differentially methylated CpGs did not reach statistically significant results for the CpGs that were identified from the systematic sample analysis. Conversely, 6 gene pathways were significantly associated with the highly differentially methylated CpGs that were identified from the target sample analysis. The corresponding pathways matched with genes involved in potassium channel regulators, potassium channel complex and regulation of potassium ion transport (**Figure 46**).

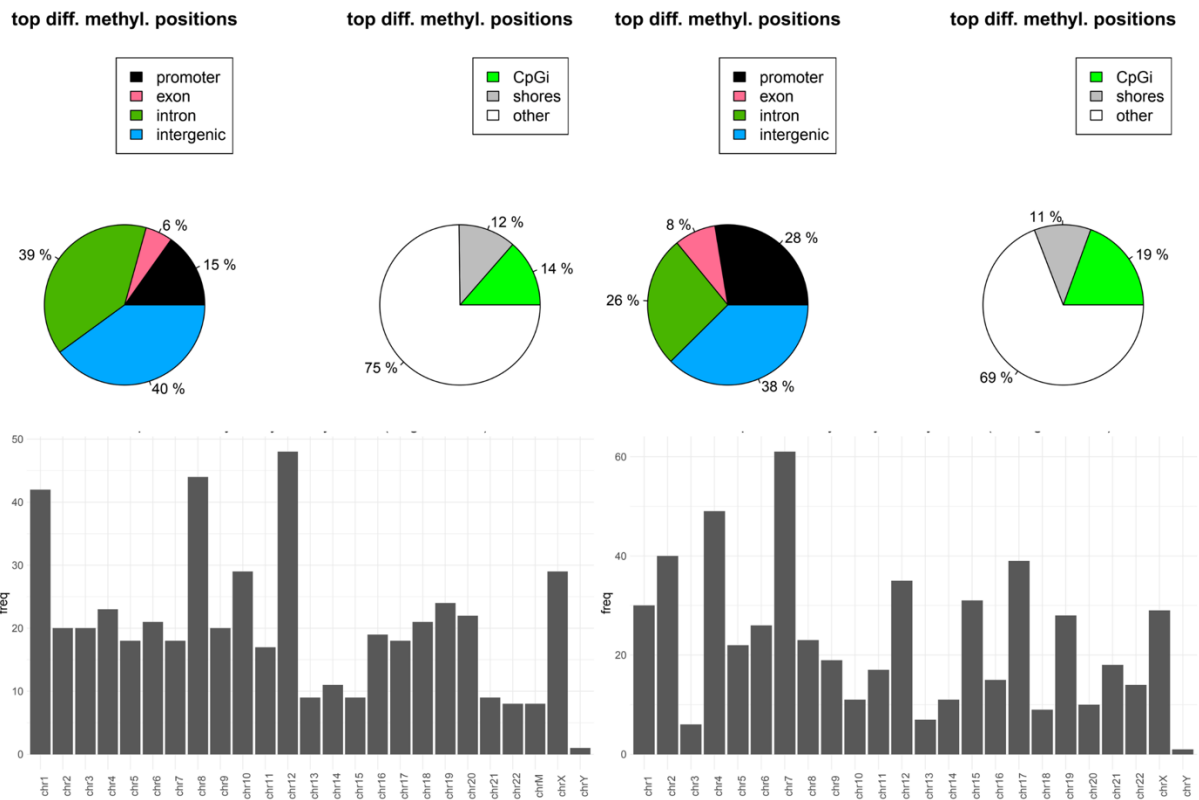


**Figure 45** – Cake plots and histograms depicting the genomic and chromosomal distribution of highly differentially methylated CpGs among target (left) and systematic (right) samples

**Top 50 significant pathways**

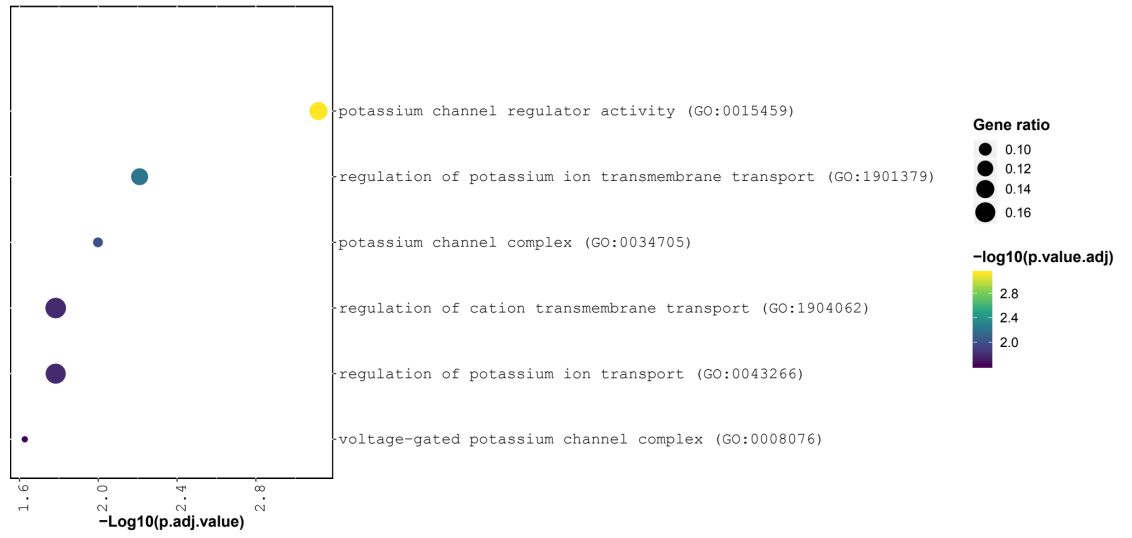


**Figure 46** – Enrichment analysis for the highly differentially methylated CpGs that were identified in the target sample analysis (FDR<0.005)

#### ***6.2.4.2 – Developing epigenetic signatures with hypermethylated CpGs***

The average methylation status for the hypermethylated CpGs sites of the target samples was highly associated with LNI risk (log Odds ratio: 0.12; 95% CI: 0.08-0.16,  $p < 0.001$ ). The same was confirmed also for the average methylation status of the hypermethylated CpGs sites of the systematic samples (log Odds ratio: 0.08; 95% CI: 0.05-0.11,  $p < 0.001$ ). The AUC of the hypermethylation score derived from target samples was higher than that from systematic samples 84.0% vs. 75.5%.

#### ***6.2.4.3 – Integrating epigenetic, clinical, and mp-MRI features***

Among all clinical and mp-MRI variables, we selected PSA at biopsy (ng/ml), T stage at mp-MRI (organ confined; EC; SVI), ISUP Gleason grade group of the target lesion (1-2, 3, 4-5) given their clinical impact and previously proven ability to predict LNI. LNI risk according to univariate logistic regression analysis is shown in **Table 9**. The AUC derived from each individual variable is also reported in **Table 9**, as well as the AUC of the models built adding to each variable the hypermethylation score from target and systematic samples, independently. All selected clinical and mp-MRI variables were able to increase the AUC of the hypermethylation signatures. **Table 10** and **Table 11** show the two multivariate logistic regression models predicting LNI that were developed from the target and systematic samples, with their AUCs. The overall cohort was then divided into training and testing sub-cohorts. These two cohorts were randomly created and this train-test validation was reiterated 500 times creating new sub-cohorts at each cycle. After reiterated train-test validation, the AUC of the target model was 86.0% (95% confidence interval [CI]: 62.0%-98.0%) and the AUC of the systematic model was 82.7% (95% CI: 70.0%-97.0%). AUCs were calculated in the testing cohorts only.

**Table 9** – Univariate logistic regression analysis for LNI prediction according with different clinical and mp-MRI predictors and corresponding AUC.

<b>Variables</b>	<b>OR (95% CI)*</b>	<b>P*</b>	<b>AUC univariable models*</b>	<b>combined AUC with the hypermethylation score (target; systematic)**</b>
PSA (ng/ml)	1.04 (1.01-1.08)	0.012	73.7%	85.4%; 81.1%
ISUP Gleason grade groups of target lesion				
1-2	Ref	Ref.	78.0%	87.1%; 82.3%
3	3.68 (1.05-17.14)	0.06		
4-5	12.47 (3.97-55.37)	<0.001		
T stage at mpMRI				
Organ confined	Ref.		73.1%	86.0%; 82.8%
ECE	3.28 (1.19-8.70)	0.02		
SVI	20.53 (5.70-97.99)	<0.001		
% Sign. prostate cancer at systematic biopsy	1.04 (1.03-1.06)	<0.001	75.6%	87.4%; 83.9%
PI-RADS				
3	Ref.		67.4%	87.3%; 84.5%
4	0.28 (0.09-0.84)	0.02		
5	2.22 (0.87-6.09)	0.1		
Diameter of index lesion at mp-MRI (mm)	1.09 (1.04-1.17)	0.003	71.0%	88.0%; 81.0%
Hypermethylation score	logOdds			
Target	0.12 (0.08-0.16)	<0.001	84.0%	-
Systematic	0.08 (0.05-0.11)	<0.001	75.5%	

\*Derived from the overall cohort; \*\* Derived from target and systematic cohorts

**Table 10** – Multivariate logistic regression model fitted on data from target samples (AUC:87.6%)

<b>Coefficients</b>	<b>Estimates</b>	<b>Std. Errors</b>	<b>z values</b>	<b>p values</b>
Intercept	-6.31	1.05	-6.00	<0.001
Hypermethylation score	0.10	0.02	4.16	<0.001
T stage at mpMRI (ECE)	0.59	0.75	0.79	0.4
T stage at mpMRI (SVI)	1.77	0.92	1.91	0.06
GGG (3)	0.78	0.80	0.98	0.3
GGG (4-5)	1.78	0.79	2.27	0.02
PSA (ng/ml)	0.03	0.02	1.46	0.1

**Table 11** – Multivariate logistic regression model fitted on data from systematic samples (AUC: 85.2%)

<b>Coefficients</b>	<b>Estimates</b>	<b>Std. Errors</b>	<b>z values</b>	<b>p values</b>
Intercept	-4.48	0.78	-5.71	<0.001
Hypermethylation score	0.07	0.02	3.66	<0.001
T stage at mpMRI (ECE)	1.22	0.67	1.80	0.07
T stage at mpMRI (SVI)	2.29	0.88	2.60	0.009
GGG (3)	0.51	0.78	0.65	0.5
GGG (4-5)	1.32	0.77	1.73	0.08
PSA (ng/ml)	0.05	0.02	2.20	0.03

The cut-off tables for the two models are reported in **Table 12** and **Table 13**. According to the model developed on the target samples, the cut-off of 5% would spare 64 (40%) PLND and would miss 3 (3.5%) lymph node metastases. According to the model developed on systematic samples, the 5% cut-off, would spare 61 (38.1%) PLND and would miss 4 (6.6%) lymph node metastases.

#### **6.2.4.4 – Comparison between developed models and existing clinical models**

The AUC of the validated 2012, 2017, and 2019 versions of Briganti nomograms were 82.9%, 81.0%, and 83.1%, respectively. Decision curve analyses comparing the two developed models with Briganti nomograms are shown in **Figure 47** and **Figure 48**. Here, both the target and systematic models showed higher net benefit for LNI prediction at any threshold probability as compared to any of the three versions of Briganti nomogram.



**Table 12** – Cut-offs tables derived from the internal validation of the model developed on the target samples

Target model cut-offs	Patients below Cut-off (PLND not recommended)			Patients above Cut-off (PLND recommended)		
	Cut-offs	N	Without LNI	With LNI	N	With LNI
1%	2	2 (100%)	0 (0%)	158	32 (20.3%)	126 (79.7%)
2%	20	20 (100%)	0 (0%)	140	32 (22.9%)	108 (77.1%)
3%	39	37 (94.9%)	2 (5.1%)	121	30 (24.8%)	91 (75.2%)
4%	53	51 (96.2%)	2 (3.8%)	107	30 (28.0%)	77 (72.0%)
5%	64	62 (96.9%)	2 (3.1%)	96	30 (31.3%)	66 (68.8%)
6%	74	71 (95.9%)	3 (4.1%)	86	29 (33.7%)	57 (66.3%)
7%	81	78 (96.3%)	3 (3.7%)	79	29 (36.7%)	50 (63.3%)
8%	85	82 (96.5%)	3 (3.5%)	75	29 (38.7%)	46 (61.3%)
9%	91	87 (95.8%)	4 (4.4%)	69	28 (40.6%)	41 (59.4%)
10%	96	92 (94.5%)	4 (4.2%)	64	28 (43.8%)	36 (56.3%)

**Table 13** – Cut-offs tables derived from the internal validation of the model developed on the systematic samples

Systematic model cut-offs	Patients below Cut-off (PLND not recommended)			Patients above Cut-off (PLND recommended)		
	Cut-offs	N	Without LNI	With LNI	N	With LNI
1%	0	0 (/)	0 (/)	160	31 (19.4%)	129 (80.6%)
2%	7	7 (96.9%)	0 (0%)	153	31 (20.3%)	122 (79.7%)
3%	32	31 (95.8%)	1 (3.1%)	128	30 (23.4%)	98 (76.6%)
4%	48	46 (93.4%)	2 (4.2%)	112	29 (25.9%)	83 (74.1%)
5%	61	57 (93.4%)	4 (6.6%)	99	27 (27.3%)	72 (72.7%)
6%	66	62 (93.9%)	4 (6.1%)	94	27 (28.7%)	67 (71.3%)
7%	72	67 (93.1%)	5 (6.9%)	88	26 (29.5%)	62 (70.5%)
8%	79	74 (93.7%)	5 (6.3%)	81	26 (32.1%)	55 (77.9%)
9%	85	79 (92.9%)	6 (7.1%)	75	25 (33.3%)	50 (66.7%)
10%	89	82 (92.1%)	7 (7.9%)	71	24 (33.8%)	47 (66.2%)

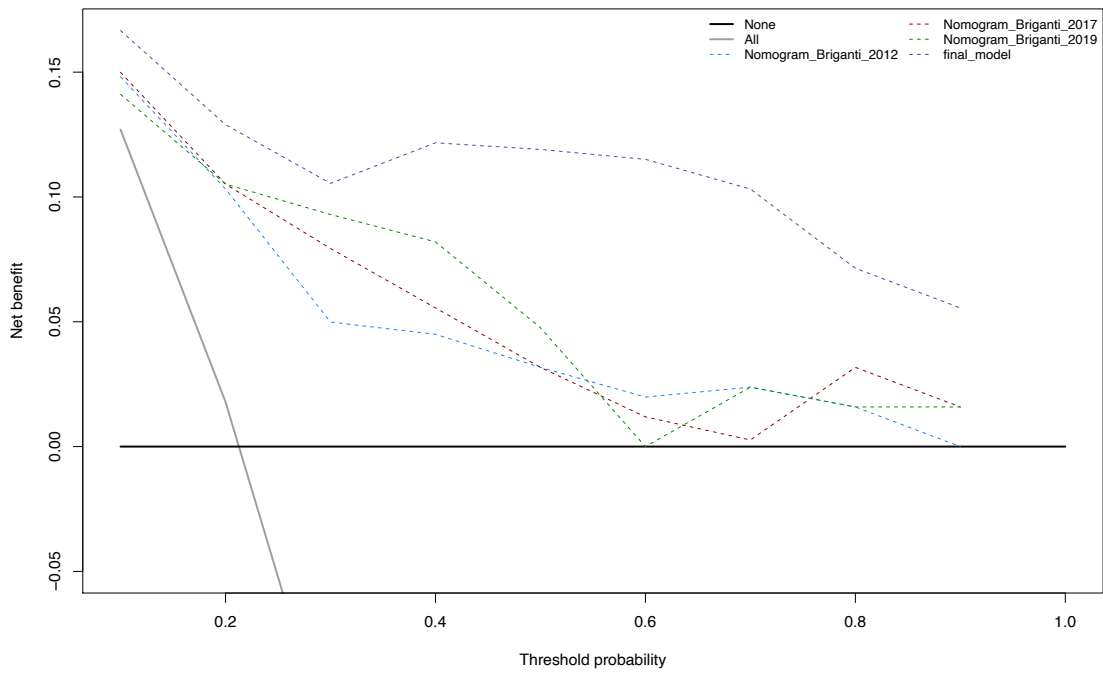


**Figure 47** – Decision curve analysis comparing the 2012, 2017, 2019 versions of the Briganti nomogram with the model developed on the target samples.

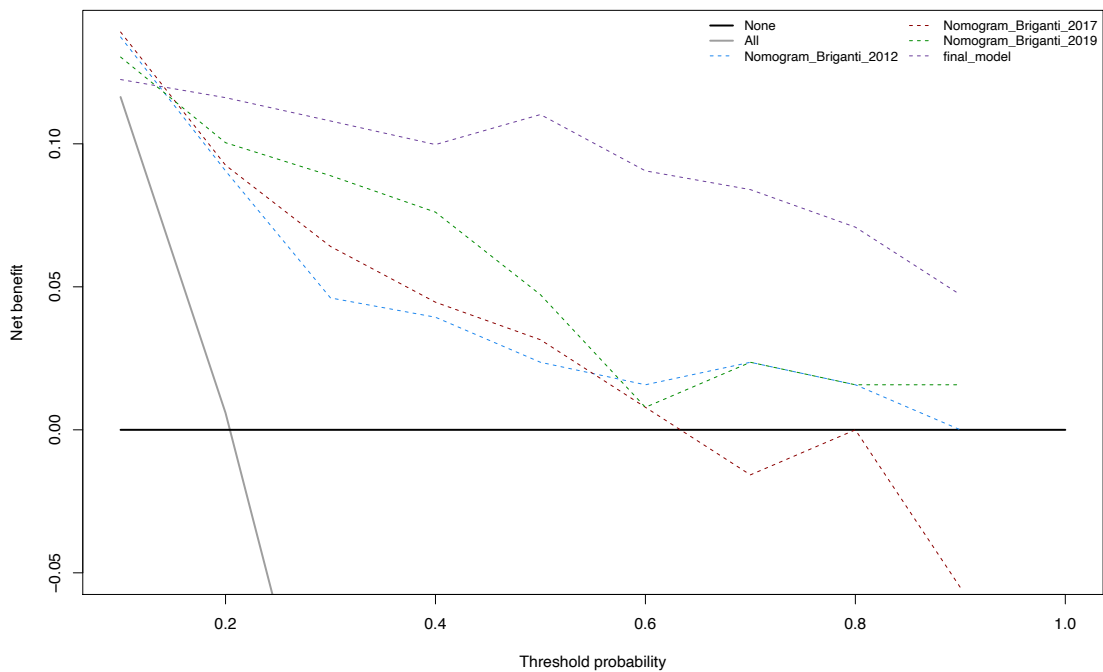


**Figure 48** – Decision curve analysis comparing the 2012, 2017, 2019 versions of the Briganti nomogram with the model developed on the systematic samples.

## **7. Materials and methods**

### ***7.1 – Cohort definition***

#### ***7.1.1 – Patient selection and ethical approval***

The study cohort included 172 patients with a diagnosis of localized prostate cancer (cTanyN0M0) who underwent radical prostatectomy and extended PLND. All patients received diagnosis and treatment at the Unit of Urology, IRCCS Ospedale San Raffaele (Milan, Italy). All included patients presented one or multiple lesions at the mp-MRI of the prostate, defined as PI-RADS 3 to 5. The diagnosis of the disease was achieved after systematic and mp-MRI target prostate biopsy. To be included in the current study, at least two biopsy cores were required: i) one positive core from the mp-MRI PI-RADS 3-5 lesion/s (target lesion), ii) one positive core from the systematic sampling (outside the target lesion). Exclusion criteria were unavailable or negative mp-MRI, unavailable or negative target or systematic biopsy, and refuse to undergo radical prostatectomy with PLND at the Ospedale San Raffaele. Data collection followed the principles outlined in the Declaration of Helsinki. All enrolled patients signed an informed consent form agreeing to supply their own anonymous information and tissue specimens for this and future studies. The study was approved by the Institutional Review Board of IRCCS Ospedale San Raffaele, Milan (89/INT/2019).

#### ***7.1.2 – Patient sample***

This study is part of a project founded by the Ministero della Salute. The main project is granted by the Finalizzata RF-2018-12368399, and it was designed to enroll 400 patients. The number of patients was established based on the need for 100 events (namely, patients with LNI) to develop and validate the multivariable model for LNI prediction. Indeed, the rate of pN1 disease in patients with a predicted risk of LNI >5% is approximately 25%(179), according to the most recent literature. Thus, to have an estimated number of 100 events, 400 patients are required. The 400 events will allow the development and validation of a model with 5 degrees of freedom (5 adjusting variables). This study focused on a preliminary cohort of 172 patients enrolled from January 2014 until April 2021, and report interim findings of the main project. This cohort of patients was selected in a two-step process. Patients who fulfilled the inclusion criteria and that

were operated on before the kick-off of the main project (July, 15<sup>th</sup> 2020) were identified retrospectively among the overall cohort of patients with prostate cancer treated with radical prostatectomy at the IRCCS Ospedale San Raffaele from January 2014. The starting date was based on the availability of mp-MRI-based fusion biopsy at our center, which came into practice in November 2013. From January 2014 to July 2020, 159 patients were identified among 214 patients treated with radical prostatectomy at our center. All had a diagnosis of prostate cancer derived from a positive target biopsy. In this retrospective phase, 55 were excluded: 31 because they did not have at least 2 positive cores from target and systematic biopsy, 18 because they did not receive PLND due to a calculated risk of LNI below 5% according to the 2012 Briganti nomogram, and 6 patients because the quality of their mp-MRI performed elsewhere was considered suboptimal. From July 2020 to April 2021, 13 patients were identified among 26 treated with radical prostatectomy at our center. All had a diagnosis of prostate cancer derived from a positive target biopsy. In this prospective phase, 13 patients were excluded: 8 because they did not have at least 2 positive cores from target and systematic biopsy, and 5 because they did not receive PLND due to a calculated risk of LNI below 5%.

## ***7.2 – Multiparametric MRI***

### ***7.2.1 – mpMRI acquisition and cohort characteristics***

Among the 172 included patients, 154 received mp-MRI at our center. We relied on a 1.5-T or 3-T mpMRI system (Achieva and Achieva dStream, Philips Medical Systems, Best, Netherlands) with both surface and endorectal coil (Prostate eCoil, Medrad®, Indianola, PA, USA). According to the European Society of Urogenital Radiology guidelines(64), the imaging protocol consisted of multiplanar turbo spin-echo T2-weighted images, echo-planar DWI with b values of 50, 800 and 1600 s/mm<sup>2</sup> (ADC maps were automatically elaborated on a pixel-by-pixel basis using b values of 50 and 800 s/mm<sup>2</sup>), 3-D fast field-echo DCE MRI and delayed axial turbo spin echo T1-weighted images with fat suppression. For DCE-MRI, an IV bolus of 0.1 mmol/kg of gadobutrol (Gadovist, Bayer Schering Pharma, Germany) at a flow rate of 4 ml/s was used. The mpMRI images were scored and reported using the most recent PI-RADS(65). A positive mp-MRI was defined as the identification of at least one lesion with PI-RADS 3 or higher (index/target lesion). For those patients who were referred from other centers to perform

the biopsy based on positive mp-MRI findings (N=18), the MRI images were reviewed by a senior radiologist of the IRCCS Ospedale San Raffaele with more than 5 year-experience in prostate cancer MRI-imaging. For those patients with external mp-MRI, only those that were performed under the same imaging protocol as ours were considered for this study. All the other referred patients that did not fulfill these requirements were excluded for this study (N=6).

### ***7.3 – Trans-perineal prostate biopsy***

#### ***7.3.1 – Prostate biopsy indications and technique***

All patients underwent combined mp-MRI target and systematic prostate biopsy in accordance with the EAU guidelines(71). Patients were admitted to the hospital on the day of the biopsy, and discharged the same day. At our center, we preferred the trans-perineal approach over the trans-rectal approach given the lower risk of urinary infection, as recommended by EAU guidelines(71). Procedures were performed under local anesthesia, whereas general anesthesia was reserved for patients with specific anesthesiologic indications. Antibiotic prophylaxis with cefoxitin 2gr was administered before the procedure. Patients were placed in social lithotomy position, with legs supported by Allen’s stirrups. Aseptic preparation of the perineal skin was achieved with povidone-iodine solutions. The target biopsy was directed towards the index lesion/s (PI-RADS 3-5), using a software-registration fusion approach, immediately followed by additional random systematic biopsies using a sextant biopsy scheme. We usually collected 3-4 cores from each PI-RADS 3-5 lesions. Biopsies were performed by experienced urologists using an 18-gauge needle and a biopsy gun providing a specimen size of 18-22 mm. Trans-rectal ultrasound was executed using a Flex Focus 500 machine with a biplanar transducer (BK Medical, Herlev, Denmark). Regarding the fusion technique, before biopsy both the prostate and the region of interest were contoured and superimposed with the TRUS image, using the BioJet fusion system (D&K Technologies, Barum, Germany)(200). Target and systematic core specimens were collected and stored separately.

## ***7.4 – Biopsy core selection***

### ***7.4.1 Selection process of biopsy cores***

As per our internal protocol, all biopsy samples were fixed with 10% neutral-buffered formalin after collection. Two cores per cassette were included. Formalin fixation time was widely variable (from 1h 30' to 24h) depending on the number and the thickness of the samples. Subsequently, tissue samples were dehydrated using alcoholic solutions with different concentration following a specific sequence (50% - 70% - 90% - 95% - 100%). The lipid solubilization and ethanol elimination “clearing process” was achieved with Xylen. Finally, tissue samples of each cassette were embedded in paraffin wax at the temperature of 60-70 °C making the FFPE blocks. For the preliminary diagnostic evaluation, each FFPE block was sliced at two different levels using a microtome to obtain (2-3µm) thin slices. Then, slices were heated in a stove with a temperature of nearly 70°C to obtain heat-induced epitope retrieval. Then each slice was dewaxed, dipping it twice in Xylene, again in alcoholic solutions with different concentrations, and finally in distilled water. Finally, slices were stained with Harris’ hematoxylin and alcoholic eosin and analyzed by a dedicated uro-pathologist to provide a diagnosis and grading of prostate cancer, as per EAU guidelines(71). The pathologist outlined the number of biopsies and the length of each needle biopsy. Gleason patterns and % of cancer involvement and extension in mm were reported for each core. Additional pathological features such as perineural extension, presence of prostatic intraepithelial neoplasia, atrophy, chronic granulomatous inflammation, acute inflammation, and benign prostatic tissue were also reported. As per our study protocol, 2 positive cores were selected for each patient:

- (i) one core from the index lesion; the core with the highest Gleason Score was selected. In case of two or more cores with the same Gleason Score, the one with the highest percentage of cancer involvement was selected;
- (ii) one core with the highest Gleason score outside the index lesion, from the systematic sampling. In case of two or more cores with the same Gleason score, the one with the highest percentage of cancer involvement was selected.

## ***7.5 – Extended pelvic lymph node dissection***

### ***7.5.1 – Surgical technique for extended PLNDs***

As previously mentioned, all included patients underwent radical prostatectomy with extended PLND. Extended PLNDs were performed by applying a standard anatomic template. The template consisted of the excision of fibrofatty tissue along the external iliac vein proximally including the bifurcation of the common iliac artery, with the genitofemoralis nerve as the lateral limit and perivescical fat as the medial limit. Lymph nodes along medially and laterally to the internal iliac vessels were removed. All fibrofatty tissue within the obturator fossa was also removed. In patients affected by pN1 disease, the positive lymph node with the larger diameter was submitted to methylation analysis. In this study, 15 patients with pN1 disease were available for methylation analysis.

## ***7.6 – Definition of the clinical variables of interest***

### ***7.6.1 – Clinical variables of the included population***

For each included patient, demographic, clinical, and disease-specific information was collected at the time of the preliminary assessment (usually at the time of prostate biopsy) and then subsequently at each relevant step of disease management, namely hospitalization for radical prostatectomy, and follow-up visits. Among the demographic information, we recorded the patient's date of birth and the date of biopsy. Clinical T stage (T1-3) and PSA at the time of prostate biopsy (in ng/ml) were also collected. Data from the mpMRI were annotated at the time of prostate biopsy, and included MRI-derived prostate volume (in ml), PI-RADS score for each identified lesion (from 3 to 5), volume of the lesion with the highest PI-RADS score (in ml), MRI tumor stage (organ confined, extracapsular extension, seminal vesicle invasion). From the prostate biopsy the following variables were collected: number of cores taken from the highest, second highest (if any), and third highest (if any) PI-RADS score (index) lesions, and number of cores taken from the systematic sampling. The pathology report of the prostate biopsy was used to collect data on the number of positive cores from the target lesion(s), systematic sampling, and overall. The ISUP grade group (1-5) was also annotated independently for the target and systematic sampling. Data from radical prostatectomy specimens were the pathological T and N stages, ISUP Gleason grade groups, evidence

of extracapsular extension (ECE), evidence of seminal vesicle invasion (SVI), surgical margin status, number of removed lymph nodes, number of lymph node metastases, size of largest lymph node metastasis. Finally, the occurrence of biochemical or clinical progression was recorded, as well as the time to these events that was calculated from the date of radical prostatectomy to respectively biochemical recurrence, clinical recurrence, or death by any cause, whichever occurred first.

## *7.7 – Preparation of the core and lymph node specimens*

### *7.7.1 – Specimen preparation*

As previously mentioned, only patients with at least two positive cores from i) target and ii) systematic biopsy were included in this study. For each patient, one FFPE block from the target and one FFPE block from systematic biopsy were identified following the aforementioned criteria. From each of the two selected FFPE blocks, 10 to 15 slices were prepared. Each slice was 6-10 $\mu$ m thin. Here, the slices were thicker than for the preliminary histopathological diagnosis. This was made with the purpose to increase the amount of tissue per slice facilitating the subsequent process of DNA extraction. This modification provided higher amount DNA for each sample as compared with standard 2-3 $\mu$ m thin slice: on average the 6-10 $\mu$ m slices provide around 100ng of DNA per core vs. less than 20ng of DNA per core for the 2-3 $\mu$ m slices. To ensure the correct location of the tumor areas within each slice, the first, an intermediate, and the last slices of the series were stained with hematoxylin and eosin. On these three stained slices, the areas involved with prostate cancer were identified under the microscope and marked with black ink (**Figure 49**). By using the first, the intermediate, and the last referenced slices, all the other unstained slices in between were marked in the corresponding areas of interest (cancer tissue). This process was performed for both the target and systematic positive cores. For the extraction of the tumor DNA contained in the lymph node metastases, we relied on the histologic material that was stored in formalin at the time of radical prostatectomy and PLND. The cassette containing the metastatic node with the largest diameter was processed with the microtome in 5-8 slices. The thickness of each slice was approximately 4-5 $\mu$ m. Again, the first, intermediate, and last slices were stained with hematoxylin and eosin to ensure the exact demarcation of tumor cells in the tissue.



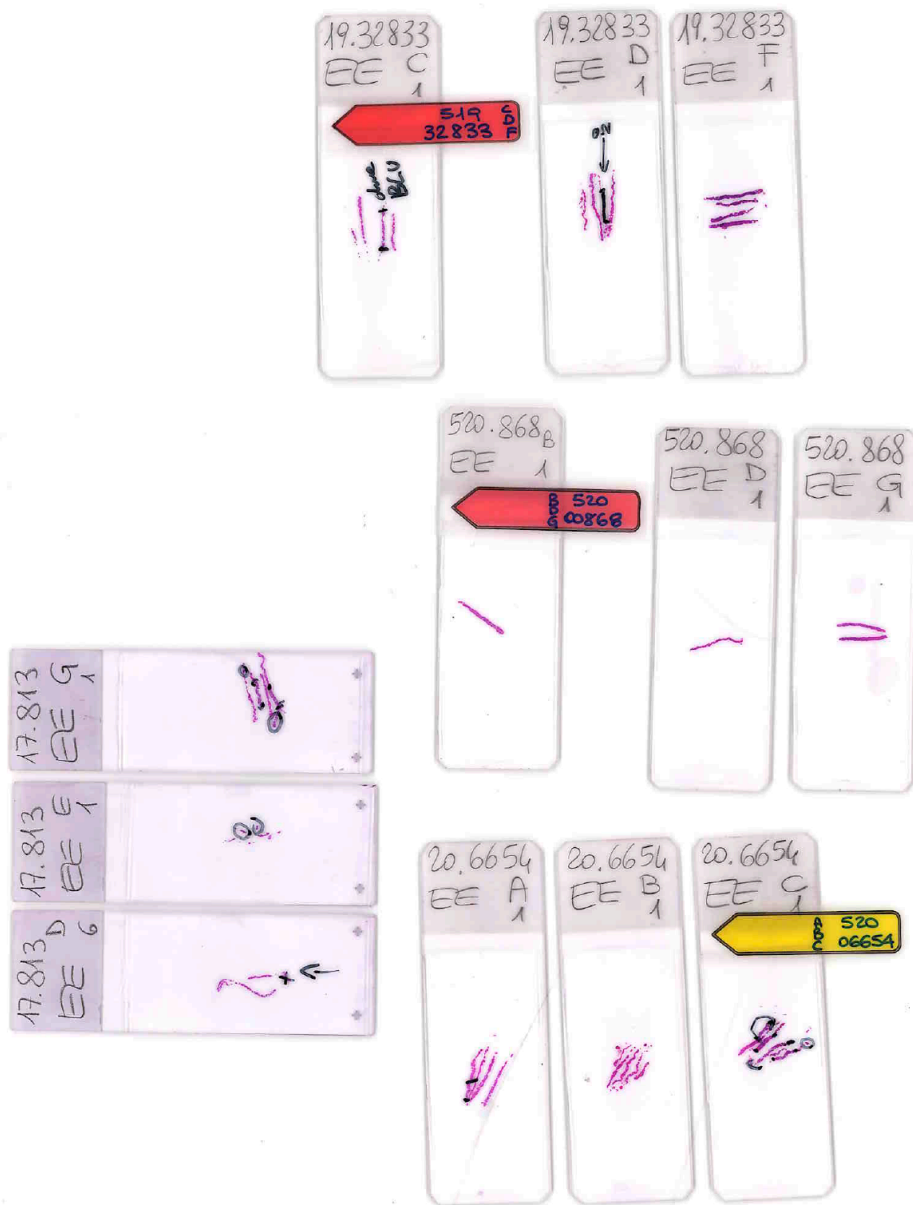


**Figure 49** – Example of prostate cancer demarcation on stained slices. The area of interest, namely the tissue occupied by prostate cancer, was marked with black ink. This process was performed on the first, the intermediate, and the last slice of the series for each FFPE block. These stained slices were used as the template for the demarcation of the same corresponding areas on the unstained slices in between of the series.

Then, the unstained slices were marked on the corresponding tumor areas, following the guide of stained slices.

## ***7.8 – Epigenetic profiling from FFPE specimens of patients with localized (cTanyN0M0) prostate cancer***

### ***7.8.1 – DNA methylation analyses***

We extracted the DNA from the 10 to 15 slices of FFPE samples of prostate biopsies using the GeneRead DNA FFPE kit (Qiagen). The GeneRead DNA FFPE kit enables the purification of genomic DNA from FFPE samples. This kit allows the removal of genomic artifacts, including artificial C>T mutations, which are common after formalin fixation and with the aging of the paraffin samples. Of note, we relied on samples that were not older than 7 years at the time of processing (Jan 2014 first patient to be enrolled, Jul 2020 starting of sample processing). Moreover, the GeneRead DNA FFPE kit enables a larger extraction of genomic DNA from small FFPE samples (1 x 10 µm slide), as compared with standard FFPE DNA isolation protocol(201–204). Briefly, all slides were deparaffined with 1-hour incubation in HistoClear (Histo-Line laboratories) and 30' incubation in degrading concentrations of Ethanol (100% and 70%). The regions of interest, indicated by the pathologist, were then removed from the slides using a scalpel and extracted after a 72h Proteinase K digestion step at 56°C. The incubation time was optimized according to our samples to maximize yield for library preparation. Extractions were then performed following the manufacturer's instructions (GeneRead™ DNA FFPE - Feb2022). After the extraction, all DNA samples were quantified using Qubit high sensitivity-DNA fluorometer (Thermo Fisher) and Agilent Tapestation 4200 (Agilent) to determine the DNA integrity number (DIN). The DIN quantifies the quality of genomic DNA. Indeed, the higher the DIN, the lower the fragmentation of DNA. With a lower DNA fragmentation, the efficiency of DNA sequencing improves. Then, we performed DNA methylome profiling using reduced representation bisulfite sequencing (RRBS) to identify the methylation status of CpG reach regions. The human genome presents methylated regions which are responsible for DNA silencing. The methylated areas occur predominantly in CpG contexts, and these CpG dinucleotides are more abundant in selected regions of the genome. RRBS facilitates the identification of CpG areas by converting unmethylated cytosine bases to uracil, and then promoting the selective DNA

amplification and sequencing of these DNA areas. To enable the RRBS process, a minimum of 10ng of genomic DNA was used as input. At this step, 12 core samples were excluded from the analyses because the amount of DNA extracted from the FFPE slices was below 10ng. The RRBS was performed with the Zymo-Seq RRBS Library Kit (Zymo). Further details on the Zymo kits can be found here ([www.zymoresearch.com](http://www.zymoresearch.com)) (Figure 50). To automate the library preparation using the epMotion 5075 (Eppendorf), we modified the original column-based purification steps with paramagnetic beads-based purification steps. All clean-up steps (section 2 step 7 and section 4 step 19 in the Zymo RRBS protocol) were performed using 1x AMPure beads (Beckman Coulter). Section 3 step 12 was modified as follows: after bisulfite conversion DNA was purified using Zymo MagBinding Beads (following the instruction for post-bisulfite purification of EZ-96 DNA Methylation-Lightning MagPrep protocol, Zymo). The library was then purified using 1x AMPure beads. The final libraries were quantified using Qubit hsDNA fluorometer and run on the HSD5000 Agilent TapeStation 4200 to determine the profile and the molar concentration. Libraries were normalized and pooled and sequenced on the Illumina NovaSeq 6000 according to manufacturer's protocols. The sequencing runs were 100-nt base paired-end runs, sequencing target was 50M cluster/sample. Sequencing data were pre-processed to remove the RRBS library specific artifacts, using the TrimGalore tool in its RRBS specific trimming mode. The retained reads were subsequently mapped on the human genome (Hg38) and the methylation status of each cytosine was assessed through the Bismark aligner and the Bismark methylation caller, respectively. Alignment on the E. Coli genome was performed to check the conversion rate of a spike sequence with a known methylation profile, and thus evaluate the efficiency of the bisulfite conversion process. Among the 172 paired samples, 12 core samples were excluded due to a low amount of extracted DNA (as previously mentioned), 7 (4 target and 3 systematic positive cores) cores failed the spike-in process reaching less than 85% conversion rate. One additional sample with low coverage was excluded (less than 5 reads on each cytosine). These samples were excluded from epigenetic analyses.

### ***7.8.2 – Bio-Informatic analyses***

The methylation data obtained were used to perform an unsupervised clustering analysis on the full cohort of patients, while differential methylation analysis was used to identify

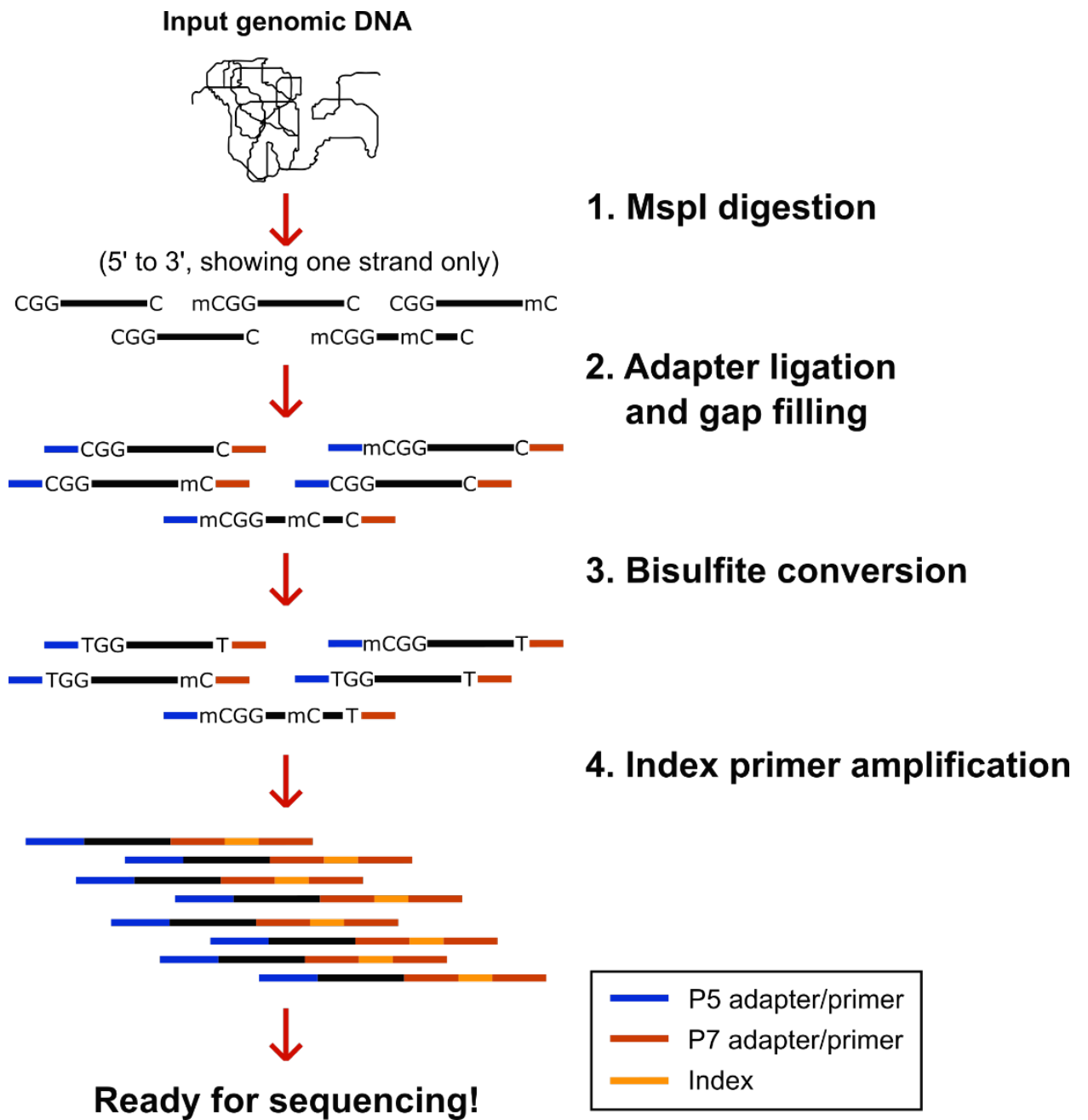


**Figure 50** – The bisulfite reaction workflow with PCR library preparation. Reprinted by permission from Zymo Research Europe GmbH (CASE29342).

hypo- and hyper-methylated regions in specific groups of samples. Cytosines and genomic regions recognized as significant by this analysis were annotated according to the corresponding genomic features, such as gene promoters and CpG islands. The analysis was performed using methylKit Bioconductor package.

#### ***7.8.2.1 – Validation of the Mundbjerg signature***

Mundbjerg and colleagues presented a DNA methylation classifier which prompted to estimate the aggressiveness of non-metastatic multifocal prostate cancer. In their study, the Authors profiled the epigenetic mutations of 14 patients with prostate cancer and lymph node metastases who underwent radical prostatectomy. They hypothesized that multiple prostate cancer foci may have different aggressiveness and metastatic propension. Moreover, they also hypothesized that metastatic progression of prostate cancer can begin from distinct cancer foci which developed proliferative, migration and aggressiveness potential through different molecular pathways, including epigenetic mutations. Thus, the epigenetic profiling of multifocal prostate cancer can reveal a similarity between the most aggressive tumor focus and the lymph node metastasis, which usually represents the initial site of extraprostatic spread. Paired analyses among prostate cancer foci and lymph node metastases identified 25 probes of hyper or hypo-methylated CpGs sites that were able to classify the aggressiveness and lymph node metastatic propension of primary prostatic sub-clones. Methylation profile of prostate cancer foci and matched lymph node metastases was performed with Illumina Infinium Human Methylation 450 Bead Array (HM450) platform. In order to test the Mundbjerg 25-probe signature in our cohort, we retrieved the genomic locations of the 25 CpGs sites in the genome of our samples. Of note, the location of the 25 probes of the original publication was expressed according to the hg19 version of the human genome, while for our study the more recent hg38 reference was used. Thus, a prior lift-over step was performed to convert the positions of the probes(205,206). The methylation status of the corresponding genomic positions in our cohort was examined, whenever available (at least one read). Then, we compared the methylation status among samples in our cohort. The Wilcoxon test compared the average methylation status of the 339 samples in the corresponding 25 positions. Comparisons were made according to i) LNI status (LNI+ vs. LNI-), and ii) sample type (target vs. systematic vs lymph node metastases). Then, methylation status

was examined for each individual probe independently according to LNI status and sample type, respectively. Here, only probes that were measured on at least 5 samples per group (LNI+ vs. LNI-) were tested. Instead, for the comparison among target vs. systematic vs. lymph node metastases, only probes that were measured on at least 5 samples per group were tested. Principal component analysis and unsupervised clustering were not performed due to the reduced set of tested positions.

#### ***7.8.2.2 – Differential Methylation analysis***

The differential methylation analysis aimed at identifying genomic loci or regions (i.e. CpGs sites or positions) with different methylation levels, namely hypo- or hyper-methylated. Data from sodium bisulfite treatment of DNA and next-generation sequencing, can be summarized as numbers of methylated and total reads at each CpG site(207). Given the aim of the study, LNI was used as a dichotomizing factor in our analyses. Thus, differential methylation analysis prompted to compare numbers of methylated and total reads among samples from patients with LNI+ and LNI-. In particular, we established the differential methylation of the two groups based on the calculated methylation status of each CpG sites. The methylation status of each CpG site was calculated as the number of reads with the considered cytosine in methylated form divided by the total number of reads (either methylated or not) that cover that particular cytosine. Differential methylation analysis was performed with methylKit R package(208), which relied on logistic regression to assign a p-value to each tested CpG. To ensure optimal outputting, we set a filter on coverage. Specifically, we considered only CpGs sites covered by at least 5 reads in at least 12 samples per group (63 LNI+ and 261 LNI-) when both sample types were included (target and systematic: N=324). Conversely, when only target or systematic samples were examined, we considered only CpGs sites covered by at least 5 reads in at least 6 samples per group (32 LNI+ and 129 LNI- for target samples [N=161]; 31 LNI+ and 132 LNI- for systematic samples [N=163]). 10% and 25% absolute changes in methylation status were set as cut-off values to identify significantly hyper- and hypo-methylated CpGs among LNI+ and LNI- samples. For both the cut-offs, the significance values were adjusted for multiple comparisons with the FDR correction set at <0.01. Due to computational limitations, the differential methylation analysis was performed on single chromosomes, merging the

results at the end. Descriptive statistics included histograms of coverage and histograms of the methylation status that were reported across all samples (target and systematic). Graphical representations of the distribution of all the tested cytosines and differentially methylated (according to both cut-offs) cytosines across chromosomes were depicted with histograms. Graphical representations of the distribution of all tested cytosines and differentially methylated cytosines (for both 10% and 25% cut-offs) according to gene parts (promoter, exon, introns, intergenic sequences) were depicted with cake plots. Differentially methylated cytosines according to both 10% and 25% cut-offs, were annotated with the corresponding CpG islands (if possible). The corresponding CpG islands were also filtered according to the number of differentially methylated cytosines contained within the islands, such as 100, 50, and 30 for the 10% cut-off, and 30, 20, and 10 for the 25% cut-off. Filtered CpG islands were associated with overlapping genes (if there were any). Annotation was performed using the Gencode annotation (v.41) related to the human genome hg38, as retrieved from the University of California-Santa Cruz (UCSC) Table Browser (**Figure 51**). Then, enrichment analysis was performed to identify biological pathways and ontologies that were significantly associated with the retrieved lists of genes (genes matching the CpG islands that contained a pre-defined amount of differentially methylated CpGs) and thus inspecting the biological processes possibly involved in the considered comparison. Tested gene collections were Gene Ontologies (GO\_BP, GO\_CC, GO\_MF); WikiPathways; Kegg; Biocarta; Reactome; Hallmarks; TF Perturbations Followed by Expression (from NCBI-GEO). The enrichment analysis was performed with the enrichR R package, which evaluated the overlap between the user-provided list of genes and the considered pathway, and assigned a significance level based on the size of this overlap. Significance levels were adjusted with the Benjamini-Hochberg correction to control the False Discovery Rate (FDR). Annotation and enrichment analyses were independently performed within combined samples (target and systematic), only target, and only systematic samples. The significant pathways derived from the enrichment analyses of the three types of samples (all, target only, systematic only) were plotted to mark the number of overlapping genes among the three sets of analyses and presented for the two different cut-offs (10% and 25%). Lastly, all the steps of the analyses were repeated accounting for the methylation status which distinguished among hyper and hypomethylated CpGs sites. Here, enrichment analyses were reported

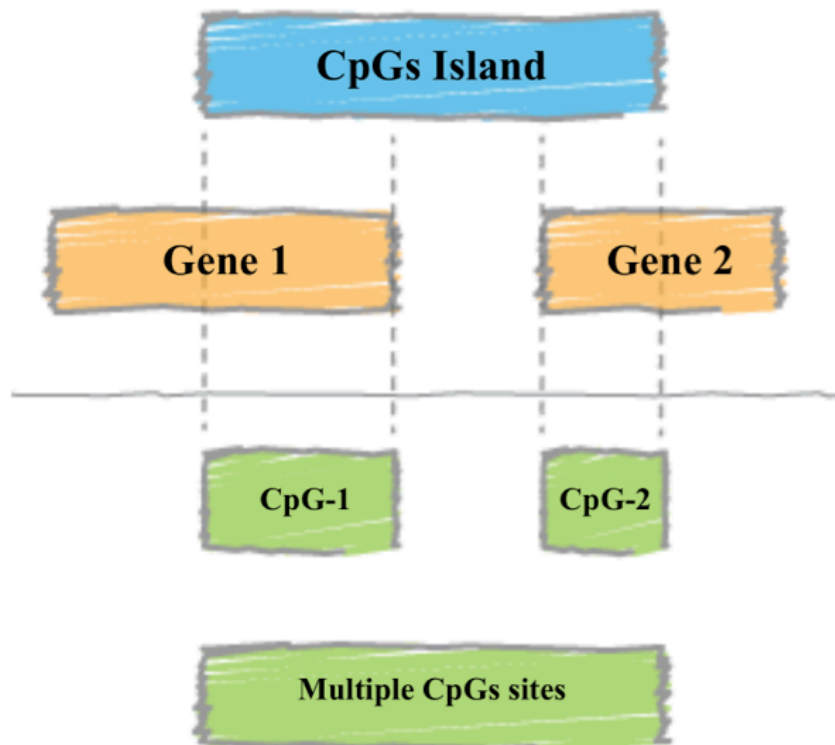


**Figure 51** – Annotation of significant CpGs positions onto the HG38. Each significant (according to the two different cut-offs: 10% and 25%) CpGs positions were annotated with the corresponding CpG islands and then overlapped with genes, whenever possible.



only for the 10% cut-off, since the application of the 25% cut-off did not lead to any significant results.

#### ***7.8.2.3 – Identification of the highly differentially methylated CpG***

The subsequent step of analyses was focused on the identification of a restricted list of CpGs sites that were highly differentially methylated among patients with and without LNI. This step aimed to restrict the number of differentially methylated CpGs selecting only the most significant in order to develop a clinically utilizable signature, which included only a limited number of genomic positions. The selection of highly differentially methylated CpGs was performed for target and systematic samples independently to allow the identification of two different lists of CpGs that could be integrated in two different epigenetic signatures. This was done to address the hypothesis of the study that target and systematic tumor foci may have different epigenetic alterations that can explain a different lymph node metastatic potential. The highly differentially methylated CpGs positions were identified by applying an absolute change in the methylation status of 50%, and  $FDR < 0.01$ . Enrichment analysis was performed on the highly differentially methylated CpGs and corresponding genes for both target and systematic samples.

#### ***7.8.2.4 – Development of epigenetic signatures***

For each sample, we calculated the average methylation status of the highly differentially methylated CpGs for the corresponding positions. The average methylation status was calculated independently for hyper and hypomethylated CpGs. In consequence, for each sample we reported two scores: i) the average methylation status of the hypermethylated CpGs; ii) the average methylation status of the hypomethylated CpGs. These two scores were calculated for target and systematic samples independently considering the two lists of highly differentially methylated CpGs. Thus, for each patient, we reported four scores: two scores (hyper-and hypomethylation score) derived from highly differentially methylated CpGs that were previously identified from the target lesion analysis; and two scores (hyper-and hypomethylation score) from highly differentially methylated CpGs that were previously identified from the systematic lesion analysis.

#### ***7.8.2.5 – Development of a model integrating clinical, mp-MRI and epigenetic features***

The development of an integrated model with epigenetic, clinical and mp-MRI variables was achieved considering the number of events (37 patients with LNI) and the available predictors. Among the two epigenetic scores, namely hypermethylation and hypomethylation score, we included in the model only the hypermethylation score. This choice was driven by the fact that uncovered cytosines and fully unmethylated cytosines were giving the same output (methylation average 0%). Thus, we were not able to differentiate between uncovered CpG and fully unmethylated CpGs. For this reason, we chose to rely only on the hypermethylation score which only included the signals from covered cytosines where the average methylation level was known. Among the clinical and mp-MRI variables, we selected those that were clinically more significant given their proven ability to predict LNI. Clinical T stage at mp-MRI, PSA value at prostate biopsy, and ISUP Gleason grade group at target biopsy are known predictors of LNI and they are also included in the 2019-version of Briganti's nomogram, which represents the current guideline's approved model for LNI prediction. The number of LNI events (37) limited the degrees of freedom of the model to 4, which was also the number of included variables. Given that the hypermethylation score was developed independently on target and systematic samples, we developed two models for LNI prediction. One model was developed on the patient population with target biopsy samples and relied on clinical T stage at mp-MRI, PSA value at prostate biopsy, ISUP Gleason grade group at target biopsy, and hypermethylation score from target samples. Here, the number of included patients was 160, due to a lack of data on clinical variables for one patient. The second model was developed on the patient population with systematic biopsy samples and relied on clinical T stage at mp-MRI, PSA value at prostate biopsy, ISUP Gleason grade group at target biopsy, and hypermethylation score from systematic samples. Here, the number of included patients was 160 due to a lack of data on clinical variables for one patient, and lower coverage for assessing the epigenetic hypermethylation score in 2 patients. The AUCs of these models were assessed. Then, we internally validated the two models in training-testing cohorts. The entire cohort of patients was randomly split into two cohorts: training (3/4 of the entire population) and testing (1/4 of the entire population) cohorts. The two multivariable logistic regression models were fitted in the training cohort and then validated in the testing cohort. The train/test validation was reiterated 500 times.

Median and 95% confidence intervals for the two AUCs of these reiterations were calculated. The use of different cut-offs for both models was investigated to quantify the number of LNI that would be missed and the number of PLND that would be spared. Lastly, we compared the AUC of the two developed models with the AUC of the validated Briganti's nomograms (2012, 2017, and 2019 versions), drawing also decision curve analyses.

## 8. Discussion

Since radical prostatectomy was introduced, sparing PLND morbidity without impairing the staging of localized prostate cancer has been an unmet clinical need for urologists. Given the paucity of reliable imaging tools for nodal staging in localized prostate cancer(162), attention was moved to developing clinical models to predict the risk of LNI. These models relied on PSA, digital rectal examination, and biopsy tumor features to estimate the probability of lymph node metastases before radical prostatectomy. The Briganti nomograms (version 2012 and 2017)(179,180), as well as the MSKCC risk calculator, are two examples of LNI predicting models, which have been externally validated several times(174,199) and are now commonly adopted in clinical practice. Nevertheless, these models were developed on data derived from men diagnosed via systematic prostate biopsies. Therefore, they might not be as accurate as they proved to be, given that contemporary patients are now diagnosed via mp-MRI target biopsy. Recently, a novel version of Briganti nomogram (2019) has been developed(98). This new version relied on mp-MRI indicators, as well as biopsy data retrieved from target plus systematic sampling. This model demonstrated higher accuracy, as compared to previous tools, and it has become the new gold standard for assessing the risk of LNI in patients eligible for radical prostatectomy. However, even this new and upgraded version still lacks specificity, given that over 70% of patients would receive PLND without the occurrence of LNI(181). Clinical and radiological features alone cannot fully describe the biological behavior of prostate cancer, but predicting models based on these factors can be improved through multi-disciplinary, disease-specific, highly informative data that derive from DNA sequencing. Indeed, genomic alterations are the real drivers of tumor aggressiveness and metastatic progression. Among them, epigenetic changings seem to influence the natural course of the disease by acting as precursors of tumor development and progression. The identification of epigenetic patterns linked with LNI would help to predict the behavior of prostate cancer even before it develops unfavorable histological features or spreads to distant sites. Nevertheless, epigenetic alterations have never been included in predicting models to assess the risk of LNI in prostate cancer. A recent study by Mundbjerg et al.(195) explored the correlation between epigenetic alterations within primary foci of prostate cancer and the occurrence of lymph node metastases in patients receiving radical prostatectomy and PLND. This epigenetic signature was strongly

associated with LNI, but not further validated in a cohort of patients with a diagnosis of tumor achieved via prostate biopsy. The model was indeed developed on radical prostatectomy specimens only. Therefore, an epigenetic signature is worthwhile being investigated further and assessed on prostate biopsy tissue to predict LNI at PLND, especially while integrating the signature with mp-MRI parameters and histological features derived from combined mp-MRI target and systematic biopsy. Indeed, mp-MRI visible tumor and systematic tumor foci may hold different epigenetic alterations with different abilities to predict LNI. With this aim, we designed the present study to examine epigenetic patterns and their correlation with LNI, by processing prostate biopsy cores from target (mp-MRI positive lesions) and systematic tumor foci. We relied on FFPE samples, which represent the most common source of storage for human tissue, to assess whether this source of tissue was reliable for epigenetic analysis. We also attempted to test the unvalidated Mundbjerg's signature in our cohort. Then, we aimed at developing a new model for LNI prediction which integrated epigenetic patterns, as well as clinical and radiological parameters derived from mp-MRI and mp-MRI target biopsy, and to test if this model was more accurate than existing clinical tools. Lastly, we investigated whether methylation patterns of target and systematic tumor samples portrayed different correlations with the risk of LNI.

### ***8.1 – The relevance of a new protocol for FFPE sample extraction and epigenetic analysis***

One of the most significant achievements of this study was the establishment of a protocol for a large-scale sequencing of FFPE samples. As known, the source of tissue for epigenetic analysis may impact the quality of results. Human tissue samples are routinely processed with formalin fixation and paraffin embedding given that FFPE has the ability to preserve tissue morphology and enable immunohistochemical analysis for histopathological diagnosis, even after many years of sample collection and at a marginal cost of manufacturing. On the other side, formalin fixation and paraffin embedding may alter the integrity of DNA, for example by increasing the artificial C>T mutations in the double strand of DNA or by riddling the DNA sequence with other artifacts(209). This degradation process may reduce the amount of extractable DNA and compromise its integrity, especially when the samples are embedded in paraffin for more than 10

years(201–204). For this study, we relied on biopsy core samples that were fixed with formalin and embedded in paraffin to identify epigenetic alterations of the DNA sequence. The main challenge was to provide a sufficient amount of good-quality DNA for the sequencing. To ensure good-quality DNA, we relied on samples that were embedded less than 10 years from the date of the biopsy. By doing so, we decreased the risk of processing DNA with mutations or artifacts. Then, we had to establish the minimum amount of DNA per sample that was required for sequencing. To accomplish this specific aim, we carefully selected the kit for epigenetic profiling among those available on the market. Two kits were compared: the RRBS and the Human Methylation 450 Bead Array (HM450), which was also employed in Mundbjerg study(195). We have chosen the RRBS kit due to the lower amount of DNA that was necessary for epigenetic sequencing according to kit manufacturing requirements. Indeed, the RRBS required a minimum of 10ng of DNA vs. over 500ng for the HM450 kit. The choice of the RRBS facilitated the sample processing but did not entirely solve the problem of the DNA quantity. Indeed, biopsy core samples are usually a limited source of tissue and tumor DNA, since cancer involvement can be only a focal spot on a core of a few millimeters' length. To increase the amount of extracted DNA from each core sample, we introduced additional modifications to the extraction protocol. First, we decided to cut our FFPE blocks in fewer but thicker slices (6-10 $\mu$ m) as compared to the standard protocol (2-3 $\mu$ m) for histopathological diagnosis. We stained with hematoxylin and eosin three slices, respectively the first, the last, and one in the middle of the series to ensure that the areas of prostate cancer were marked and extracted without sampling errors. This step increased the amount of tissue per slice, as well as the amount of extracted DNA per core sample. Second, to reduce DNA damaging during its extraction, we modified the purification step, which is usually carried out to isolate and selectively extract the double strain of DNA from cell components. Purification of human DNA is usually achieved with a spin-column based process, which requires multiple steps of vacuum and centrifugations of human samples in solutions at varying pH, salt and alcohol concentrations(210). Instead, we adopted a paramagnetic beads-based protocol which removed the need of vacuum and centrifugations in multiple solutions. The magnetic beads selectively attracted the DNA particles among other cell components and reagents, minimizing the stress and shearing forces on the DNA. Paramagnetic beads required fewer steps and reagents than other

DNA extraction protocols reducing DNA damaging and maximizing the amount of DNA(211). In summary, these protocol modifications were crucial to ensure reliable epigenetic sequencing. The outlined protocol represents a valid reference for upcoming epigenetic studies, which rely on FFPE core samples.

### ***8.2 – Chromosomic positions of differentially methylated CpG***

We examined the chromosomic positions of CpGs and differentially methylated CpGs among patients with and without LNI in target and systematic samples and found that these positions were similar among the two sample types. We achieved similar results also when the analyses were run including both samples combined. Differentially methylated CpGs were more common on chromosomes 16, 17, and 19, while hypomethylated CpGs were more abundant on chromosome 8. These chromosomes are known to host some of the genes that are highly associated with prostate cancer such as *BRCA1* (17q21), *HOXB13* (17q21-22)(212), *p53* (17p13), and C-myc (8q24)(213). Similarly, chromosome 16 is known to be enriched with tumor suppressor genes, which are correlated with prostate cancer progression(214–216). This said, we can assume that these chromosomes are enriched in areas that may play a role in prostate cancer aggressiveness and LNI risk. On the other hand, it is also important to highlight that chromosome X was not among the list of chromosomes with a higher amount of differentially methylated CpGs. Chromosome X is the site of genes encoding for the dihydrotestosterone receptor complex, which is known to play a key role in prostate cancer, especially in castration resistance disease. Probably the reason why the androgen receptor (*AR*) gene was not involved in epigenetic alterations was that we included patients with localized prostate cancer at the initial stage when no systemic treatment was administered. Androgen deprivation therapy is known to be a factor in inducing clonal selection and facilitating the proliferation of tumor cells with *AR* mutations. Based on this observation, we hypothesized that initial forms of prostate cancer did not exhibit significant epigenetic changing on chromosome X. Another relevant finding from the epigenetic profiling was that the majority of differentially methylated CpG positions, especially when cut-offs 10% and 25% were applied, were among intergenic parts of the genome. These findings may seem unexpected considering that methylation of onco-suppressor genes or demethylation of oncogenes happen more commonly in the

promoter's area. Nevertheless, a recent study from Zhao and colleagues highlighted that the epigenetic modifications of the DNA within intergenic parts of the genome might play a role in advanced metastatic prostate cancer(217). In this study, the investigators found that the methylation of intergenic regions was associated with variable expression of RNA of oncogenic driver genes such as *AR*, *MYC*, and *ERG*. The study suggested that epigenetic changings within potential intergenic regulatory regions might participate in tumorigenesis and facilitate the development of androgen deprivation therapy resistance in metastatic prostate cancer. Given this recent discovery, it is not surprising to find that intergenic regions were also enriched with differentially methylated CpGs in our samples. Nevertheless, how these intergenic CpGs are promoting gene silencing or gene activation, and then increasing the risk of LNI, remains unknown.

### ***8.3 – Validation of the Mundbjerg signature***

This study aimed to validate a previously developed epigenetic signature, designed for LNI prediction. The Mundbjerg signature(195) is a genomic prognostic score that was developed to predict cancer aggressiveness among different tumor loci within prostatectomy specimens. The Authors identified 25 probes that were differentially methylated among cancer foci and benign prostate tissue or intraepithelial neoplasia and that were closely correlated with the epigenetic profile of metastatic cells in the pelvic lymph nodes. This signature was developed in a restricted cohort of 14 patients and then its predictivity was explored in a cohort of 496 patients retrieved from the Cancer Genome Atlas project database. Among the large cohort of the CGA, 351 prostate samples (312 tumors and 39 normal tissue samples) were classified using the signature. The signature showed a 97.4% specificity and a 96.2% cancer sensitivity to identify prostate cancer compared to normal tissue samples. Besides this experimental validation, no further external validation of the signature was performed. Our study represents the first external validation of Mundbjerg signature. From this external validation, we achieved some interesting findings. First and foremost, we failed to consistently measure the 25 genomic positions of this signature in our tumor samples. The 25 positions did not match with the genome of the tumor samples from target and systematic biopsy cores, but also with the genome of tumor samples from the lymph node metastases. This can be explained by two reasons: i) the signature was developed using HM450 platform, while we relied on RRBS.



HM450 interrogates approximately 900 000 methylation sites of the human DNA and it differs from the RRBS kit which explores over 4 000 000 CpG sites and is based on next-generation sequencing. Indeed, even if the number of explored CpG sites was higher for the RRBS kit, the investigated sites were different; ii) the location of these sites was annotated in Mundbjerg's study using the human reference genome HG19, while for our study we relied on the human reference genome HG38. Annotation and conversion can be hampered when two different versions of the human reference genome(205) are considered, resulting in a miss-match of CpG sites. Overall, we were able to consistently measure six probes among the 25 of the Mundbjerg's signature. None of the tested probes was differentially methylated among LNI-positive and LNI-negative patients when either target or systematic samples were examined. Of note, only the *chr17:17810978* was significantly hypermethylated in the metastatic lymph nodes as compared to prostatic tumor samples (both target and systematic). The probe *chr17:17810978* is located on the gene *RAII* (Retinoic acid induced 1), which is a transcriptional regulator through chromatin remodeling. The gene is located within chromosome 17 and it is involved in the Smith-Magenis syndrome, influencing both the phenotype and response to medical treatments in schizophrenic patients. The gene *RAII* has never been associated with prostate cancer, so far. Conversely, other retinoic acid receptor genes have been closely investigated in the setting of castration-resistant prostate cancer (CRPC). The retinoid acid receptor-related orphan receptor  $\gamma$  (ROR- $\gamma$ ) has been recently identified as a potential key player in CRPC. ROR- $\gamma$  can stimulate androgen receptor transcription in prostate cancer, facilitating cancer growth and progression under androgenic boost. ROR- $\gamma$  antagonists seemed to block tumor progression in CRPC treated with enzalutamide by acting upstream in the androgen receptor transcription(218). The analogy between *RAII*-derived protein and ROR- $\gamma$  is difficult to define but truly worth studying in the future. In summary, Mundbjerg's signature failed to classify patients according to LNI. The 25 genomic positions of the signature were not constantly measured in our samples limiting its applicability in RRBS-processed samples, especially when the annotation is performed with the updated version of human reference genome HG38.

#### ***8.4 – Analysis of differentially methylated CpG sites among samples from target and systematic biopsy core***

Differential methylation analyses on target, systematic, and combined samples identified many CpG positions, CpG islands, and genes within these islands for both cut-offs. The stream of our analyses aimed at identifying the correlation among these CpG sites with genomic pathways. To accomplish this aim, we relied on enrichment analysis, which applied a powerful algorithm to establish whether, among those genes harboring many differentially methylated CpG, there were some participating in specific biological functions. Firstly, it is important to highlight that gene pathways analyses reached statistically significant results only when we applied a less stringent cut-off. Indeed, only with the 10% cut-off we reached an  $FDR < 0.005$ . Gene pathways are collecting hundreds of genes, so it is not surprising that only when the lists of identified genes were numerous, such as when we applied the 10% cut-off, we had enough events to reach statistical significance. Additionally, we found that regardless of the sample type, we identified the same gene pathways for target, systematic, and combined samples. In other words, for either target, systematic and combined samples, the differentially methylated CpGs positions were annotated in common genes or genes that were involved in the same gene pathways. Thus, we can hypothesize that gene pathways associated with LNI did not differ among sample types. The top four most significant gene pathways were sequence-specific double-stranded DNA binding (GO:1990837), sequence-specific DNA binding (GO:0043565), double-stranded DNA binding (GO:0003690), and RNA polymerase II transcription regulatory region sequence-specific DNA binding (GO:0000977). The same four pathways resulted from the analysis of all the differentially methylated CpGs, but also when hyper- and hypo-methylated CpGs were considered independently. These pathways are known to be crucially involved in DNA transcription and replications, especially in binding the double strain of DNA in specific positions such as promoters and transcription regulatory regions. These pathways are involved in gene silencing and activation, and they are considered the main actors of epigenetic mechanisms. No previous study has identified these pathways as significantly associated with LNI in prostate cancer. Thus, this result is relevant for its novelty but deserves further validation. Of note, another pathway, the neuron differentiation (GO:0030182) achieved statistical significance on enrichment analysis. Neuron differentiation has been previously linked

with prostate cancer. Three proteins, namely staurosporine, reelin, and beta III tub, have been found to play a role in promoting neuronal differentiation in prostate cancer cells. Staurosporine is a protein kinase inhibitor, which stimulates several gene expression profiles which ultimately suppress malignancy of human prostate cancer(219). Reelin, on the contrary, can regulate cell migration and it was associated with higher Gleason score and cancer aggressiveness(220). Lastly, beta III tubulin, another neuronal inducer protein, was linked with prostate cancer, and apparently, it seems to promote progression to castration resistance forms where this class III beta-tubulin is overexpressed(221). Our analysis supports the hypothesis that neuronal differentiation may play a role in cancer aggressiveness and may increase the risk of LNI, pending further validations. In the last step of the analyses focusing on differentially methylated CpGs, we examined the list of genes in common among target, systematic, and combined samples that were harboring the highest number of differentially methylated CpGs. Thus, we selected those genes that were annotated among those harboring CpGs with at least 25% methylation difference. We established also that the genes had to overlap CpGs islands with at least 10 differentially methylated CpGs per island. Six genes were overlapping the results of the analyses on target, systematic, and combined samples: *CBX4*, *CHD5*, *ENSG00000285629*, *ENSG00000287655*, *RNF126*, *SHTNI*(222,223). Three of them, have been previously linked with prostate cancer. *CBX4* is a negative regulator of the RNA polymerase II, but is also a regulator of prostate cancer cell growth. Indeed, the bound among *CBX4* and the long non-coding RNAs *RAMS11*, a known promoter of prostate cancer cell growth, activates *Top2 $\alpha$*  which contrasts the activity of *RAMS11* by attenuating its pro-cancer effects(224). *CHD5* is a chromatin-remodeling protein, and it modulates the transcription of genes, including tumor promoter genes. Promoter silencing of *CHD5* has been linked with several tumors(225), including prostate cancer(226). *RNF126* (Ring Finger Protein 126) encodes for a protein that regulates the interaction among DNA and proteins. *RNF126* seems to function as an oncogene in prostate cancer, by destabilizing cell-cycle and increasing cell proliferation when it is upregulated(227). Our findings support the hypothesis that epigenetic alterations within these 6 genes may significantly correlate with a higher risk of LNI in localized disease regardless the tumor samples were collected from mp-MRI visible lesions or not. In conclusion, enrichment analysis identified similar pathways among different sample types. Tumor epigenetic may

not be as differentiated among target and systematic tumor foci as we expected, at least from a gene pathways perspective. This result could be justified if we consider the lack of environmental factors, such as radiotherapy or systemic therapies that usually facilitate the selection of specific tumor clones with unique genetic or epigenetic features. Our population was exclusively composed of patients with localized disease, with a primary diagnosis of prostate cancer and no previous treatment. Systemic treatments, such as hormonal therapy, are known to play a role in clone selection facilitating disease heterogeneity. Thus, large epigenetic modifications or activation of different genomic pathways was not yet initiated at this stage, or at least was not statistically different among tumor foci.

### ***8.5 – Highly differentially methylated CpGs sites and their correlation with gene pathways***

The development of an epigenetic signature was achieved through the identification of highly differentially methylated CpG spots among patients with and without LNI. We applied an average methylation difference cut-off of 50% among LNI-positive and negative patients to restrict the number of significant CpGs. The first and most interesting result was that target and systematic samples have no CpGs sites in common. Indeed, the two lists of highly differentially methylated cytosines for target and systematic samples were not overlapping in any genomic positions. Annotation analysis partially confirmed this finding. Indeed, annotation of the highly differentially methylated CpGs on the human genome identified 360 and 411 genes for target and systematic samples, respectively. Among them, only 18 were overlapping. These 18 genes were *ANO2*, *CDH4*, *CSMD1*, *CSMD3*, *DPP10*, *LINC01166*, *LINGO2*, *MIR3667HG*, *RAI1*, *RBFOX1*, *RIMBP2*, *SBNO2*, *SCAMP5*, *SEMA3A*, *TMEM132C*, *TP73*, *TSPEAR*, *WSCD2*. Among them, *CSMD1*, *DPP10*, *SEMA3A*, *TP53*, and *TSPEAR* have been previously correlated with prostate cancer, while the link was not fully elucidated for *TSPEAR* and *CSMD3*(228). *CSMD1* is a tumor suppressor located on chromosome 8 and its lower expression was associated with a higher Gleason score tumor(229,230); it encodes for a complement control protein, and its lower expression may facilitate the tumor's abilities to divide, migrate and invade. *DPP10* regulates the cell surface expression of the potassium channels, which have a pivotal role in carcinogenesis(231). *SEMA3A* acts as

an inhibitor of angiogenesis, and its expression is aberrant in prostate cancer, as it affects adhesion and motility of prostate cancer cells indicating a key role of this gene in cancer progression(232,233). Lastly, *TP73* is a gene encoding for a protein which is one of the p53 family of transcription factors. It is involved in cell cycle regulation, and it can stimulate cell apoptosis. It is a well-known tumor suppressor, linked with prostate cancer(234–236). We can postulate that epigenetic modifications affecting these genes are significantly associated with LNI regardless they are present on tumor cells from target or systematic foci. We then run enrichment analyses including both lists of genes identified from target and systematic sample analyses. However, statistically significant results were achieved only with genes from target samples. Here, the most significant gene pathways were on potassium channels and their regulators. It is known that potassium channels play a pivotal role in cancer cell proliferation, migration, and invasion(237). Potassium channels are overexpressed in prostate cancer cells, as well as in the tumor stroma compartment tissue(238). Potassium channels have been implicated also in the proliferation of prostate cancer cells, as well as their metastatic propension(239). Our findings showed that gene pathways associated with potassium channels were enriched with genes with differentially methylated CpGs, suggesting a possible correlation with LNI risk. Interestingly, these pathways emerged only from the analyses of target samples. We believe that further investigations can elucidate the correlation between potassium channel expression and the risk of LNI, and explore how the regulation of gene expression of potassium channels is linked mp-MRI visible lesions, but not with systematic tumor foci.

### ***8.6 – Developing an integrated model for LNI prediction***

The primary aim of the study was to develop a model predicting LNI while integrating clinical, radiological, and epigenetic features. We also aimed to assess whether mp-MRI visible and systematic tumor foci were holding different epigenetic alterations, which were somehow differently associated with the risk of LNI. Thus, we chose to explore differentially methylated CpGs among patients with and without LNI including either target or systematic samples. As previously mentioned, the list of relevant CpGs was different among target and systematic samples. In other words, we found that the epigenetic alterations, namely CpG sites, which were significantly associated with the

risk of LNI, were not the same among target and systematic tumor samples. This is a relevant finding which is supporting the hypothesis that epigenetic alterations driving tumor spreading are different among target (mp-MRI lesions with PI-RADS 3-5) and systematic tumor foci, at least in terms of involved cytosines. Additionally, when we combined these two signatures with clinical (PSA), mp-MRI (clinical T stage at mp-MRI), and target biopsy features (Gleason score at target biopsy), the resulting models presented different accuracies for LNI prediction (86% for the target model vs. 82.7% for the systematic model). Caution should be paid while interpreting these findings because no external validation of the models was performed. Nevertheless, it is encouraging to see that epigenetic patterns highlighted within tumor samples of the target lesions, seemed, at least in this initial developing stage, more accurate to predict the risk of LNI, as compared to the systematic counterparts. Our findings may encourage the hypothesis that epigenetic profiling of mp-MRI target biopsy samples may predict more accurately the characteristics of the tumor, and its metastatic propensity, as compared to the epigenetic profiling of systematic biopsy samples. In recent years, the hypothesis that target biopsy was holding more relevant prognostic information on tumor aggressiveness, as compared to systematic biopsy has been postulated and tested several times. Randomized trials(67,72,240) proved that mp-MRI target biopsy is more accurate than systematic biopsy to detect clinically significant prostate cancer. These trials prompted the scientific community to hypothesize that prostate cancer detection and characterization could be achieved through the sampling of mp-MRI visible lesions alone, as this sampling is more informative and clinically useful for tailoring curative treatments as compared to systematic sampling. Another relevant finding of this study was that both the developed models integrating clinical, mp-MRI, and epigenetic features were superior to existing tools for LNI prediction. The accuracy, as well as the clinical net benefit of the two developed models, were outperforming the 2012, 2017, and 2019 versions of Briganti's nomogram. Pending external validation, this is an encouraging finding.

### ***8.7 – Study limitations***

This study is not devoid of limitations. First and foremost, we did not validate our findings and our models within an external cohort. As previously specified, the main project is ongoing and we planned to reach a population of 400 patients at the final recruiting. Given

that LNI occurs approximately in 25% of patients with localized disease receiving PLND, we estimated that the final number of events, namely LNI, will be 100. Considering that 40 events were necessary to develop the models, 60 events will be sufficient for their validation and comparison with existing tools. Secondly, the choice to rely on the 50% cut-offs for the identification of highly differentially methylated CpGs positions was arbitrary. The RRBS kit manufacturer suggests the use of 10% and 25% cut-offs for differential methylation analyses. We relied on these two cut-offs for explorative analyses, but we chose a more stringent one for the development of the signatures. This was done in order to reduce the number of relevant CpGs sites, that were included in the signatures. A limited number of CpGs will help future validations of our findings. Indeed, a small number of genomic positions can be selectively explored with target sequencing instead of whole genome sequencing, which is more time-consuming and expensive. Lastly, we did not explore the methylation status of relevant CpGs sites, within the lymph node metastases. Our study lacks a match-paired analysis among prostate tumor samples and lymph node samples. This analysis will be integrated into the main project and it will help to corroborate our findings providing a direct epigenetic correlation among tumor cores and lymph node metastases, and not just a probabilistic correlation, as the one achieved in the present study.

### **8.8 – Conclusions**

The present study successfully profiled the epigenetic alterations of a large number of FFPE tumor samples. We described a protocol that maximizes DNA tumor extraction from biopsy cores and its processing, with a considerable output in terms of CpG positions. RRBS kit was appropriate for this task given that biopsy core samples contained a limited amount of genomic DNA which would have been insufficient for generating a reliable output with array-based kits (HM450). Our study represents the first external validation of Mundbjerg signature. We found that the majority of genomic positions of the signature were not constantly measured in our samples, and they were not differentially methylated among patients with and without LNI, as well as among prostatic and lymph node samples. The only probe that was hypermethylated in the lymph node metastases as compared to tumor samples was the *RAI1* probe. To date, the correlation between this gene and the risk of LNI in prostate cancer has not been fully

elucidated. Enrichment analysis of differentially methylated CpGs identified similar genomic pathways among target and systematic tumor foci. This result is not surprising if we consider that we included only patients with localized prostate cancer, who did not receive previous treatments such as radiotherapy or systemic agents. At this disease stage, where no environmental factors have induced a clonal tumor selection, the identification of similar gene pathways is expected, especially because we applied the cut-offs of 10% and 25% that identified a less stringent number of CpG positions and correlated genes. Conversely, the application of the 50% cut-off successfully segregated different CpGs and genes among target and systematic samples. Here, also enrichment analysis found genomic pathways that were enriched in target samples and unexpressed in systematic samples. These pathways were involved in the transcription of potassium channels which are known to play a role in prostate cancer proliferation and metastatization. The correlation between the epigenetic regulation of potassium channel genes and LNI is worth to be investigated further. Lastly, we successfully developed a model integrating clinical, radiological, and epigenetic features that outperformed existing clinical models in predicting the risk of LNI. The model that was developed from target samples seemed more accurate than that developed on systematic samples, pending their external validations.



## 9. References

1. IARC: Home [Internet]. [cited 2022 Oct 9]. Available from: <https://www.iarc.who.int/>
2. Cancer (IARC) TIA for R on. Global Cancer Observatory [Internet]. [cited 2022 Oct 9]. Available from: <https://gco.iarc.fr/>
3. Culp MB, Soerjomataram I, Efstathiou JA, Bray F, Jemal A. Recent Global Patterns in Prostate Cancer Incidence and Mortality Rates. *Eur Urol*. 2020 Jan;77(1):38–52.
4. Baade PD, Youlten DR, Krnjacki LJ. International epidemiology of prostate cancer: geographical distribution and secular trends. *Mol Nutr Food Res*. 2009 Feb;53(2):171–84.
5. Tonon L, Fromont G, Boyault S, Thomas E, Ferrari A, Sertier AS, et al. Mutational Profile of Aggressive, Localised Prostate Cancer from African Caribbean Men Versus European Ancestry Men. *Eur Urol*. 2019 Jan;75(1):11–5.
6. Tikkinen KAO, Dahm P, Lytvyn L, Heen AF, Vernooij RWM, Siemieniuk RAC, et al. Prostate cancer screening with prostate-specific antigen (PSA) test: a clinical practice guideline. *BMJ*. 2018 Sep 5;362:k3581.
7. Rawla P. Epidemiology of Prostate Cancer. *World J Oncol*. 2019 Apr;10(2):63–89.
8. Attard G, Parker C, Eeles RA, Schröder F, Tomlins SA, Tannock I, et al. Prostate cancer. *Lancet*. 2016 Jan 2;387(10013):70–82.
9. Verze P, Cai T, Lorenzetti S. The role of the prostate in male fertility, health and disease. *Nat Rev Urol*. 2016 Jul;13(7):379–86.
10. Timms BG. Prostate development: a historical perspective. *Differentiation*. 2008 Jul;76(6):565–77.

11. McNeal JE. Normal and pathologic anatomy of prostate. *Urology*. 1981 Mar;17(Suppl 3):11–6.
12. Toivanen R, Shen MM. Prostate organogenesis: tissue induction, hormonal regulation and cell type specification. *Development*. 2017 Apr 15;144(8):1382–98.
13. Carm KT, Hoff AM, Bakken AC, Axcrone U, Axcrone K, Lothe RA, et al. Interfocal heterogeneity challenges the clinical usefulness of molecular classification of primary prostate cancer. *Sci Rep*. 2019 Sep 19;9(1):13579.
14. Sfanos KS, Yegnasubramanian S, Nelson WG, De Marzo AM. The inflammatory microenvironment and microbiome in prostate cancer development. *Nat Rev Urol*. 2018 Jan;15(1):11–24.
15. Bandini M, Gandaglia G, Briganti A. Obesity and prostate cancer. *Curr Opin Urol*. 2017 Sep;27(5):415–21.
16. Rebello RJ, Oing C, Knudsen KE, Loeb S, Johnson DC, Reiter RE, et al. Prostate cancer. *Nat Rev Dis Primers*. 2021 Feb 4;7(1):9.
17. Humphrey PA. Gleason grading and prognostic factors in carcinoma of the prostate. *Mod Pathol*. 2004 Mar;17(3):292–306.
18. Epstein JI, Zelefsky MJ, Sjoberg DD, Nelson JB, Egevad L, Magi-Galluzzi C, et al. A Contemporary Prostate Cancer Grading System: A Validated Alternative to the Gleason Score. *Eur Urol*. 2016 Mar;69(3):428–35.
19. Rao AR, Motiwala HG, Karim OMA. The discovery of prostate-specific antigen. *BJU Int*. 2008 Jan;101(1):5–10.
20. Balk SP, Ko YJ, Bubley GJ. Biology of prostate-specific antigen. *J Clin Oncol*. 2003 Jan 15;21(2):383–91.
21. Kouriefs C, Sahoyl M, Grange P, Muir G. Prostate specific antigen through the years. *Arch Ital Urol Androl*. 2009 Dec;81(4):195–8.

22. Catalona WJ, Smith DS, Ratliff TL, Dodds KM, Coplen DE, Yuan JJ, et al. Measurement of prostate-specific antigen in serum as a screening test for prostate cancer. *N Engl J Med*. 1991 Apr 25;324(17):1156–61.
23. Charatan FB. FDA approves test for prostatic cancer. *BMJ*. 1994 Sep 10;309(6955):628–9.
24. Bangma CH, Roemeling S, Schröder FH. Overdiagnosis and overtreatment of early detected prostate cancer. *World J Urol*. 2007 Mar;25(1):3–9.
25. Hayes JH, Barry MJ. Screening for prostate cancer with the prostate-specific antigen test: a review of current evidence. *JAMA*. 2014 Mar 19;311(11):1143–9.
26. U.S. Preventive Services Task Force. Screening for prostate cancer: U.S. Preventive Services Task Force recommendation statement. *Ann Intern Med*. 2008 Aug 5;149(3):185–91.
27. Va M. Screening for prostate cancer: U.S. Preventive Services Task Force recommendation statement. *Annals of internal medicine* [Internet]. 2012 Jul 17 [cited 2022 Oct 9];157(2). Available from: <https://pubmed.ncbi.nlm.nih.gov/22801674/>
28. Andriole GL, Crawford ED, Grubb RL, Buys SS, Chia D, Church TR, et al. Mortality Results from a Randomized Prostate-Cancer Screening Trial. *New England Journal of Medicine*. 2009 Mar 26;360(13):1310–9.
29. Schröder FH, Hugosson J, Roobol MJ, Tammela TLJ, Ciatto S, Nelen V, et al. Screening and Prostate-Cancer Mortality in a Randomized European Study. *New England Journal of Medicine*. 2009 Mar 26;360(13):1320–8.
30. Prasad SM, Drazer MW, Huo D, Hu JC, Eggener SE. 2008 US Preventive Services Task Force recommendations and prostate cancer screening rates. *JAMA*. 2012 Apr 25;307(16):1692–4.
31. Bandini M, Mazzone E, Preisser F, Nazzani S, Zaffuto E, Marchioni M, et al. Increase in the Annual Rate of Newly Diagnosed Metastatic Prostate Cancer: A

- Contemporary Analysis of the Surveillance, Epidemiology and End Results Database. *Eur Urol Oncol*. 2018 Sep;1(4):314–20.
32. US Preventive Services Task Force, Grossman DC, Curry SJ, Owens DK, Bibbins-Domingo K, Caughey AB, et al. Screening for Prostate Cancer: US Preventive Services Task Force Recommendation Statement. *JAMA*. 2018 May 8;319(18):1901–13.
  33. Van Poppel H, Roobol MJ, Chapple CR, Catto JWF, N'Dow J, Sønksen J, et al. Prostate-specific Antigen Testing as Part of a Risk-Adapted Early Detection Strategy for Prostate Cancer: European Association of Urology Position and Recommendations for 2021. *Eur Urol*. 2021 Dec;80(6):703–11.
  34. Giri VN, Knudsen KE, Kelly WK, Cheng HH, Cooney KA, Cookson MS, et al. Implementation of Germline Testing for Prostate Cancer: Philadelphia Prostate Cancer Consensus Conference 2019. *J Clin Oncol*. 2020 Aug 20;38(24):2798–811.
  35. Siegel RL, Miller KD, Jemal A. Cancer statistics, 2018. *CA Cancer J Clin*. 2018 Jan;68(1):7–30.
  36. Han Y, Rand KA, Hazelett DJ, Ingles SA, Kittles RA, Strom SS, et al. Prostate Cancer Susceptibility in Men of African Ancestry at 8q24. *J Natl Cancer Inst*. 2016 Jul;108(7).
  37. Zeigler-Johnson CM, Spangler E, Jalloh M, Gueye SM, Rennert H, Rebbeck TR. Genetic susceptibility to prostate cancer in men of African descent: implications for global disparities in incidence and outcomes. *Can J Urol*. 2008 Feb;15(1):3872–82.
  38. Shenoy D, Packianathan S, Chen AM, Vijayakumar S. Do African-American men need separate prostate cancer screening guidelines? *BMC Urol*. 2016 May 10;16(1):19.
  39. Kimura T, Egawa S. Epidemiology of prostate cancer in Asian countries. *Int J Urol*. 2018 Jun;25(6):524–31.

40. Hemminki K. Familial risk and familial survival in prostate cancer. *World J Urol.* 2012 Apr;30(2):143–8.
41. Stewart RW, Lizama S, Peairs K, Sateia HF, Choi Y. Screening for prostate cancer. *Semin Oncol.* 2017 Feb;44(1):47–56.
42. Tan DSW, Mok TSK, Rebbeck TR. Cancer Genomics: Diversity and Disparity Across Ethnicity and Geography. *J Clin Oncol.* 2016 Jan 1;34(1):91–101.
43. Nyberg T, Frost D, Barrowdale D, Evans DG, Bancroft E, Adlard J, et al. Prostate Cancer Risks for Male BRCA1 and BRCA2 Mutation Carriers: A Prospective Cohort Study. *Eur Urol.* 2020 Jan;77(1):24–35.
44. Nyberg T, Govindasami K, Leslie G, Dadaev T, Bancroft E, Ni Raghallaigh H, et al. Homeobox B13 G84E Mutation and Prostate Cancer Risk. *Eur Urol.* 2019 May;75(5):834–45.
45. Dominguez-Valentin M, Sampson JR, Seppälä TT, Ten Broeke SW, Plazzer JP, Nakken S, et al. Cancer risks by gene, age, and gender in 6350 carriers of pathogenic mismatch repair variants: findings from the Prospective Lynch Syndrome Database. *Genet Med.* 2020 Jan;22(1):15–25.
46. Ahmadiyeh N, Pomerantz MM, Grisanzio C, Herman P, Jia L, Almendro V, et al. 8q24 prostate, breast, and colon cancer risk loci show tissue-specific long-range interaction with MYC. *Proc Natl Acad Sci U S A.* 2010 May 25;107(21):9742–6.
47. Li-Sheng Chen S, Ching-Yuan Fann J, Sipeky C, Yang TK, Yueh-Hsia Chiu S, Ming-Fang Yen A, et al. Risk Prediction of Prostate Cancer with Single Nucleotide Polymorphisms and Prostate Specific Antigen. *J Urol.* 2019 Mar;201(3):486–95.
48. Esposito K, Chiodini P, Capuano A, Bellastella G, Maiorino MI, Parretta E, et al. Effect of metabolic syndrome and its components on prostate cancer risk: meta-analysis. *J Endocrinol Invest.* 2013 Feb;36(2):132–9.

49. Zhao J, Stockwell T, Roemer A, Chikritzhs T. Is alcohol consumption a risk factor for prostate cancer? A systematic review and meta-analysis. *BMC Cancer*. 2016 Nov 15;16(1):845.
50. De Nunzio C, Andriole GL, Thompson IM, Freedland SJ. Smoking and Prostate Cancer: A Systematic Review. *Eur Urol Focus*. 2015 Aug;1(1):28–38.
51. Bylsma LC, Alexander DD. A review and meta-analysis of prospective studies of red and processed meat, meat cooking methods, heme iron, heterocyclic amines and prostate cancer. *Nutr J*. 2015 Dec 21;14:125.
52. Paner GP, Stadler WM, Hansel DE, Montironi R, Lin DW, Amin MB. Updates in the Eighth Edition of the Tumor-Node-Metastasis Staging Classification for Urologic Cancers. *Eur Urol*. 2018 Apr;73(4):560–9.
53. Siegel RL, Miller KD, Fuchs HE, Jemal A. Cancer statistics, 2022. *CA Cancer J Clin*. 2022 Jan;72(1):7–33.
54. Key Statistics for Prostate Cancer | Prostate Cancer Facts [Internet]. [cited 2022 Oct 9]. Available from: <https://www.cancer.org/cancer/prostate-cancer/about/key-statistics.html>
55. Ross HM, Kryvenko ON, Cowan JE, Simko JP, Wheeler TM, Epstein JI. Do adenocarcinomas of the prostate with Gleason score (GS)  $\leq 6$  have the potential to metastasize to lymph nodes? *Am J Surg Pathol*. 2012 Sep;36(9):1346–52.
56. Anderson BB, Oberlin DT, Razmaria AA, Choy B, Zagaja GP, Shalhav AL, et al. Extraprostatic Extension Is Extremely Rare for Contemporary Gleason Score 6 Prostate Cancer. *Eur Urol*. 2017 Sep;72(3):455–60.
57. Bill-Axelson A, Holmberg L, Garmo H, Taari K, Busch C, Nordling S, et al. Radical Prostatectomy or Watchful Waiting in Prostate Cancer - 29-Year Follow-up. *N Engl J Med*. 2018 Dec 13;379(24):2319–29.

58. Wilt TJ, Jones KM, Barry MJ, Andriole GL, Culin D, Wheeler T, et al. Follow-up of Prostatectomy versus Observation for Early Prostate Cancer. *N Engl J Med*. 2017 Jul 13;377(2):132–42.
59. Hamdy FC, Donovan JL, Lane JA, Mason M, Metcalfe C, Holding P, et al. 10-Year Outcomes after Monitoring, Surgery, or Radiotherapy for Localized Prostate Cancer. *N Engl J Med*. 2016 13;375(15):1415–24.
60. D’Amico AV, Whittington R, Malkowicz SB, Schultz D, Blank K, Broderick GA, et al. Biochemical outcome after radical prostatectomy, external beam radiation therapy, or interstitial radiation therapy for clinically localized prostate cancer. *JAMA*. 1998 Sep 16;280(11):969–74.
61. Mazzone E, Gandaglia G, Ploussard G, Marra G, Valerio M, Campi R, et al. Risk Stratification of Patients Candidate to Radical Prostatectomy Based on Clinical and Multiparametric Magnetic Resonance Imaging Parameters: Development and External Validation of Novel Risk Groups. *Eur Urol*. 2022 Feb;81(2):193–203.
62. Johnson DC, Raman SS, Mirak SA, Kwan L, Bajgiran AM, Hsu W, et al. Detection of Individual Prostate Cancer Foci via Multiparametric Magnetic Resonance Imaging. *Eur Urol*. 2019 May;75(5):712–20.
63. Drost FJH, Osses DF, Nieboer D, Steyerberg EW, Bangma CH, Roobol MJ, et al. Prostate MRI, with or without MRI-targeted biopsy, and systematic biopsy for detecting prostate cancer. *Cochrane Database Syst Rev*. 2019 Apr 25;4:CD012663.
64. Barentsz JO, Richenberg J, Clements R, Choyke P, Verma S, Villeirs G, et al. ESUR prostate MR guidelines 2012. *Eur Radiol*. 2012 Apr;22(4):746–57.
65. Weinreb JC, Barentsz JO, Choyke PL, Cornud F, Haider MA, Macura KJ, et al. PI-RADS Prostate Imaging - Reporting and Data System: 2015, Version 2. *Eur Urol*. 2016 Jan;69(1):16–40.
66. Turkbey B, Rosenkrantz AB, Haider MA, Padhani AR, Villeirs G, Macura KJ, et al. Prostate Imaging Reporting and Data System Version 2.1: 2019 Update of

Prostate Imaging Reporting and Data System Version 2. *Eur Urol.* 2019 Sep;76(3):340–51.

67. Kasivisvanathan V, Rannikko AS, Borghi M, Panebianco V, Mynderse LA, Vaarala MH, et al. MRI-Targeted or Standard Biopsy for Prostate-Cancer Diagnosis. *N Engl J Med.* 2018 May 10;378(19):1767–77.
68. Rouvière O, Puech P, Renard-Penna R, Claudon M, Roy C, Mège-Lechevallier F, et al. Use of prostate systematic and targeted biopsy on the basis of multiparametric MRI in biopsy-naive patients (MRI-FIRST): a prospective, multicentre, paired diagnostic study. *Lancet Oncol.* 2019 Jan;20(1):100–9.
69. van der Leest M, Cornel E, Israël B, Hendriks R, Padhani AR, Hoogenboom M, et al. Head-to-head Comparison of Transrectal Ultrasound-guided Prostate Biopsy Versus Multiparametric Prostate Resonance Imaging with Subsequent Magnetic Resonance-guided Biopsy in Biopsy-naïve Men with Elevated Prostate-specific Antigen: A Large Prospective Multicenter Clinical Study. *Eur Urol.* 2019 Apr;75(4):570–8.
70. Wegelin O, Exterkate L, van der Leest M, Kummer JA, Vreuls W, de Bruin PC, et al. The FUTURE Trial: A Multicenter Randomised Controlled Trial on Target Biopsy Techniques Based on Magnetic Resonance Imaging in the Diagnosis of Prostate Cancer in Patients with Prior Negative Biopsies. *Eur Urol.* 2019 Apr;75(4):582–90.
71. Mottet N, van den Bergh RCN, Briers E, Van den Broeck T, Cumberbatch MG, De Santis M, et al. EAU-EANM-ESTRO-ESUR-SIOG Guidelines on Prostate Cancer-2020 Update. Part 1: Screening, Diagnosis, and Local Treatment with Curative Intent. *Eur Urol.* 2021 Feb;79(2):243–62.
72. Ahdoot M, Wilbur AR, Reese SE, Lebastchi AH, Mehralivand S, Gomella PT, et al. MRI-Targeted, Systematic, and Combined Biopsy for Prostate Cancer Diagnosis. *N Engl J Med.* 2020 Mar 5;382(10):917–28.



73. Farrell C, Noyes SL, Joslin J, Varma M, Moriarity A, Buchach C, et al. Prostate Multiparametric Magnetic Resonance Imaging Program Implementation and Impact: Initial Clinical Experience in a Community Based Health System. *Urology Practice*. 2018 May 1;5(3):165–71.
74. Hessels D, Klein Gunnewiek JMT, van Oort I, Karthaus HFM, van Leenders GJL, van Balken B, et al. DD3(PCA3)-based molecular urine analysis for the diagnosis of prostate cancer. *Eur Urol*. 2003 Jul;44(1):8–15; discussion 15-16.
75. Van Neste L, Hendriks RJ, Dijkstra S, Trooskens G, Cornel EB, Jannink SA, et al. Detection of High-grade Prostate Cancer Using a Urinary Molecular Biomarker-Based Risk Score. *Eur Urol*. 2016 Nov;70(5):740–8.
76. Bryant RJ, Sjoberg DD, Vickers AJ, Robinson MC, Kumar R, Marsden L, et al. Predicting high-grade cancer at ten-core prostate biopsy using four kallikrein markers measured in blood in the ProtecT study. *J Natl Cancer Inst*. 2015 Jul;107(7):djv095.
77. Loeb S, Catalona WJ. The Prostate Health Index: a new test for the detection of prostate cancer. *Ther Adv Urol*. 2014 Apr;6(2):74–7.
78. Partin AW, Van Neste L, Klein EA, Marks LS, Gee JR, Troyer DA, et al. Clinical validation of an epigenetic assay to predict negative histopathological results in repeat prostate biopsies. *J Urol*. 2014 Oct;192(4):1081–7.
79. Jonsson E, Sigbjarnarson HP, Tomasson J, Benediktsdottir KR, Tryggvadottir L, Hrafnkelsson J, et al. Adenocarcinoma of the prostate in Iceland: a population-based study of stage, Gleason grade, treatment and long-term survival in males diagnosed between 1983 and 1987. *Scand J Urol Nephrol*. 2006;40(4):265–71.
80. Adolfsson J, Tribukait B, Levitt S. The 20-Yr outcome in patients with well- or moderately differentiated clinically localized prostate cancer diagnosed in the pre-PSA era: the prognostic value of tumour ploidy and comorbidity. *Eur Urol*. 2007 Oct;52(4):1028–35.

81. Bill-Axelsson A, Holmberg L, Ruutu M, Häggman M, Andersson SO, Bratell S, et al. Radical prostatectomy versus watchful waiting in early prostate cancer. *N Engl J Med*. 2005 May 12;352(19):1977–84.
82. Johansson JE, Adami HO, Andersson SO, Bergström R, Krusemo UB, Kraaz W. Natural history of localised prostatic cancer. A population-based study in 223 untreated patients. *Lancet*. 1989 Apr 15;1(8642):799–803.
83. Sandblom G, Dufmats M, Varenhorst E. Long-term survival in a Swedish population-based cohort of men with prostate cancer. *Urology*. 2000 Sep 1;56(3):442–7.
84. Chodak GW, Thisted RA, Gerber GS, Johansson JE, Adolfsson J, Jones GW, et al. Results of conservative management of clinically localized prostate cancer. *N Engl J Med*. 1994 Jan 27;330(4):242–8.
85. J H, Mj R, M M, Tlj T, M Z, V N, et al. A 16-yr Follow-up of the European Randomized study of Screening for Prostate Cancer. *European urology* [Internet]. 2019 Jul [cited 2022 Oct 9];76(1). Available from: <https://pubmed.ncbi.nlm.nih.gov/30824296/>
86. Wilt TJ, Vo TN, Langsetmo L, Dahm P, Wheeler T, Aronson WJ, et al. Radical Prostatectomy or Observation for Clinically Localized Prostate Cancer: Extended Follow-up of the Prostate Cancer Intervention Versus Observation Trial (PIVOT). *Eur Urol*. 2020 Jun;77(6):713–24.
87. Graversen PH, Nielsen KT, Gasser TC, Corle DK, Madsen PO. Radical prostatectomy versus expectant primary treatment in stages I and II prostatic cancer. A fifteen-year follow-up. *Urology*. 1990 Dec;36(6):493–8.
88. Vernooij RW, Lancee M, Cleves A, Dahm P, Bangma CH, Aben KK. Radical prostatectomy versus deferred treatment for localised prostate cancer. *Cochrane Database Syst Rev*. 2020 Jun 4;6:CD006590.

89. Thomsen FB, Brasso K, Klotz LH, Røder MA, Berg KD, Iversen P. Active surveillance for clinically localized prostate cancer--a systematic review. *J Surg Oncol*. 2014 Jun;109(8):830–5.
90. Tosoian JJ, Mamawala M, Epstein JI, Landis P, Wolf S, Trock BJ, et al. Intermediate and Longer-Term Outcomes From a Prospective Active-Surveillance Program for Favorable-Risk Prostate Cancer. *J Clin Oncol*. 2015 Oct 20;33(30):3379–85.
91. Donovan JL, Hamdy FC, Lane JA, Mason M, Metcalfe C, Walsh E, et al. Patient-Reported Outcomes after Monitoring, Surgery, or Radiotherapy for Prostate Cancer. *N Engl J Med*. 2016 Oct 13;375(15):1425–37.
92. McLeod DG, Iversen P, See WA, Morris T, Armstrong J, Wirth MP, et al. Bicalutamide 150 mg plus standard care vs standard care alone for early prostate cancer. *BJU Int*. 2006 Feb;97(2):247–54.
93. Willemse PPM, Davis NF, Grivas N, Zattoni F, Lardas M, Briers E, et al. Systematic Review of Active Surveillance for Clinically Localised Prostate Cancer to Develop Recommendations Regarding Inclusion of Intermediate-risk Disease, Biopsy Characteristics at Inclusion and Monitoring, and Surveillance Repeat Biopsy Strategy. *Eur Urol*. 2022 Apr;81(4):337–46.
94. Lam TBL, MacLennan S, Willemse PPM, Mason MD, Plass K, Shepherd R, et al. EAU-EANM-ESTRO-ESUR-SIOG Prostate Cancer Guideline Panel Consensus Statements for Deferred Treatment with Curative Intent for Localised Prostate Cancer from an International Collaborative Study (DETECTIVE Study). *Eur Urol*. 2019 Dec;76(6):790–813.
95. Loeb S, Bruinsma SM, Nicholson J, Briganti A, Pickles T, Kakehi Y, et al. Active surveillance for prostate cancer: a systematic review of clinicopathologic variables and biomarkers for risk stratification. *Eur Urol*. 2015 Apr;67(4):619–26.
96. Klotz L, Pond G, Loblaw A, Sugar L, Moussa M, Berman D, et al. Randomized Study of Systematic Biopsy Versus Magnetic Resonance Imaging and Targeted

- and Systematic Biopsy in Men on Active Surveillance (ASIST): 2-year Postbiopsy Follow-up. *Eur Urol.* 2020 Mar;77(3):311–7.
97. Studer UE, Collette L, Whelan P, Albrecht W, Casselman J, de Reijke T, et al. Using PSA to guide timing of androgen deprivation in patients with T0-4 N0-2 M0 prostate cancer not suitable for local curative treatment (EORTC 30891). *Eur Urol.* 2008 May;53(5):941–9.
  98. Gandaglia G, Ploussard G, Valerio M, Mattei A, Fiori C, Fossati N, et al. A Novel Nomogram to Identify Candidates for Extended Pelvic Lymph Node Dissection Among Patients with Clinically Localized Prostate Cancer Diagnosed with Magnetic Resonance Imaging-targeted and Systematic Biopsies. *Eur Urol.* 2019;75(3):506–14.
  99. Bolla M, Van Tienhoven G, Warde P, Dubois JB, Mirimanoff RO, Storme G, et al. External irradiation with or without long-term androgen suppression for prostate cancer with high metastatic risk: 10-year results of an EORTC randomised study. *Lancet Oncol.* 2010 Nov;11(11):1066–73.
  100. Pilepich MV, Winter K, Lawton CA, Krisch RE, Wolkov HB, Movsas B, et al. Androgen suppression adjuvant to definitive radiotherapy in prostate carcinoma--long-term results of phase III RTOG 85-31. *Int J Radiat Oncol Biol Phys.* 2005 Apr 1;61(5):1285–90.
  101. Roach M, Bae K, Speight J, Wolkov HB, Rubin P, Lee RJ, et al. Short-term neoadjuvant androgen deprivation therapy and external-beam radiotherapy for locally advanced prostate cancer: long-term results of RTOG 8610. *J Clin Oncol.* 2008 Feb 1;26(4):585–91.
  102. D'Amico AV, Chen MH, Renshaw AA, Loffredo M, Kantoff PW. Androgen suppression and radiation vs radiation alone for prostate cancer: a randomized trial. *JAMA.* 2008 Jan 23;299(3):289–95.
  103. Denham JW, Steigler A, Lamb DS, Joseph D, Turner S, Matthews J, et al. Short-term neoadjuvant androgen deprivation and radiotherapy for locally advanced

- prostate cancer: 10-year data from the TROG 96.01 randomised trial. *Lancet Oncol.* 2011 May;12(5):451–9.
104. Viani GA, Viana BS, Martin JEC, Rossi BT, Zuliani G, Stefano EJ. Intensity-modulated radiotherapy reduces toxicity with similar biochemical control compared with 3-dimensional conformal radiotherapy for prostate cancer: A randomized clinical trial. *Cancer.* 2016 Jul 1;122(13):2004–11.
  105. Wortel RC, Incrocci L, Pos FJ, van der Heide UA, Lebesque JV, Aluwini S, et al. Late Side Effects After Image Guided Intensity Modulated Radiation Therapy Compared to 3D-Conformal Radiation Therapy for Prostate Cancer: Results From 2 Prospective Cohorts. *Int J Radiat Oncol Biol Phys.* 2016 Jun 1;95(2):680–9.
  106. James ND, Sydes MR, Clarke NW, Mason MD, Dearnaley DP, Spears MR, et al. Addition of docetaxel, zoledronic acid, or both to first-line long-term hormone therapy in prostate cancer (STAMPEDE): survival results from an adaptive, multiarm, multistage, platform randomised controlled trial. *Lancet.* 2016 Mar 19;387(10024):1163–77.
  107. Krauss D, Kestin L, Ye H, Brabbins D, Ghilezan M, Gustafson G, et al. Lack of benefit for the addition of androgen deprivation therapy to dose-escalated radiotherapy in the treatment of intermediate- and high-risk prostate cancer. *Int J Radiat Oncol Biol Phys.* 2011 Jul 15;80(4):1064–71.
  108. Kupelian PA, Ciezki J, Reddy CA, Klein EA, Mahadevan A. Effect of increasing radiation doses on local and distant failures in patients with localized prostate cancer. *Int J Radiat Oncol Biol Phys.* 2008 May 1;71(1):16–22.
  109. Spratt DE, Malone S, Roy S, Grimes S, Eapen L, Morgan SC, et al. Prostate Radiotherapy With Adjuvant Androgen Deprivation Therapy (ADT) Improves Metastasis-Free Survival Compared to Neoadjuvant ADT: An Individual Patient Meta-Analysis. *J Clin Oncol.* 2021 Jan 10;39(2):136–44.
  110. King MT, Keyes M, Frank SJ, Crook JM, Butler WM, Rossi PJ, et al. Low dose rate brachytherapy for primary treatment of localized prostate cancer: A systemic

- review and executive summary of an evidence-based consensus statement. *Brachytherapy*. 2021 Dec;20(6):1114–29.
111. Viani GA, Arruda CV, Assis Pellizzon AC, De Fendi LI. HDR brachytherapy as monotherapy for prostate cancer: A systematic review with meta-analysis. *Brachytherapy*. 2021 Apr;20(2):307–14.
112. Morris WJ, Tyldesley S, Rodda S, Halperin R, Pai H, McKenzie M, et al. Androgen Suppression Combined with Elective Nodal and Dose Escalated Radiation Therapy (the ASCENDE-RT Trial): An Analysis of Survival Endpoints for a Randomized Trial Comparing a Low-Dose-Rate Brachytherapy Boost to a Dose-Escalated External Beam Boost for High- and Intermediate-risk Prostate Cancer. *Int J Radiat Oncol Biol Phys*. 2017 Jun 1;98(2):275–85.
113. Parry MG, Nossiter J, Sujenthiran A, Cowling TE, Patel RN, Morris M, et al. Impact of High-Dose-Rate and Low-Dose-Rate Brachytherapy Boost on Toxicity, Functional and Cancer Outcomes in Patients Receiving External Beam Radiation Therapy for Prostate Cancer: A National Population-Based Study. *Int J Radiat Oncol Biol Phys*. 2021 Apr 1;109(5):1219–29.
114. Guillaumier S, Peters M, Arya M, Afzal N, Charman S, Dudderidge T, et al. A Multicentre Study of 5-year Outcomes Following Focal Therapy in Treating Clinically Significant Nonmetastatic Prostate Cancer. *Eur Urol*. 2018 Oct;74(4):422–9.
115. van der Poel HG, van den Bergh RCN, Briers E, Cornford P, Govorov A, Henry AM, et al. Focal Therapy in Primary Localised Prostate Cancer: The European Association of Urology Position in 2018. *Eur Urol*. 2018 Jul;74(1):84–91.
116. Yaxley JW, Coughlin GD, Chambers SK, Occhipinti S, Samaratunga H, Zajdlewicz L, et al. Robot-assisted laparoscopic prostatectomy versus open radical retropubic prostatectomy: early outcomes from a randomised controlled phase 3 study. *Lancet*. 2016 10;388(10049):1057–66.

117. Walz J, Gallina A, Saad F, Montorsi F, Perrotte P, Shariat SF, et al. A nomogram predicting 10-year life expectancy in candidates for radical prostatectomy or radiotherapy for prostate cancer. *J Clin Oncol*. 2007 Aug 20;25(24):3576–81.
118. Efstathiou E, Davis JW, Pisters L, Li W, Wen S, McMullin RP, et al. Clinical and Biological Characterisation of Localised High-risk Prostate Cancer: Results of a Randomised Preoperative Study of a Luteinising Hormone-releasing Hormone Agonist with or Without Abiraterone Acetate plus Prednisone. *Eur Urol*. 2019 Oct;76(4):418–24.
119. Kumar S, Shelley M, Harrison C, Coles B, Wilt TJ, Mason MD. Neo-adjuvant and adjuvant hormone therapy for localised and locally advanced prostate cancer. *Cochrane Database Syst Rev*. 2006 Oct 18;(4):CD006019.
120. Lawton CA, DeSilvio M, Roach M, Uhl V, Kirsch R, Seider M, et al. An update of the phase III trial comparing whole pelvic to prostate only radiotherapy and neoadjuvant to adjuvant total androgen suppression: updated analysis of RTOG 94-13, with emphasis on unexpected hormone/radiation interactions. *Int J Radiat Oncol Biol Phys*. 2007 Nov 1;69(3):646–55.
121. Murthy V, Maitre P, Bhatia J, Kannan S, Krishnatry R, Prakash G, et al. Late toxicity and quality of life with prostate only or whole pelvic radiation therapy in high risk prostate cancer (POP-RT): A randomised trial. *Radiother Oncol*. 2020 Apr;145:71–80.
122. Murthy V, Maitre P, Kannan S, Panigrahi G, Krishnatry R, Bakshi G, et al. Prostate-Only Versus Whole-Pelvic Radiation Therapy in High-Risk and Very High-Risk Prostate Cancer (POP-RT): Outcomes From Phase III Randomized Controlled Trial. *J Clin Oncol*. 2021 Apr 10;39(11):1234–42.
123. Walsh PC, Donker PJ. Impotence following radical prostatectomy: insight into etiology and prevention. *J Urol*. 1982 Sep;128(3):492–7.
124. Schuessler WW, Schulam PG, Clayman RV, Kavoussi LR. Laparoscopic radical prostatectomy: initial short-term experience. *Urology*. 1997 Dec;50(6):854–7.

125. Guillonneau B, Cathelineau X, Barret E, Rozet F, Vallancien G. [Laparoscopic radical prostatectomy. Preliminary evaluation after 28 interventions]. *Presse Med.* 1998 Oct 17;27(31):1570–4.
126. Binder J, Jones J, Bentas W, Wolfram M, Bräutigam R, Probst M, et al. [Robot-assisted laparoscopy in urology. Radical prostatectomy and reconstructive retroperitoneal interventions]. *Urologe A.* 2002 Mar;41(2):144–9.
127. Kawachi MH. Counterpoint: robot-assisted laparoscopic prostatectomy: perhaps the surgical gold standard for prostate cancer care. *J Natl Compr Canc Netw.* 2007 Aug;5(7):689–92.
128. Lovegrove C, Novara G, Mottrie A, Guru KA, Brown M, Challacombe B, et al. Structured and Modular Training Pathway for Robot-assisted Radical Prostatectomy (RARP): Validation of the RARP Assessment Score and Learning Curve Assessment. *Eur Urol.* 2016 Mar;69(3):526–35.
129. Coughlin GD, Yaxley JW, Chambers SK, Occhipinti S, Samaratunga H, Zajdlewicz L, et al. Robot-assisted laparoscopic prostatectomy versus open radical retropubic prostatectomy: 24-month outcomes from a randomised controlled study. *Lancet Oncol.* 2018 Aug;19(8):1051–60.
130. Semerjian A, Pavlovich CP. Extraperitoneal Robot-Assisted Radical Prostatectomy: Indications, Technique and Outcomes. *Curr Urol Rep.* 2017 Jun;18(6):42.
131. Guillonneau B, Vallancien G. Laparoscopic radical prostatectomy: the Montsouris technique. *J Urol.* 2000 Jun;163(6):1643–9.
132. Menon M, Shrivastava A, Bhandari M, Satyanarayana R, Siva S, Agarwal PK. Vattikuti Institute prostatectomy: technical modifications in 2009. *Eur Urol.* 2009 Jul;56(1):89–96.
133. Montorsi F, Wilson TG, Rosen RC, Ahlering TE, Artibani W, Carroll PR, et al. Best practices in robot-assisted radical prostatectomy: recommendations of the Pasadena Consensus Panel. *Eur Urol.* 2012 Sep;62(3):368–81.



134. Li H, Liu C, Zhang H, Xu W, Liu J, Chen Y, et al. The Use of Unidirectional Barbed Suture for Urethrovesical Anastomosis during Robot-Assisted Radical Prostatectomy: A Systematic Review and Meta-Analysis of Efficacy and Safety. *PLoS One*. 2015;10(7):e0131167.
135. Kowalewski KF, Tapking C, Hetjens S, Nickel F, Mandel P, Nuhn P, et al. Interrupted versus Continuous Suturing for Vesicourethral Anastomosis During Radical Prostatectomy: A Systematic Review and Meta-analysis. *Eur Urol Focus*. 2019 Nov;5(6):980–91.
136. Bubendorf L, Schöpfer A, Wagner U, Sauter G, Moch H, Willi N, et al. Metastatic patterns of prostate cancer: an autopsy study of 1,589 patients. *Hum Pathol*. 2000 May;31(5):578–83.
137. Saitoh H, Yoshida K, Uchijima Y, Kobayashi N, Suwata J, Kamata S. Two different lymph node metastatic patterns of a prostatic cancer. *Cancer*. 1990 Apr 15;65(8):1843–6.
138. Briganti A, Blute ML, Eastham JH, Graefen M, Heidenreich A, Karnes JR, et al. Pelvic lymph node dissection in prostate cancer. *Eur Urol*. 2009 Jun;55(6):1251–65.
139. Briganti A, Chun FKH, Salonia A, Gallina A, Zanni G, Scattoni V, et al. Critical assessment of ideal nodal yield at pelvic lymphadenectomy to accurately diagnose prostate cancer nodal metastasis in patients undergoing radical retropubic prostatectomy. *Urology*. 2007 Jan;69(1):147–51.
140. Briganti A, Chun FKH, Salonia A, Gallina A, Farina E, Da Pozzo LF, et al. Validation of a nomogram predicting the probability of lymph node invasion based on the extent of pelvic lymphadenectomy in patients with clinically localized prostate cancer. *BJU Int*. 2006 Oct;98(4):788–93.
141. Heidenreich A, Varga Z, Von Knobloch R. Extended pelvic lymphadenectomy in patients undergoing radical prostatectomy: high incidence of lymph node metastasis. *J Urol*. 2002 Apr;167(4):1681–6.

142. Allaf ME, Palapattu GS, Trock BJ, Carter HB, Walsh PC. Anatomical extent of lymph node dissection: impact on men with clinically localized prostate cancer. *J Urol*. 2004 Nov;172(5 Pt 1):1840–4.
143. Bader P, Burkhard FC, Markwalder R, Studer UE. Is a limited lymph node dissection an adequate staging procedure for prostate cancer? *J Urol*. 2002 Aug;168(2):514–8; discussion 518.
144. Touijer K, Rabbani F, Otero JR, Secin FP, Eastham JA, Scardino PT, et al. Standard versus limited pelvic lymph node dissection for prostate cancer in patients with a predicted probability of nodal metastasis greater than 1%. *J Urol*. 2007 Jul;178(1):120–4.
145. Heidenreich A, Ohlmann CH, Polyakov S. Anatomical extent of pelvic lymphadenectomy in patients undergoing radical prostatectomy. *Eur Urol*. 2007 Jul;52(1):29–37.
146. Masterson TA, Bianco FJ, Vickers AJ, DiBlasio CJ, Fearn PA, Rabbani F, et al. The association between total and positive lymph node counts, and disease progression in clinically localized prostate cancer. *J Urol*. 2006 Apr;175(4):1320–4; discussion 1324-1325.
147. McLaughlin AP, Saltzstein SL, McCullough DL, Gittes RF. Prostatic carcinoma: incidence and location of unsuspected lymphatic metastases. *J Urol*. 1976 Jan;115(1):89–94.
148. Filimonova I, Schmidt D, Mansoorian S, Weissmann T, Siavooshhaghghi H, Cavallaro A, et al. The Distribution of Pelvic Nodal Metastases in Prostate Cancer Reveals Potential to Advance and Personalize Pelvic Radiotherapy. *Front Oncol*. 2020;10:590722.
149. Touijer KA, Sjoberg DD, Benfante N, Laudone VP, Ehdaie B, Eastham JA, et al. Limited versus Extended Pelvic Lymph Node Dissection for Prostate Cancer: A Randomized Clinical Trial. *Eur Urol Oncol*. 2021 Aug;4(4):532–9.

150. Lestingi JFP, Guglielmetti GB, Trinh QD, Coelho RF, Pontes J, Bastos DA, et al. Extended Versus Limited Pelvic Lymph Node Dissection During Radical Prostatectomy for Intermediate- and High-risk Prostate Cancer: Early Oncological Outcomes from a Randomized Phase 3 Trial. *Eur Urol.* 2021 May;79(5):595–604.
151. Golimbu M, Morales P, Al-Askari S, Brown J. Extended pelvic lymphadenectomy for prostatic cancer. *J Urol.* 1979 May;121(5):617–20.
152. Mattei A, Fuechsel FG, Bhatta Dhar N, Warncke SH, Thalmann GN, Krause T, et al. The template of the primary lymphatic landing sites of the prostate should be revisited: results of a multimodality mapping study. *Eur Urol.* 2008 Jan;53(1):118–25.
153. Mattei A, Würnschimmel C, Baumeister P, Hyseni A, Afferi L, Moschini M, et al. Standardized and Simplified Robot-assisted Superextended Pelvic Lymph Node Dissection for Prostate Cancer: The Monoblock Technique. *Eur Urol.* 2020 Sep;78(3):424–31.
154. Preisser F, Bandini M, Marchioni M, Nazzani S, Tian Z, Pompe RS, et al. Extent of lymph node dissection improves survival in prostate cancer patients treated with radical prostatectomy without lymph node invasion. *Prostate.* 2018 May;78(6):469–75.
155. Fossati N, Willemse PPM, Van den Broeck T, van den Bergh RCN, Yuan CY, Briers E, et al. The Benefits and Harms of Different Extents of Lymph Node Dissection During Radical Prostatectomy for Prostate Cancer: A Systematic Review. *Eur Urol.* 2017 Jul;72(1):84–109.
156. Cacciamani GE, Maas M, Nassiri N, Ortega D, Gill K, Dell’Oglio P, et al. Impact of Pelvic Lymph Node Dissection and Its Extent on Perioperative Morbidity in Patients Undergoing Radical Prostatectomy for Prostate Cancer: A Comprehensive Systematic Review and Meta-analysis. *Eur Urol Oncol.* 2021 Apr;4(2):134–49.
157. Weight CJ, Reuther AM, Gunn PW, Zippe CR, Dhar NB, Klein EA. Limited pelvic lymph node dissection does not improve biochemical relapse-free survival

- at 10 years after radical prostatectomy in patients with low-risk prostate cancer. *Urology*. 2008 Jan;71(1):141–5.
158. Berglund RK, Sadetsky N, DuChane J, Carroll PR, Klein EA. Limited pelvic lymph node dissection at the time of radical prostatectomy does not affect 5-year failure rates for low, intermediate and high risk prostate cancer: results from CaPSURE. *J Urol*. 2007 Feb;177(2):526–9; discussion 529-530.
159. Makarov DV, Trock BJ, Humphreys EB, Mangold LA, Walsh PC, Epstein JI, et al. Updated nomogram to predict pathologic stage of prostate cancer given prostate-specific antigen level, clinical stage, and biopsy Gleason score (Partin tables) based on cases from 2000 to 2005. *Urology*. 2007 Jun;69(6):1095–101.
160. Briganti A, Karnes RJ, Gandaglia G, Spahn M, Gontero P, Tosco L, et al. Natural history of surgically treated high-risk prostate cancer. *Urol Oncol*. 2015 Apr;33(4):163.e7-13.
161. Tosco L, Laenen A, Briganti A, Gontero P, Karnes RJ, Bastian PJ, et al. The EMPaCT Classifier: A Validated Tool to Predict Postoperative Prostate Cancer-related Death Using Competing-risk Analysis. *Eur Urol Focus*. 2018 Apr;4(3):369–75.
162. Harisinghani MG, Barentsz J, Hahn PF, Deserno WM, Tabatabaei S, van de Kaa CH, et al. Noninvasive detection of clinically occult lymph-node metastases in prostate cancer. *N Engl J Med*. 2003 Jun 19;348(25):2491–9.
163. Hövels AM, Heesakkers R a. M, Adang EM, Jager GJ, Strum S, Hoogeveen YL, et al. The diagnostic accuracy of CT and MRI in the staging of pelvic lymph nodes in patients with prostate cancer: a meta-analysis. *Clin Radiol*. 2008 Apr;63(4):387–95.
164. Flanigan RC, McKay TC, Olson M, Shankey TV, Pyle J, Waters WB. Limited efficacy of preoperative computed tomographic scanning for the evaluation of lymph node metastasis in patients before radical prostatectomy. *Urology*. 1996 Sep;48(3):428–32.

165. Tiguert R, Gheiler EL, Tefilli MV, Oskanian P, Banerjee M, Grignon DJ, et al. Lymph node size does not correlate with the presence of prostate cancer metastasis. *Urology*. 1999 Feb;53(2):367–71.
166. Spevack L, Killion LT, West JC, Rooker GM, Brewer EA, Cuddy PG. Predicting the patient at low risk for lymph node metastasis with localized prostate cancer: an analysis of four statistical models. *Int J Radiat Oncol Biol Phys*. 1996 Feb 1;34(3):543–7.
167. von Eyben FE, Kairemo K. Meta-analysis of (11)C-choline and (18)F-choline PET/CT for management of patients with prostate cancer. *Nucl Med Commun*. 2014 Mar;35(3):221–30.
168. Van den Bergh L, Lerut E, Haustermans K, Deroose CM, Oyen R, Isebaert S, et al. Final analysis of a prospective trial on functional imaging for nodal staging in patients with prostate cancer at high risk for lymph node involvement. *Urol Oncol*. 2015 Mar;33(3):109.e23-31.
169. van Kalmthout LWM, van Melick HHE, Lavalaye J, Meijer RP, Kooistra A, de Klerk JMH, et al. Prospective Validation of Gallium-68 Prostate Specific Membrane Antigen-Positron Emission Tomography/Computerized Tomography for Primary Staging of Prostate Cancer. *J Urol*. 2020 Mar;203(3):537–45.
170. Jansen BHE, Bodar YJL, Zwezerijnen GJC, Meijer D, van der Voorn JP, Nieuwenhuijzen JA, et al. Pelvic lymph-node staging with 18F-DCFPyL PET/CT prior to extended pelvic lymph-node dissection in primary prostate cancer - the SALT trial. *Eur J Nucl Med Mol Imaging*. 2021 Feb;48(2):509–20.
171. Cimino S, Reale G, Castelli T, Favilla V, Giardina R, Russo GI, et al. Comparison between Briganti, Partin and MSKCC tools in predicting positive lymph nodes in prostate cancer: a systematic review and meta-analysis. *Scand J Urol*. 2017 Oct;51(5):345–50.

172. Yu JB, Makarov DV, Sharma R, Peschel RE, Partin AW, Gross CP. Validation of the partin nomogram for prostate cancer in a national sample. *J Urol*. 2010 Jan;183(1):105–11.
173. Abdollah F, Cozzarini C, Suardi N, Gallina A, Capitanio U, Bianchi M, et al. Indications for pelvic nodal treatment in prostate cancer should change. Validation of the Roach formula in a large extended nodal dissection series. *Int J Radiat Oncol Biol Phys*. 2012 Jun 1;83(2):624–9.
174. Bandini M, Marchioni M, Pompe RS, Tian Z, Gandaglia G, Fossati N, et al. First North American validation and head-to-head comparison of four preoperative nomograms for prediction of lymph node invasion before radical prostatectomy. *BJU Int*. 2017 Nov 10;
175. Briganti A, Chun FKH, Salonia A, Zanni G, Gallina A, Dehò F, et al. A nomogram for staging of exclusive nonobturator lymph node metastases in men with localized prostate cancer. *Eur Urol*. 2007 Jan;51(1):112–9; discussion 119–120.
176. Godoy G, Chong KT, Cronin A, Vickers A, Laudone V, Touijer K, et al. Extent of pelvic lymph node dissection and the impact of standard template dissection on nomogram prediction of lymph node involvement. *Eur Urol*. 2011 Aug;60(2):195–201.
177. Prostate Cancer Nomograms: Pre-Radical Prostatectomy | Memorial Sloan Kettering Cancer Center [Internet]. [cited 2022 Oct 9]. Available from: [https://www.mskcc.org/nomograms/prostate/pre\\_op](https://www.mskcc.org/nomograms/prostate/pre_op)
178. Pre-Radical Prostatectomy [Internet]. Memorial Sloan Kettering Cancer Center. [cited 2017 Nov 22]. Available from: [https://www.mskcc.org/nomograms/prostate/pre\\_op](https://www.mskcc.org/nomograms/prostate/pre_op)
179. Briganti A, Larcher A, Abdollah F, Capitanio U, Gallina A, Suardi N, et al. Updated nomogram predicting lymph node invasion in patients with prostate

- cancer undergoing extended pelvic lymph node dissection: the essential importance of percentage of positive cores. *Eur Urol.* 2012 Mar;61(3):480–7.
180. Gandaglia G, Fossati N, Zaffuto E, Bandini M, Dell’Oglio P, Bravi CA, et al. Development and Internal Validation of a Novel Model to Identify the Candidates for Extended Pelvic Lymph Node Dissection in Prostate Cancer. *Eur Urol.* 2017 Apr 12;
181. Gandaglia G, Martini A, Ploussard G, Fossati N, Stabile A, De Visschere P, et al. External Validation of the 2019 Briganti Nomogram for the Identification of Prostate Cancer Patients Who Should Be Considered for an Extended Pelvic Lymph Node Dissection. *Eur Urol.* 2020 Aug;78(2):138–42.
182. Willard SS, Koochekpour S. Regulators of gene expression as biomarkers for prostate cancer. *Am J Cancer Res.* 2012;2(6):620–57.
183. Damaschke NA, Yang B, Bhusari S, Svaren JP, Jarrard DF. Epigenetic susceptibility factors for prostate cancer with aging. *Prostate.* 2013 Dec;73(16):1721–30.
184. Kumaraswamy A, Welker Leng KR, Westbrook TC, Yates JA, Zhao SG, Evans CP, et al. Recent Advances in Epigenetic Biomarkers and Epigenetic Targeting in Prostate Cancer. *Eur Urol.* 2021 Jul;80(1):71–81.
185. Geybels MS, Zhao S, Wong CJ, Bibikova M, Klotzle B, Wu M, et al. Epigenomic profiling of DNA methylation in paired prostate cancer versus adjacent benign tissue. *Prostate.* 2015 Dec;75(16):1941–50.
186. Patel PG, Wessel T, Kawashima A, Okello JBA, Jamaspishvili T, Guérard KP, et al. A three-gene DNA methylation biomarker accurately classifies early stage prostate cancer. *Prostate.* 2019 Oct;79(14):1705–14.
187. Stewart GD, Van Neste L, Delvenne P, Delrée P, Delga A, McNeill SA, et al. Clinical utility of an epigenetic assay to detect occult prostate cancer in histopathologically negative biopsies: results of the MATLOC study. *J Urol.* 2013 Mar;189(3):1110–6.

188. Carroll PH, Mohler JL. NCCN Guidelines Updates: Prostate Cancer and Prostate Cancer Early Detection. *Journal of the National Comprehensive Cancer Network*. 2018 May 1;16(5S):620–3.
189. Zhao S, Geybels MS, Leonardson A, Rubicz R, Kolb S, Yan Q, et al. Epigenome-Wide Tumor DNA Methylation Profiling Identifies Novel Prognostic Biomarkers of Metastatic-Lethal Progression in Men Diagnosed with Clinically Localized Prostate Cancer. *Clin Cancer Res*. 2017 Jan 1;23(1):311–9.
190. Zhao S, Leonardson A, Geybels MS, McDaniel AS, Yu M, Kolb S, et al. A five-CpG DNA methylation score to predict metastatic-lethal outcomes in men treated with radical prostatectomy for localized prostate cancer. *Prostate*. 2018 Jun 28;
191. Henrique R, Ribeiro FR, Fonseca D, Hoque MO, Carvalho AL, Costa VL, et al. High promoter methylation levels of APC predict poor prognosis in sextant biopsies from prostate cancer patients. *Clin Cancer Res*. 2007 Oct 15;13(20):6122–9.
192. Richiardi L, Fiano V, Vizzini L, De Marco L, Delsedime L, Akre O, et al. Promoter methylation in APC, RUNX3, and GSTP1 and mortality in prostate cancer patients. *J Clin Oncol*. 2009 Jul 1;27(19):3161–8.
193. Rosenbaum E, Hoque MO, Cohen Y, Zahurak M, Eisenberger MA, Epstein JI, et al. Promoter hypermethylation as an independent prognostic factor for relapse in patients with prostate cancer following radical prostatectomy. *Clin Cancer Res*. 2005 Dec 1;11(23):8321–5.
194. Vasiljević N, Ahmad AS, Thorat MA, Fisher G, Berney DM, Møller H, et al. DNA methylation gene-based models indicating independent poor outcome in prostate cancer. *BMC Cancer*. 2014 Sep 6;14:655.
195. Mundbjerg K, Chopra S, Alemozaffar M, Duymich C, Lakshminarasimhan R, Nichols PW, et al. Identifying aggressive prostate cancer foci using a DNA methylation classifier. *Genome Biol*. 2017 12;18(1):3.



196. Preisser F, Marchioni M, Nazzani S, Bandini M, Tian Z, Pompe RS, et al. The Impact of Lymph Node Metastases Burden at Radical Prostatectomy. *Eur Urol Focus*. 2018 Jan 3;
197. Bandini M, Fossati N, Gandaglia G, Preisser F, Dell'Oglio P, Zaffuto E, et al. Neoadjuvant and adjuvant treatment in high-risk prostate cancer. *Expert Rev Clin Pharmacol*. 2018 Apr;11(4):425–38.
198. Oderda M, Diamand R, Albisinni S, Callaris G, Carbone A, Falcone M, et al. Indications for and complications of pelvic lymph node dissection in prostate cancer: accuracy of available nomograms for the prediction of lymph node invasion. *BJU Int*. 2021 Mar;127(3):318–25.
199. Bandini M, Marchioni M, Preisser F, Nazzani S, Tian Z, Fossati N, et al. A Head-to-head Comparison of Four Prognostic Models for Prediction of Lymph Node Invasion in African American and Caucasian Individuals. *Eur Urol Focus*. 2017 Dec 14;
200. Tewes S, Hueper K, Hartung D, Imkamp F, Herrmann TRW, Weidemann J, et al. Targeted MRI/TRUS fusion-guided biopsy in men with previous prostate biopsies using a novel registration software and multiparametric MRI PI-RADS scores: first results. *World J Urol*. 2015 Nov;33(11):1707–14.
201. Williams C, Pontén F, Moberg C, Söderkvist P, Uhlén M, Pontén J, et al. A high frequency of sequence alterations is due to formalin fixation of archival specimens. *Am J Pathol*. 1999 Nov;155(5):1467–71.
202. Yost SE, Smith EN, Schwab RB, Bao L, Jung H, Wang X, et al. Identification of high-confidence somatic mutations in whole genome sequence of formalin-fixed breast cancer specimens. *Nucleic Acids Res*. 2012 Aug;40(14):e107.
203. Do H, Wong SQ, Li J, Dobrovic A. Reducing sequence artifacts in amplicon-based massively parallel sequencing of formalin-fixed paraffin-embedded DNA by enzymatic depletion of uracil-containing templates. *Clin Chem*. 2013 Sep;59(9):1376–83.

204. Kerick M, Isau M, Timmermann B, Sülthmann H, Herwig R, Krobitch S, et al. Targeted high throughput sequencing in clinical cancer settings: formaldehyde fixed-paraffin embedded (FFPE) tumor tissues, input amount and tumor heterogeneity. *BMC Med Genomics*. 2011 Sep 29;4:68.
205. Pan B, Kusko R, Xiao W, Zheng Y, Liu Z, Xiao C, et al. Similarities and differences between variants called with human reference genome HG19 or HG38. *BMC Bioinformatics*. 2019 Mar 14;20(Suppl 2):101.
206. Pan B, Kusko R, Xiao W, Zheng Y, Liu Z, Xiao C, et al. Correction to: Similarities and differences between variants called with human reference genome HG19 or HG38. *BMC Bioinformatics*. 2019 May 15;20(1):252.
207. Park Y, Wu H. Differential methylation analysis for BS-seq data under general experimental design. *Bioinformatics*. 2016 May 15;32(10):1446–53.
208. Akalin A, Kormaksson M, Li S, Garrett-Bakelman FE, Figueroa ME, Melnick A, et al. methylKit: a comprehensive R package for the analysis of genome-wide DNA methylation profiles. *Genome Biol*. 2012 Oct 3;13(10):R87.
209. Guo Q, Lakatos E, Bakir IA, Curtius K, Graham TA, Mustonen V. The mutational signatures of formalin fixation on the human genome. *Nat Commun*. 2022 Sep 6;13(1):4487.
210. Tan SC, Yiap BC. DNA, RNA, and protein extraction: the past and the present. *J Biomed Biotechnol*. 2009;2009:574398.
211. Oberacker P, Stepper P, Bond D, Hipp K, Hore TA, Jurkowski TP. Simple Synthesis of Functionalized Paramagnetic Beads for Nucleic Acid Purification and Manipulation. *Bio Protoc*. 2019 Oct 20;9(20):e3394.
212. Ewing CM, Ray AM, Lange EM, Zuhlke KA, Robbins CM, Tembe WD, et al. Germline mutations in HOXB13 and prostate-cancer risk. *N Engl J Med*. 2012 Jan 12;366(2):141–9.

213. Sato K, Qian J, Slezak JM, Lieber MM, Bostwick DG, Bergstralh EJ, et al. Clinical significance of alterations of chromosome 8 in high-grade, advanced, nonmetastatic prostate carcinoma. *J Natl Cancer Inst.* 1999 Sep 15;91(18):1574–80.
214. Strup SE, Pozzatti RO, Florence CD, Emmert-Buck MR, Duray PH, Liotta LA, et al. Chromosome 16 allelic loss analysis of a large set of microdissected prostate carcinomas. *J Urol.* 1999 Aug;162(2):590–4.
215. Osman I, Scher H, Dalbagni G, Reuter V, Zhang ZF, Cordon-Cardo C. Chromosome 16 in primary prostate cancer: a microsatellite analysis. *Int J Cancer.* 1997 May 16;71(4):580–4.
216. Carter BS, Ewing CM, Ward WS, Treiger BF, Aalders TW, Schalken JA, et al. Allelic loss of chromosomes 16q and 10q in human prostate cancer. *Proc Natl Acad Sci U S A.* 1990 Nov;87(22):8751–5.
217. Zhao SG, Chen WS, Li H, Foye A, Zhang M, Sjöström M, et al. The DNA methylation landscape of advanced prostate cancer. *Nat Genet.* 2020 Aug;52(8):778–89.
218. Wang J, Zou JX, Xue X, Cai D, Zhang Y, Duan Z, et al. ROR- $\gamma$  drives androgen receptor expression and represents a therapeutic target in castration-resistant prostate cancer. *Nat Med.* 2016 May;22(5):488–96.
219. Shimizu T, Okayama A, Inoue T, Takeda K. Analysis of gene expression during staurosporine-induced neuronal differentiation of human prostate cancer cells. *Oncol Rep.* 2005 Aug;14(2):441–8.
220. Perrone G, Vincenzi B, Zagami M, Santini D, Panteri R, Flammia G, et al. Reelin expression in human prostate cancer: a marker of tumor aggressiveness based on correlation with grade. *Mod Pathol.* 2007 Mar;20(3):344–51.
221. Terry S, Ploussard G, Allory Y, Nicolaiew N, Boissière-Michot F, Maillé P, et al. Increased expression of class III beta-tubulin in castration-resistant human prostate cancer. *Br J Cancer.* 2009 Sep 15;101(6):951–6.

222. Expression of SHTN1 in cancer - Summary - The Human Protein Atlas [Internet]. [cited 2022 Oct 9]. Available from: <https://www.proteinatlas.org/ENSG00000187164-SHTN1/pathology>
223. Jong Jin O, Seo YE, Shivakumar M, Jason M, Shefali V, Lee H, et al. P067 - Association of rare variants with Prostate Cancer in South Korean population. *European Urology Supplements*. 2017 Nov 1;16(10):e2714–5.
224. Zheng Z, Qiu K, Huang W. Long Non-Coding RNA (lncRNA) RAMS11 Promotes Metastasis and Cell Growth of Prostate Cancer by CBX4 Complex Binding to Top2 $\alpha$ . *Cancer Manag Res*. 2021;13:913–23.
225. Kolla V, Zhuang T, Higashi M, Naraparaju K, Brodeur GM. Role of CHD5 in human cancers: 10 years later. *Cancer Res*. 2014 Feb 1;74(3):652–8.
226. Robbins CM, Tembe WA, Baker A, Sinari S, Moses TY, Beckstrom-Sternberg S, et al. Copy number and targeted mutational analysis reveals novel somatic events in metastatic prostate tumors. *Genome Res*. 2011 Jan;21(1):47–55.
227. Zhi X, Zhao D, Wang Z, Zhou Z, Wang C, Chen W, et al. E3 ubiquitin ligase RNF126 promotes cancer cell proliferation by targeting the tumor suppressor p21 for ubiquitin-mediated degradation. *Cancer Res*. 2013 Jan 1;73(1):385–94.
228. Zhao X, Lei Y, Li G, Cheng Y, Yang H, Xie L, et al. Integrative analysis of cancer driver genes in prostate adenocarcinoma. *Mol Med Rep*. 2019 Apr;19(4):2707–15.
229. Pi P, A A, J F, An J, V W, D K, et al. Whole genome scanning identifies genotypes associated with recurrence and metastasis in prostate tumors. *Human molecular genetics* [Internet]. 2004 Jul 1 [cited 2022 Oct 9];13(13). Available from: <https://pubmed.ncbi.nlm.nih.gov/15138198/>
230. Hornstein M, Hoffmann MJ, Alexa A, Yamanaka M, Müller M, Jung V, et al. Protein phosphatase and TRAIL receptor genes as new candidate tumor genes on chromosome 8p in prostate cancer. *Cancer Genomics Proteomics*. 2008 Apr;5(2):123–36.

231. Zhou Y, Zhou Z, Ji Z, Yan W, Li H, Yu X. Tetramethylpyrazine reduces prostate cancer malignancy through inactivation of the DPP10-AS1/CBP/FOXM1 signaling pathway. *Int J Oncol.* 2020 Jul;57(1):314–24.
232. Blanc V, Nariculam J, Munson P, Freeman A, Klocker H, Masters J, et al. A role for class 3 semaphorins in prostate cancer. *Prostate.* 2011 May;71(6):649–58.
233. Liu F, Wang C, Huang H, Yang Y, Dai L, Han S, et al. SEMA3A-mediated crosstalk between prostate cancer cells and tumor-associated macrophages promotes androgen deprivation therapy resistance. *Cell Mol Immunol.* 2021 Mar;18(3):752–4.
234. Takahashi H, Ichimiya S, Nimura Y, Watanabe M, Furusato M, Wakui S, et al. Mutation, allelotyping, and transcription analyses of the p73 gene in prostatic carcinoma. *Cancer Res.* 1998 May 15;58(10):2076–7.
235. Arslan A, Batar B, Temiz E, Tozgir H, Koyuncu I, Bozgeyik E. Silencing of TP73-AS1 impairs prostate cancer cell proliferation and induces apoptosis via regulation of TP73. *Mol Biol Rep.* 2022 Jul;49(7):6859–69.
236. Bozgeyik E, Arslan A, Temiz E, Batar B, Koyuncu I, Tozgir H. miR-320a promotes p53-dependent apoptosis of prostate cancer cells by negatively regulating TP73-AS1 invitro. *Biochem Biophys Res Commun.* 2022 Sep 3;619:130–6.
237. Pardo LA, Stühmer W. The roles of K(+) channels in cancer. *Nat Rev Cancer.* 2014 Jan;14(1):39–48.
238. Abdul M, Hoosein N. Expression and activity of potassium ion channels in human prostate cancer. *Cancer Lett.* 2002 Dec 1;186(1):99–105.
239. Song MS, Park SM, Park JS, Byun JH, Jin HJ, Seo SH, et al. Kv3.1 and Kv3.4, Are Involved in Cancer Cell Migration and Invasion. *Int J Mol Sci.* 2018 Apr 2;19(4):E1061.

240. Ahmed HU, El-Shater Bosaily A, Brown LC, Gabe R, Kaplan R, Parmar MK, et al. Diagnostic accuracy of multi-parametric MRI and TRUS biopsy in prostate cancer (PROMIS): a paired validating confirmatory study. *Lancet*. 2017 Feb 25;389(10071):815–22.

A handwritten signature in black ink, appearing to read "Marco Banti". The signature is written in a cursive style with a prominent initial 'M' and a long, sweeping tail.